Politecnico di Torino

Department of Mechanical and Aerospace Engineering
Master's Degree in Aerospace Engineering
Academic Year 2023/2024

Fuel Cell Simulation Model for Aircraft Integration Analysis in Early Design Phases

Supervisors
Prof. Nicole Viola
Dr. Susan Liscouët-Hanke

Candidate
Leonardo Cavini

July 2024

Leonardo Cavini.
Fuel Cell Simulation Model for Aircraft Integration Analysis in Early Design Phases.

email: leonardo.cavini7@gmail.com
Contact the author for the model code.

Abstract

Air traffic's rapid expansion necessitates aircraft reconfiguring to mitigate greenhouse gas emissions. Hydrogen propulsion presents a potential alternative to reduce aviation's environmental impact, yet it introduces numerous new challenges, particularly in the design of novel system architectures. One promising solution is the hydrogen fuel cell (FC), which can generate electricity without CO_2 emissions, with water as its unique byproduct. A versatile mathematical model is essential to analyze the behaviour and performance of these innovative devices during the early stages of aircraft design. This model must interact seamlessly with all Balance of Plant (BoP) components—devices facilitating the fuel cell's operation.

A fuel cell modelling approach based on defining an equivalent circuit is adopted. This approach can capture these devices' typical losses and dynamic behaviour. The core model, adapted and refined from a zero-dimensional model in existing literature, includes several key assumptions: dynamic effects during transients are considered, the operating temperature is constant, the membrane is optimally hydrated, and high current densities are excluded. This model can accurately represent the behaviour of both Proton Exchange Membrane Fuel Cells (PEMFCs) and Solid Oxide Fuel Cells (SOFCs).

To enhance the model's fidelity, two formulations for modelling heat production are incorporated: one employs a detailed enthalpy balance of reactants and products, while the other uses a simplified energy balance. The mathematical model is implemented in the Modelica language, enabling the creation of a fuel cell block with acausal interfaces. These interfaces allow integration with other components, such as electrical loads, the hydrogen tank, the air intake, and a cooling system. Specifically, the acausal model is designed to represent the behaviour of PEMFCs. Validation with real PEMFC stack data, sourced from the market and collected in databases, confirmed the model's accuracy. Importantly, the model's parameters are directly derived from fuel cell stack datasheets, guaranteeing flexibility and ease of use.

To demonstrate the model's practical application, a rudimentary BoP was constructed around it to simulate a realistic case study. The mission profile of an ATR 72-based aircraft using hydrogen-powered electric propulsion is simulated. This model allows for examining various parameters, including the quantity of hydrogen required for the mission, electrical and thermal energy production, and overall system efficiency. Simulations were conducted using two different fuel cells: one from the early 2000s with lower performance and another incorporating the latest aviation technologies.

This comprehensive model is a valuable tool for studying different configurations of hydrogen fuel cell systems during the preliminary design phases of new aircraft. It allows detailed analysis of hydrogen consumption, energy production, and system efficiency and facilitates the development of more sustainable aircraft.

Contents

List of Figures

List of Tables

Listings

Acronyms

AC	Alternating Current
APU	Auxiliary Power Unit
ATR	Avions de Transport Régional
BPP	BiPolar Plate
CFD	Computational Fluid Dynamics
CL	Catalyst Layer
DASSL	Differential/Algebraic System Solver
DC	Direct Current
EIS	Electrochemical Impedance Spectroscopy
EVD	Electrochemical Vapor Deposition
FC	Fuel Cell
GDL	Gas Diffusion Layer
GC	Gas Channel
GT	Gas Turbine
HEFA	Hydroprocessing production process of Esters and Fatty Acids
HHV	Higher Heating Value
IATA	International Air Transport Association
ICAO	International Civil Aviation Organization
ICE	Internal Combustion Engine
ISA	International Standard Atmosphere
LHV	Lower Heating Value
MBD	Model-Based Design
MEA	Membrane Electrode Assembly
MEM	Membrane
NASA	National Aeronautics and Space Administration
OCV	Open Circuit Voltage
PEMFC	Proton Exchange Membrane Fuel Cell
PTFE	PolyTetraFluoroEthylene
RC	Resistor-Capacitor circuit
RLC	Resistor, Capacitor, and inductor (L) circuit
SAF	Sustainable Aviation Fuel
SOFC	Solid Oxide Fuel Cell
YSZ	Yttria-Stabilized Zirconia

Symbols

A	Surface of the fuel cell, or Tafel slope
c_p	Specific heat capacity
E	Electrical potential difference, reversible voltage of fuel cell
E^0	Reversible voltage in standard condition
E_T	Reversible cell voltage at temperature T and constant pressure
E_n	Nernst Voltage
E_{oc}	Open Circuit Voltage
F	Faraday's Constant (96485 As/mol)
G, g	Gibbs free energy, specific Gibbs free energy
g_0	Gravity acceleration
ΔG	Activation energy barrier
H, h_i	Enthalpy, specific enthalpy of species i
h	Planck's constant (6.626e-34 Js), or altitude
h_{fg}	Water heat of vaporization
i	Current density
i_0	Exchange current
i_{fc}	Fuel Cell current
K_1	Adimensional parameter
K_c	Voltage constant at the nominal condition
k	Boltzmann's constant (1.38e-23 J/K)
M	Mass
Ma	Mach number
M_{air}	Molar mass of air (28.9646 g/mol)
M_{H2}	Molar mass of molecular hydrogen (2.01568 g/mol)
M_{H2O}	Molar mass of water (18.01528 g/mol)
M_{O2}	Molar mass of molecular oxygen (31.9988 g/mol)
$\dot{m}$	Mass flow rate
N	Number of cells in series in a stack
$n, \dot{n}$	Mole rate
P, p, p_i	Pressure, or partial pressure of species i
P_{fuel}	Preussure of the fuel
P_{air}	Preussure of the air
P	Power
Q	Heat, or charge
R	Gas constant (8.3145 J/(mol K))
R^2	Coefficient of determination
R_{ohm}	Ohmic resistance
S, s	Entropy, specific entropy

T	Temperature
T_0	Reference temperature
T_d	Settling time
t_i	Thickness of a fuel cell layer
U	Internal energy
$U_{f_{H2}}$	Rate of utilization of hydrogen
$U_{f_{O2}}$	Rate of utilization of oxygen
V	Volume, or Voltage
V_{act}	Activation voltage drop
V_{air}	Air flow rate
V_{fc}	Fuel cell voltage
V_{fuel}	Fuel flow rate
Δv	Activation barrier volume factor ($1m^3$)
v	Efficiency
W	Work
w	Molar fraction of water in the exhaust air, or general mass fraction
x	Molar fraction (of hydrogen in the fuel if not specified)
y	Molar fraction of oxygen in the air
z	Number of moving electrons

Greek Letters

α	Charge transfer coefficient
γ	Air heat capacity ratio (=1.4)
λ	Stoichiometric ratio
ρ	Density
ϕ	Scaling factor

Superscripts

0	Standard state condition, or condition at 0°C
25	Standard condition at 25°C

Subscripts

0	Sea level condition
11	Related to tropopause
1	Related to 1 Ampere
c	Cooling, or related to point c
$cell$	Related to a single cell
dis	Dissipated
$elec$, el	Electric
gen	Generated
$H2$	Related to molecular hydrogen
$H2O$	Related to water
max	Maximum
min	Minimum
nom	Related to nominal condition
out	Output
$O2$	Related to molecular oxygen

rev	Reversible
rxn	Related to a reaction
start	Initial condition
std	Related to standard condition
T	Related to a specific temperature
trop	Related to tropopause

Chapter 1

Introduction

Studying new aircraft configurations is essential to make commercial and non-commercial flights more environmentally sustainable. This chapter will address the challenges of aviation's decarbonization and how this thesis contributes to this process. Some technologies contributing to reduce the impact of aviation will be explained, such as new fuels and devices capable of converting their energy, providing the necessary background to understand the following chapters better. Finally, the purpose and objectives of this thesis will be exposed.

1.1 Decarbonization of Aviation

The expansion of air travel is evident as passenger and cargo air traffic is expected to double within the next two decades, driven by tourism and a globalized economy [1]. Despite being the safest and most efficient means of long-distance travel, aviation faces challenges such as managing increased traffic and reducing emissions [1]. Currently, aviation contributes between 2 and 3.5% of global anthropogenic greenhouse gas emissions [2], a figure expected to increase if countermeasures are not implemented. However, initiatives such as those presented at the 41st Assembly of the International Civil Aviation Organization (ICAO) aim to achieve the goal of net zero carbon emissions by 2050. These initiatives ensure the sustainability of aviation and its crucial role in society and the global economy through collaborative efforts to mitigate greenhouse gas emissions from aviation operations.

The International Air Transport Association (IATA) has identified three areas in which action can be taken to achieve the objective set for 2050. The first area of intervention is reducing the energy used by aircraft, acting on the propulsion and aerodynamic efficiency of the aircraft, air traffic management, and airport operations. The second area of intervention is the reduction of the carbon footprint by using alternative fuels. Finally, the third area aims to capture the carbon dioxide emitted, which cannot be avoided in other ways [3]. These actions involve the entire aviation sector, from aircraft design to ground and airborne operations.

Changing the emission source is a substantial way to reduce the impact of aviation. The root of the emissions lies in the fuel used, as Jet fuel is a mix of hydrocarbons that produce greenhouse gases if combusted in the burner. As shown in Figure 1.1, an aviation turbine engine produces a massive quantity of carbon dioxide CO_2, nitrogen oxides NO_x, and several other substances harmful to the environment. Three possibilities for replacing aviation fuel as an energy carrier have been identified: sustainable aviation fuels (SAFs), batteries, and hydrogen [4].

SAFs are the most promising fuels for reducing aviation emissions in the short and medium term. These fuels must be chemically similar to standard aviation fuels to be used within current airport infrastructure, fuel tanks, and aircraft engines. SAFs do not seek to reduce emissions during

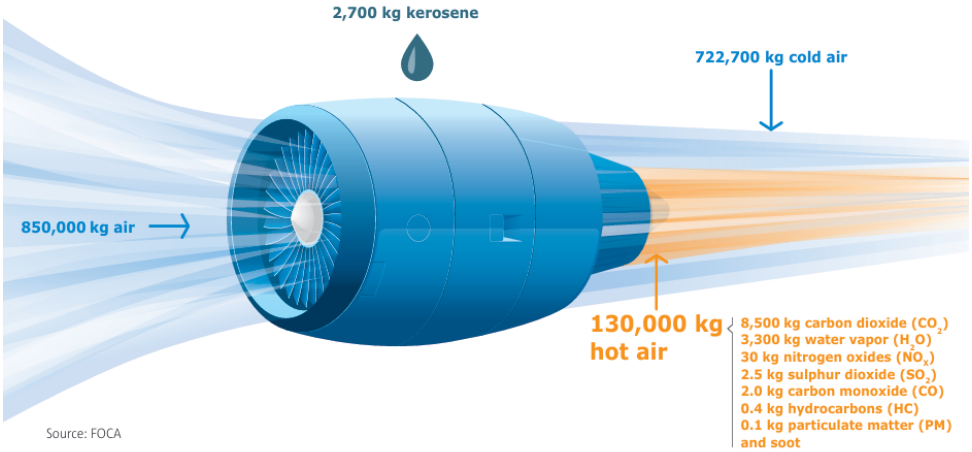

Figure 1.1: Emissions of an engine of a 150-passenger aircraft during one-hour flight. Source: *European aviation environmental report 2019.*[5]

the flight, which remain unchanged. Still, they are crucial for reducing greenhouse gas emissions over the entire life cycle of fuels, particularly in their production [2]. One of the problems with these fuels is the future large demand from airports that may not be met by the companies currently producing these sustainable fuels [6].

Batteries may be a prospect to reduce the production of emissions completely, but currently, there are still several challenges that limit their application. Unlike sustainable fuels, batteries do not produce emissions during flight as there is no combustion. Aviation is observing other sectors where this technology is in a more advanced state of development, such as the automotive sector, to understand if and how it can be used in aircraft. Nowadays, the specific energy of the batteries is significantly lower than that of conventional fuel and can only be considered for short-haul flights for regional aircraft. For aeronautical applications, where weight and reliability are fundamental concerns, it is necessary to improve the available technologies to increase power density and safety [7].

Finally, hydrogen can also be considered as a promising avenue to achieve zero emissions in aviation by 2050. This fuel can be produced from water and renewable electricity through electrolysis or other environmentally friendly methods [8]. Experimentation with the use of this fuel in aviation since the 1950s and a good overview of the current state of the art of this technology in aviation can be found in the work of Adler et al. [9].

This thesis will explore the use of hydrogen and fuel cells, i.e. devices that convert the chemical energy of hydrogen into electrical energy.

1.2 Hydrogen in Aviation

Aviation has used hydrogen since its beginnings, well before the invention of the first airplane. As Yusaf et al. [10] recall in their work, the first flying machines that used hydrogen were hot air balloons at the end of the 1700s and airships in the 1800s. Subsequently, this fuel was studied for modern aeronautical applications starting in the middle of the last century, when the fuel cost began to increase. The projects discussed in this section are summarized in Table 1.1. For example, Lockheed studied the feasibility of using hydrogen in commercial aviation with the CL-400 Suntan [9]. In addition to the United States, the Soviet Union was also working on a large-scale

Company	Year of first flight	Aircraft	Technology
Lockheed's Skunk Works [9]	-	CL-400 Suntan	Hydrogen combustion
Aviakor [11]	1988	Tupolev Tu-155	Hydrogen combustion
ZeroAvia [12, 13]	2023	Dornier 228	Fuel Cell
Universal Hydrogen [14]	2023	Dash 8	Fuel Cell
Airbus ZEROe	-	New Fleet of Aircraft	Fuel Cell and Hydrogen Combustion

Table 1.1: Past and future projects using hydrogen in aviation

project using hydrogen. In 1988, the modified Tupolev-155 performed the first 21-minute flight with hydrogen powering the turbine engines, setting a record for the time with this fuel [11]. By the late 1900s, only a few airplanes flew with liquid hydrogen burned in turbine engines.

The application of hydrogen to aviation brings essential challenges to future aircraft design. Hydrogen has properties that are different from those of current aviation fuel. On the one hand, it has a three times greater specific energy (approximately 120 MJ/kg); on the other hand, there is an energy density much lower than Jet-A1, which is further reduced when considering hydrogen stored in gaseous form. For this reason, configurations considering different hydrogen storage methods are studied, including using cryogenic liquid hydrogen at very low temperatures, around 20 K. Innovative cooling systems are required to maintain hydrogen at these low temperatures. The presence of cryogenic liquids radically changes on-board architectures, leading to new application possibilities such as the use of superconducting technologies [15].

Hydrogen has been a controversial fluid since 1937 when the LZ 129 Hindenburg airship caught fire, and many considered hydrogen as the cause of the accident [16]. Hydrogen has advantages and disadvantages in terms of safety. Regarding flammability, hydrogen has a lower combustion temperature than kerosene, but its low density means the fire develops upwards, dispersing into the atmosphere very quickly and avoiding remaining on the ground for a long time like conventional fuel. In developing the CL-400, Lockheed engineers cataloged this material as fairly safe to handle. A problem with hydrogen is its ability to permeate materials, make them more fragile, and produce gas leaks.

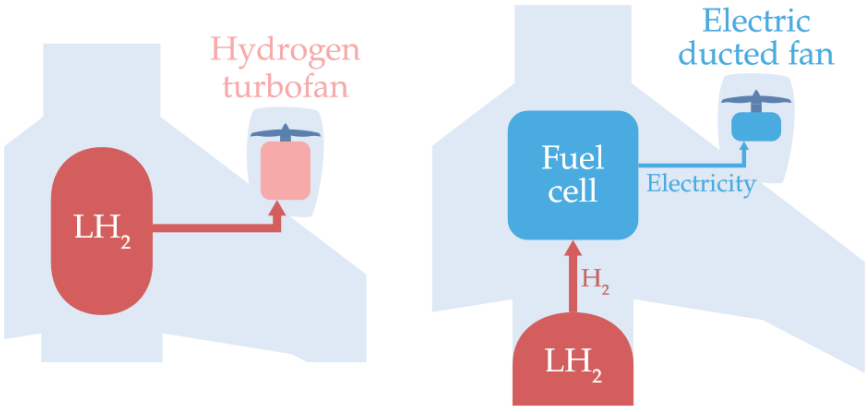

Figure 1.2: The two basic architectures most commonly studied for the use of hydrogen. Source: Adler et al. [9]

Since the beginning of the new millennium, many companies have begun to study the applica-

tion of hydrogen in aviation to reduce greenhouse gas emissions. In particular, as shown in Figure 1.2, two possible technologies are studied: hydrogen combustion or hybrid-electric devices. The first architecture supplies hydrogen directly to a turbine engine where combustion occurs. This technology takes advantage of the knowledge and technical capabilities in designing and producing turbine engines developed since the middle of the last century; in fact, many large motor companies plan to develop hydrogen-powered turbine engines in the following years [17]. The second architecture supplies hydrogen to a fuel cell, which converts the chemical energy of hydrogen into electrical energy to provide electricity to a hybrid-electric system. This latest architecture is more complex than the first and has some limitations due to current technology, but it can be considered the only one that avoids greenhouse gas emissions due to the absence of combustion. For these reasons, it is initially studied for regional aircraft applications.

The simplest example, which considers the second architecture, requires fuel cells sized for the maximum power required by the aircraft and a compressor capable of providing air at the right pressure for each phase of flight [18]. The electricity provides power to an electric motor via an inverter. This solution has been studied in recent years by ZeroAvia [12, 13] and Universal Hydrogen [14], which have carried out a retrofit of the Dornier 228 (Figure 1.3a) and Dash 8 (Figure 1.3b), respectively, by inserting electric propulsion powered by a fuel cell and starting flight tests around 2020 with their prototypes. One of the most ambitious projects is the one carried out by Airbus ZEROe, where a new fleet of aircraft will be developed, using both architectures that use hydrogen to produce power (Figures 1.3c and 1.3d).

(a) Dornier 228 retrofitted by ZeroAvia. Source: `https://zeroavia.com/`

(b) Dash 8 retrofitted by Universal Hydrogen. Source: `https://hydrogen.aero/`

(c) Innovative turboprop design in Airbus' ZEROe project. Source: `https://www.airbus.com/en`

(d) Innovative blended-wing body design in Airbus' ZEROe project. Source: `https://edition.cnn.com/`

Figure 1.3: Actual and future projects for the use of hydrogen in aviation.

Hydrogen can become an essential means in the service of decarbonization of aviation. There are many challenges that researchers will have to overcome to use this fuel in the medium and long term, but despite this, many companies want to bring this technology to the market before the end

of the decade. Among the significant challenges is the design of the fuel system and hydrogen tanks, considering the high safety standards of aviation. It will be designed, for example, considering the presence of bulkier tanks, more significant structural requirements compared to the previous generation and leak detectors to prevent flammable scenarios. Therefore, the use of hydrogen in aviation will be anticipated by a change in the design methodologies of the configuration of new aircraft [9, 10]. The use of the architecture containing the fuel cells will be explored in depth, starting by explaining the operating principles of these devices

1.3 Fuel Cells Technology

Fuel cells are electrochemical devices that directly convert the chemical energy contained in fuels into electrical energy, promising energy generation with high efficiency and low environmental impact. They do not have thermodynamic or mechanical limitations as heat engines. Fuel cell systems are complex devices comprising several components: the unit cells, where the chemical reaction takes place; the stacks, where the unit cells are combined to provide the desired capacity; and the Balance of Plant (BoP), including all auxiliary devices useful for the operation of the fuel cell [19].

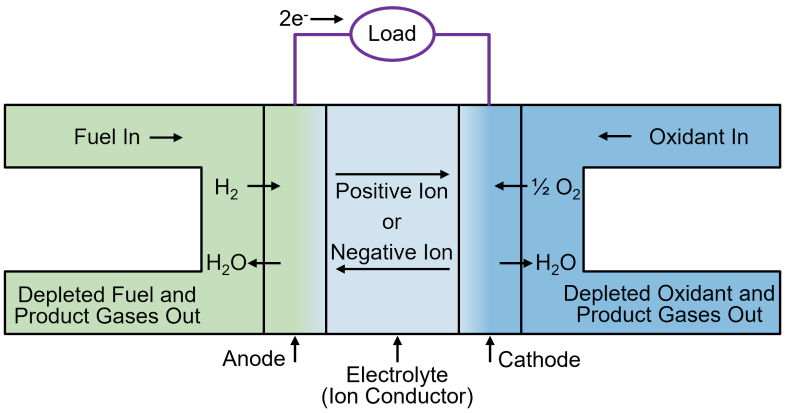

Figure 1.4: Basic structure of a fuel cell unit. Adapted from [19]

The fundamental unit of a fuel cell is made of different layers, each with a specific function. Figure 1.4 shows the basic structure of a fuel cell, where fuel and oxidant are fed to the anode and cathode, respectively, through two separate gas channels. The anode and cathode are called electrodes, and they are connected by the electrolyte layer.

The electrodes are where the half-reactions occur, producing ions and electrons. Ions are transferred to the other electrode via the electrolyte, and electrons make up the current that passes through the applied electrical load. The material these layers are made of is essential to determining the correct and high-performance functioning of the fuel cell.

Many types of fuel cells have been studied and built. Fuel cells are classified according to the composition of the electrolyte and the fuel used. This chapter will consider two types of fuel cells: Proton Exchange Membrane Fuel Cells (PEMFC) and Solid Oxide Fuel Cells (SOFC), and their operating characteristics and differences will be described.

As will be seen later, a single fuel cell can deliver a very low voltage, around 1 Volt. Placing more fuel cells within a stack is necessary to increase the total voltage supplied and to apply this technology to real cases. Two important strategies for connecting cells are utilizing bipolar plates or tubular cells.

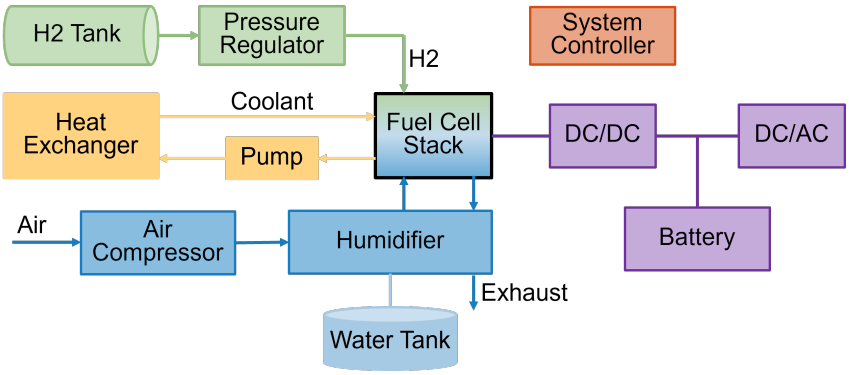

Figure 1.5: Example of Balance of Plant. Adapted from [20]

Using bipolar plates to connect two adjacent cells is the most widely used method. This plate is designed to transport oxidizer and fuel in different channels without mutual contamination. Furthermore, this component electrically connects two adjacent cells.

However, in the case of high-temperature fuel cells, tubular cells are often preferred due to their ability to provide sealing and enhance the structural integrity of the stack, despite the challenges involved in their design.

A fuel cell stack cannot work alone but needs supporting devices. The set of devices that allow the fuel cell stack to function correctly is called Balance of Pant. This complex system comprises several subsystems connected to different fuel cell parts, as shown in Figure 1.5. The cooling system is necessary to remove the heat generated inside the fuel cell by various phenomena. As Ohm's law describes, the absorption of current by the electrical load connected to the fuel cell generates heat proportional to the current. Furthermore, the water formation reaction inside the fuel cell is exothermic, with a negative enthalpy variation (See Section 3.1). These and other reasons make it necessary to have a complex cooling system that maintains the right temperature inside the stack to stabilize its performance.

The water management system maintains a correct humidity inside the polymer membrane in the case of PEMFC. Membrane wetting can vary due to changes in pressure and flow of reagents or changes in temperature. The presence of this system prevents significant changes in performance.

The system that manages the flow of reactants must guarantee the correct supply of hydrogen and air to the anode and cathode in each operational phase. This system uses valves and compressors that maintain the correct pressure of the reactants when the required current is high.

Finally, the electrical system converts the current generated by the fuel cell stack into current that can be used by the electrical load. The stack produces direct current with variable voltage depending on the load required. Electrical users generally require a constant voltage, whether direct or alternating, so a DC/DC converter stabilizes the voltage. Then, a DC/AC converter is used to modify its nature and adapt it to the demands of the electrical users [21]. The BoP is fundamental for implementing fuel cells in transportation applications while increasing the mass and volume of the electrical generation system.

As mentioned previously, among the main and most studied types of fuel cells, there are PEMFCs and SOFCs. Table 1.2 shows the main differences between these two devices, and their structure will be explored in detail in the next paragraphs.

	PEMFC	**SOFC**
Electrodes	Carbon (cloth or paper)	Metal Cermet: Anode $Ni + ZrO_2$ Cathode Sr-doped $LaMnO_3$
Catalyst	Platinum (0.2 mg/cm^2)	Non-noble metal
Electrolyte	Solid ion conduction Polymer (PTFE)	Dense ceramic Yttria-stabilized Zirconia (YSZ)
Operating Temperature [°C]	50-80	600-1000
Charge Ion Carrier	H^+	O^{2-}
CO Tolerance	No (<50ppm)	Yes, carbon-based fuel
Electrical Efficiency [%]	40-50	50-60
Power Density [mW/cm^2]	300-1000	250-350
Power Range [kW]	10^{-3}-10^3	5-10^5

Table 1.2: Comparison between PEMFC and SOFC. Sources: *Fuel cell systems explained* [22] and *Modeling and control of fuel cells* [23].

1.3.1 Proton Exchange Membrane Fuel Cell

The proton exchange membrane fuel cell (PEMFC), also called solid polymer fuel cell or polymer electrolyte fuel cell, found its first uses in human spacecraft developed by NASA in the second half of the 20th century.

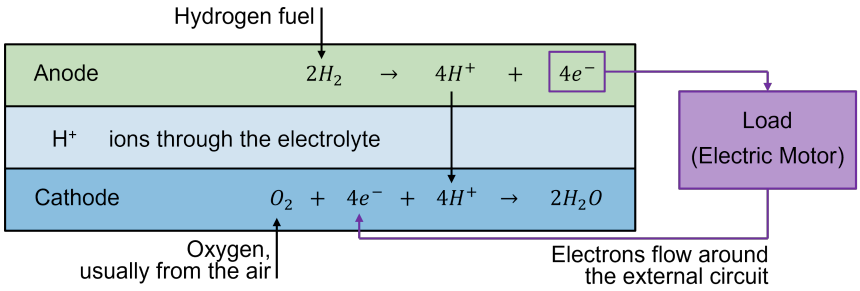

Figure 1.6: Semi-reactions within the PEMFC. Adapted from [22]

This type of fuel cell requires the use of high-purity hydrogen. The chemical process represented in Figure 1.6 begins with the hydrogen arriving at the anode, where the first half-reaction takes place:

$$2\,\mathrm{H_2} \longrightarrow 4\,\mathrm{H^+} + 4\,\mathrm{e^-} \tag{1.1}$$

From here, the electrons pass through the circuit and the electrical load, while the hydrogen ions pass through the membrane. The second half-reaction occurs at the cathode, where water is produced:

$$\mathrm{O_2} + 4\,\mathrm{e^-} + 4\,\mathrm{H^+} \longrightarrow 2\,\mathrm{H_2O} \tag{1.2}$$

The polymer electrolyte membrane of this fuel cell is made of a material called sulfonated fluoropolymers. This material, known commercially as *Nafion*, is developed starting from a polyethylene chain in which the hydrogen atoms are replaced with fluorine atoms, obtaining Polytetrafluoroethylene (PTFE), and is subsequently sulfonated with a side chain ending with sulphonic acid.

This hydrophilic termination allows abundant hydration of the membrane (up to doubling its dry weight) and the movement of hydrogen ions.

The half-reactions occur at the electrodes and are favoured by the presence of a catalyst, usually platinum. In recent years, attempts have been made to reduce the presence of platinum to reduce the cost of the device, as this material is expensive [24]. The electrodes are made of structural porous materials, generally made of carbon paper or cloth, on which fine carbon particles, with small particles of platinum on their surface, are fixed.

To connect more cells and increase the total voltage supplied, a bipolar plate must be inserted between the cells. The design of these bulky components is complex and will not be explored here. Despite this, these bipolar plates are essential for electrically connecting adjacent cells, correctly distributing reagents on the electrodes without them coming into contact with each other and, in some cases, for circulating liquids for the cooling system. To meet many project requirements, graphite modelled using various techniques is often chosen [22].

PEMFC is a technology developed and studied in multiple transport fields. Despite its widespread diffusion, it is essential to identify the limitations relating to application in aviation, which research will try to overcome in the coming years. In particular, the variation in inertia forces due to the different flight phases can modify water distribution on the fuel cell membrane, reducing its performance. PEMFC also has a complex BoP and can only be powered by pure hydrogen. However, among the advantages is a fast start-up time and good reactivity to variations in the electrical load [25]. Nowadays, PEMFCs are mainly designed for road applications, such as cars or small trucks, of which the first prototypes are already being tested [19].

1.3.2 Solid Oxide Fuel Cell

The solid oxide fuel cell (SOFC) has been developed by Nernst since the late 19th century.

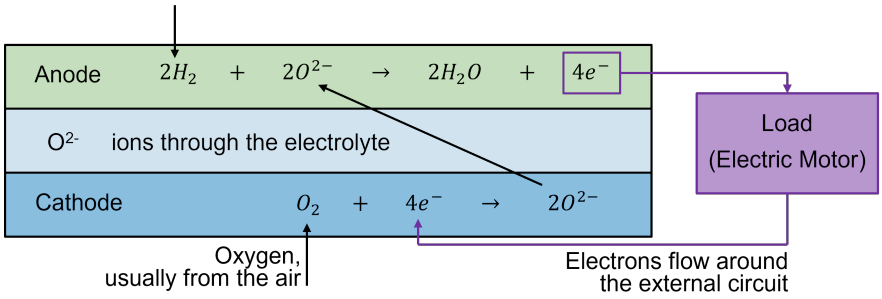

Figure 1.7: Semi-reactions within the SOFC. Adapted from [22]

The chemical process represented in Figure 1.7 begins with the oxygen arriving at the cathode, which reacts with the electrons from the electrical load:

$$\mathrm{O_2 + 4\,e^- \longrightarrow 2\,O^{2-}} \tag{1.3}$$

The oxygen ions pass through the electrolyte and react with hydrogen at the anode, where water is produced:

$$\mathrm{2\,H_2 + 2\,O^{2-} \longrightarrow 2\,H_2O + 4\,e^-} \tag{1.4}$$

The electrolyte in the core of the SOFC is composed of yttria-stabilized Zirconia (YSZ). This material is stable in both reducing and oxidizing environments, thanks to Zirconia, and it is capable of conducting oxygen-negative ions at high temperatures (around 1000°C) through its crystalline structure, thanks to yttria ions used to dope Zirconia.

The anode is composed of a highly porous YSZ structure, which maintains a similar thermal expansion coefficient to the electrolyte, together with a cermet made of metallic nickel. The cathode is composed of a porous structure of Storntium-doped Lanthanum manganite. There are no expensive catalysts because the high temperatures facilitate chemical reactions. The interconnection materials between different cells vary greatly depending on the structure of the cells, which can be planar or tubular. In the case of planar cells, there is a bipolar plate made of special alloys that try to satisfy structural and chemical requirements due to the high operating temperatures. In the case of the tubular configuration, which is more common for this type of fuel cell, the interconnection materials are mainly ceramic [22]. Table 1.3 shows the main differences between the two SOFC configurations.

These fuel cells bring some advantages for aeronautical use, as there is no water management system in the membrane, and the latter is not sensitive to the inertia forces typical of aeronautical flight. Furthermore, high-temperature exhaust gases can be recovered and used by other systems that require high thermal loads. This technology is promising for aviation applications because it can also be powered by aviation fuel, so it is possible to study its behaviour in the short term before the introduction of hydrogen [25].

	Tubular SOFC	**Planar SOFC**
Connection between cells	Complex geometry	Simple geometry
Fabrication methods	Expensive: - Electrochemical vapour deposition (EVD)	Cheap: - Screen printing - Tape casting
Stack	Big and heavy	Compact
Sealing	Seal-less configuration	Difficult gas-tight sealing
Power density [mW/cm^2]	∼100	∼800
Oper. current density [mA/cm^2]	∼200	∼900
Ohmic loss	High	Low

Table 1.3: Comparison between Tubular and Planar SOFC. Sources: Santarelli et al.[25], Nehrir et al.[23], and Mendonça et al.[26].

Nowadays, SOFCs are used in some parts of the world to produce energy for residential buildings, using the electricity created by transferring electrons, and hot exhaust gases to power thermal consumers, such as heating.

1.3.3 Polarization Curve

The voltage produced by the fuel cell is not constant but varies depending on the operating conditions. As will be discussed later in Chapter 3, the maximum ideal voltage that the fuel cell can provide is called the open circuit voltage (OCV). This is the fuel cell voltage when no electrical loads are applied under standard temperature and pressure conditions. However, electrical loads are applied to the circuit during its use, such as an electric motor, which requires a certain current. As current production increases, the voltage decreases at different rates depending on the type of fuel cell. For PEMFCs, there is an initial rapid reduction in voltage and then a linear decrease. In the case of high-temperature fuel cells, the initial jump is less significant, and then a linear region occurs. In both cases, there is again a steep potential drop for high currents.

These potential drops are due to irreversible phenomena that are triggered at different current densities during the different operating conditions of the fuel cell. Among these, four main ones can be identified:

- Activation losses: An energy barrier must be overcome to start a chemical reaction. This can be done by increasing the temperature (in the case of SOFC), inserting a catalyst (such as platinum in PEMFC) or increasing the reaction surface. Despite this, the activation energy causes a slowdown of the reaction and, therefore, a highly nonlinear potential drop for low current densities.
- Fuel crossover and internal currents depend on the unwanted fuel passage inside the membrane, reducing the voltage.
- Ohmic losses: these losses are proportional to the current supplied by the fuel cell, as there is a certain resistance to the passage of both the electrons in the electrodes and the positive ions in the electrolyte.
- Mass transport or concentration losses: these are due to high consumption of the reagents and, therefore, to the decrease in their concentration at the electrodes due to high current densities.

Figure 1.8 shows the different contributions that make up the losses of the polarization curve, neglecting the voltage drop due to the fuel crossover. The polarization curve represents the fulcrum of fuel cell modelling.

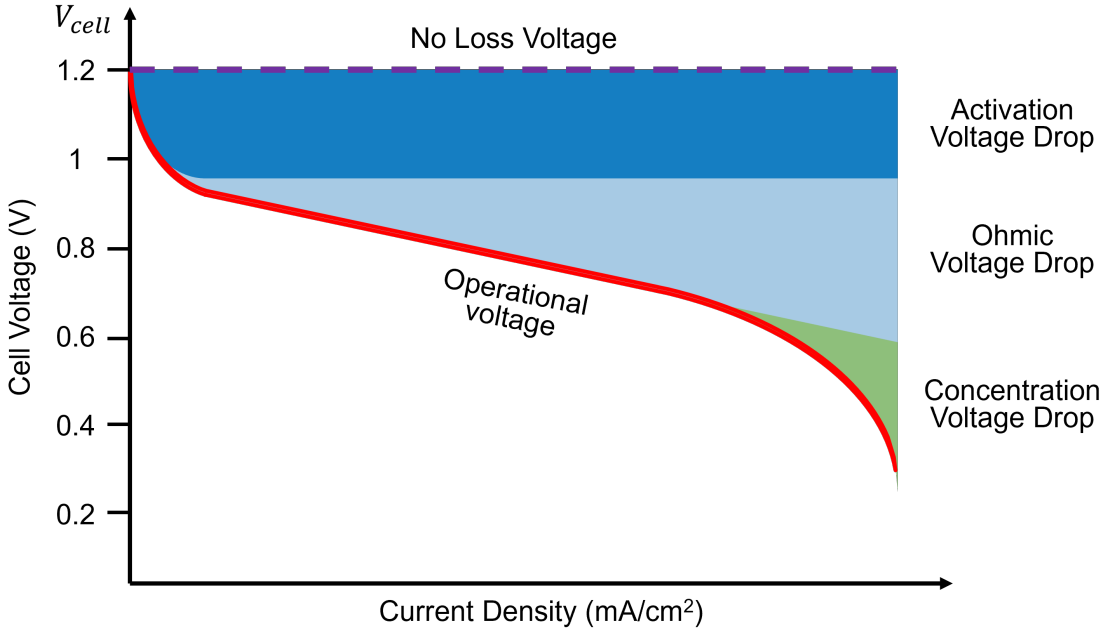

Figure 1.8: Polarization curve (red) with voltage drops. Adapted from [19, 22]

1.4 Scope and Objectives of the Thesis

This thesis aims to create a simulation model of a fuel cell stack for aircraft integration analysis in the early phases of the design process. It is essential to define a model that can be used to integrate a fuel cell stack in an electrical power architecture of the future aircraft and provide valuable data to compare the performances of various configurations.

The work has the following objectives:

1. literature review on fuel cell sizing, simulation models for PEMFC and SOFC, and their application in the aviation framework;
2. development of a dynamic simulation model of the two fuel cell technologies model using the Modelica software. The model must be integrated into an aircraft-level analysis, providing information on the fuel cell's electrical and thermal power and reagents' use;
3. validation of the model with actual fuel cell;
4. development of a simplified Balance of Plant to analyze the system integration in realistic case studies;
5. define and perform case studies to analyze the integration challenges of the fuel cell within an aircraft context (e.g., mission profile, hydrogen supply).

In this chapter, some valuable concepts have been explained to help understand the rest of the thesis, such as the difference between fuel cells and the reason for this work. Chapter 2 shows the literature review and research carried out in recent years regarding the modelling of fuel cells and their application in aviation. Chapter 3 explains the mathematical approach followed to create the fuel cell model, starting from the thermodynamics of this device, describing the contributions that determine the voltage of the fuel cell, illustrating the chosen mathematical model and its implementation with a numerical language, until the validation of the model with actual fuel cells. Chapter 4 reports the definition of the case studies and the analysis of the results of the simulations carried out with commercial software. Finally, Chapter 5 reports a critical analysis of the work carried out and the next steps for improving this model.

Chapter 2

Literature Review

Numerical models are used in the preliminary stages of designing innovative fuel cell systems because of their ease of use, and low cost compared to making real models and testing under actual operating conditions [27]. To define a mathematical model, it is essential to follow very specific steps. The phenomenon is first observed, and then an attempt is made to describe it with mathematical equations. These equations must first be adapted to experimental data and then validated under different operating conditions, comparing them with further experimental data. If the validation is successful, the model can be used; otherwise, it is necessary to reconsider the equations that make up the model, as illustrated in the process in Figure 2.1.

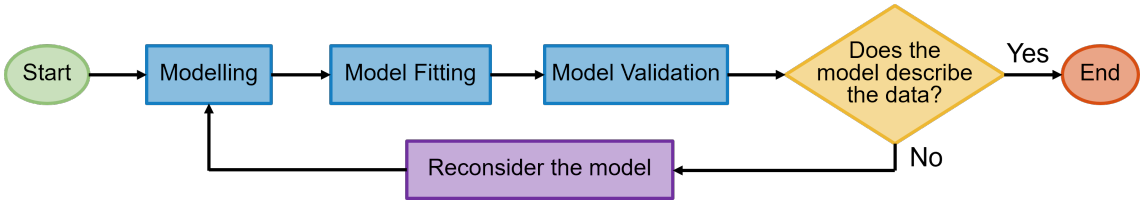

Figure 2.1: Approach for developing a mathematical model. Adapted from [28]

This literature review aims to show how the numerical simulation problem of two different types of fuel cells (PEMFC and SOFC) has been addressed over the years and how to use these models in the preliminary design phases of aircraft design. Extensive reviews of the models and issues related to fuel cells were carried out by Rossetti [29] and Mendonça et al. [26].

This chapter starts by reviewing mathematical approaches to models of PEMFC and SOFC, then shows the application to aviation case studies using PEMFC and SOFC models. Finally, the model chosen as a starting point for this thesis and what this work aims to add to research on the application of fuel cells to aviation is introduced.

2.1 Fuel Cell Mathematical Modelling

There are many approaches to modelling the behaviour and performance of fuel cells. It all starts with defining the purpose of the model, which depends on the level of accuracy of the equations used and the spatial dimensions involved. Among the characteristics of the models analyzed in this chapter is the number of spatial dimensions of the model, along which the state variables can vary. For example, in 3D models, partial differential equations are written on three spatial dimensions and integrated into a three-dimensional domain representing the cell or part of it.

Similar methodologies exist in 1D and 2D models but using equations with spatial derivatives along one or two spatial axes. In the case of 0D models, the equations do not have spatial derivatives but are only algebraic equations. Another feature of the models considered is their ability to represent transients when time-dependent differential equations are present, in the case of dynamic models.

The different fuel cell models reviewed are summarized in Table 2.1 (ordered by years of publication), which shows the type of fuel cell distinguished between PEMFC (P) and SOFC (S), the size of the mathematical model, the source of experimental data used to the validation of the models, and the focus of the research. This table shows many articles use Ticianelli et al. [30] data to validate their models. In the next sections, the PEMFC models will be reviewed in detail first and then the SOFC models.

Ref.	**Fuel Cell**		**Model Dim.**	**Validation with Exp. Data**	**Research focus**
	P	**S**			
[31]	X		1D	Ballard Technologies Corporation (1988)	Membrane humidification requirements
[32]	X		1D	[30]	Internal resistances of the cathode and membrane
[33]	X		1D	Prototech electrodes	Water transport influence on performances
[34]	X		1D	[30]	Current density limitation
[35]	X		2D	Nafion 117 cell	Effect of water on current density
[36]	X		3D	[37, 38]	Three-dimensional effects in membrane mass transport
[39]	X		1D	[30]	Temperature and water distribution
[40]	X		3D	[30]	Transport phenomena in membrane
[41]	X		0D	PEMFC Test station	Simulation study and control analysis
[42]	X	X	0D	NedStack PS6 Hpower EPAC-500	Use of data from the FC datasheet
[43]		X	0D	Tubular SOFC by NanoDynamics	Real-time simulation with equivalent circuit
[44]	X		1D	-	Multiple FC effect using Modelica
[45]		X	1D	Forschungszentrum Jülich, Germany	Flexible tool for integration studies
[46]		X	0D	[43]	Model with a single transfer function
[47]		X	2D	Rolls-Royce Fuel Cell System Ltd. Data	Reactants composition and temperature relationship
[48]		X	3D	Previous studies	Dynamic response of different parameter
[49]	X		0D-1D	-	PEMFC controllability
[50]		X	2D	EIS analysis on real fuel cell	Study on the composition of the membrane

Table 2.1: Summary of models developed for PEMFC and SOFC, sorted by year of publication.

2.2 Proton Exchange Membrane Fuel Cell Models

Many researchers have studied several effects and elements that compose a PEMFC model. Bernardi [31] has started with creating a one-dimensional model of the solid polymer electrolyte derived from

the basic equation of gas transportation. From this study, the researcher has identified the humidification requirements for the membrane. Later Bernardi et al. [32] created a mathematical model for the oxygen electrode of a PEMFC. Finally, a completed model is presented in [34] to investigate the limit of cell performance and the transport of species in the complex multi-phase network of the cell. This investigation showed no need for external water requirements because the water produced by the reaction is enough to satisfy the water demand.

Springer et al. [33] presented a one-dimensional, steady-state, isothermal mathematical model for a PEMFC, that includes transport phenomena due to diffusivities in the membrane. They validated and verified the model with experimental data. Bussel et al. [35] published a two-dimensional dynamic model to study the water management in each fuel cell membrane. They showed that variations in local humidity cause a strong change in current density along the gas channel.

At the beginning of the new millennium, researchers were led to increase the complexity of the fuel cells model to study their deeper behaviours, such as Dutta et al. [36, 51] who presented three-dimensional models of the fuel cell, by solving complete Navier-Stokes equations with a multispecies mixture. Berning et al. [40] have developed a three-dimensional, non-isothermal PEMFC model that can provide information about transport phenomena in the membrane. This model has considerable potential for parametric studies of fuel cells.

Complex models developed in the early 2000s can show detailed phenomena inside the fuel cell, such as temperature gradient, mass transport, velocity and pressure distribution, but they require great computation effort. To apply this model to complex systems architecture in aircraft or vehicle integration studies, it is necessary to simplify the models to improve the computational speed of great models. A first step in that direction is made by Rowe et al. [39], who presented a one-dimensional, non-isothermal model of a PEMFC. With this model, they can study the effect on performance due to variations in design and operating conditions. The model's objective was to show the temperature and water distribution inside the cell. A mathematical model for simulation study and control analysis, validated with a testbed, of a PEMFC is described in Thanapalan et al. [41] paper. A zero-dimensional thermodynamically consistent electrochemical model is presented by Kravos et al. [49] to investigate PEMFC performance and controllability. To this model, the authors also integrated equations to describe the transport of gaseous species, making it a quasi-one-dimensional electrochemical model. The resulting model shows strong prediction and generalization capabilities.

New models and libraries of PEMFC have been introduced with the development of commercial model-based design software. *FuelCellLib* is a free Modelica library that was released in 2005 and then updated by Rubio Gonzalez et al. in 2010 [44]. The authors relied on physical and chemical principles to formulate a one-dimensional dynamic model of PEMFC, leaving freedom for the user to choose whether to consider certain phenomena: double-layer effect, the influence of the pore size in the Knudsen diffusion, the effect of electro-osmotic drag in the electrolyte, and the dependence of the electrolyte conductivity with the water load. Models implemented in MathWorks®' more popular Simulink® platform were also not slow to arrive. Sumeshan et al. [52] show how they created a robust model with Simulink® blocks.

MathWorks® provides three different possibilities for simulating a fuel cell in its software, shown in Figure 2.2 and explained below.

The first and simplest (Figure 2.2a) is the block from the Simscape™ Electrical library called *Fuel Cell*, which has two levels of accuracy: simplified and detailed. The simplified model calculates the main parameters in nominal temperature and pressure conditions, while the detailed model considers the possibility of varying the pressure and flow rate of the reagents, as well as calculating the heat released by the cell. This block is compatible with the new Simscape libraries but does not provide information on fuel cell products.

The second block (Figure 2.2b), called *Fuel Cell Stack*, uses the mathematical model of Soule-

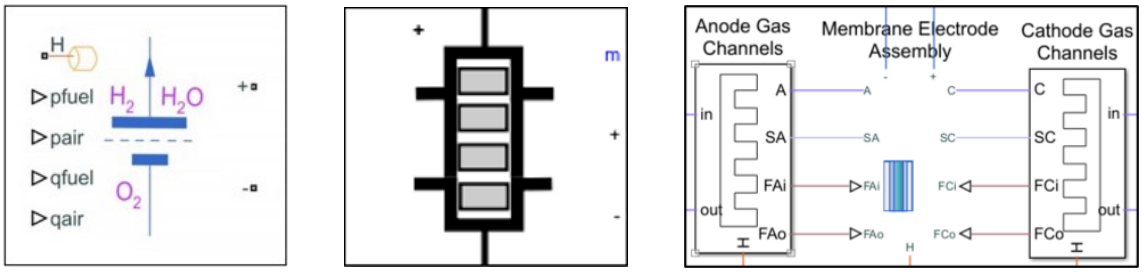

(a) Simscape^{TM} Electrical Fuel Cell block.

(b) Simscape^{TM} Electrical Fuel Cell Stack block.

(c) PEMFC system modelled with Simscape^{TM} libraries.

Figure 2.2: Fuel cell model implemented in Simulink®. Source: MathWorks

man et al. [42], who has developed two models, with similar levels of accuracy to the previous block, of fuel cells based on the available information of the stack datasheet, to facilitate the parameter search. This generic model (for PEMFC or SOFC) can be used in electrical simulation software and can represent the operating parameters of the fuel cell with little error. The model does not consider the effect of the temperature and humidity of the membrane on the stack resistance; on the other hand, it considers dynamic effects in the transient. The problem with this block is that it was created with old versions of Simscape, which prevents its use with the latest libraries.

Finally, MathWorks® has created a very detailed model (Figure 2.2c) of the Balance of Plant of a PEMFC using their Simscape^{TM} library [53]. In this model, they used predefined physical blocks to describe the BoP and a customized block (Membrane Electrode Assembly - MEA) to show the behaviour of the membrane, with the equation derived from the book of Spiegel [28].

Finally, many researchers have presented the challenge of obtaining the parameters that characterize the equations of their models. There may be several ways, including using experimental data to derive the parameters or through the use of more sophisticated and innovative techniques, as reported by Rossetti [29] in her review of the current strategies to modelling fuel cells.

This type of fuel cell is also widely studied at an industrial level for real applications; despite this, SOFCs have limitations. For this reason, mathematical models that describe the behaviour of another type of fuel cell are now shown.

2.3 Solide Oxide Fuel Cell Models

Interest in Solid Oxide Fuel Cells has grown in the new millennium, leading to the development of new simulation models of these devices' performance. However, the first one-dimensional and three-dimensional models date back to the early 1990s, as reported in the review of Beale et al. [54]. This review also includes many other models developed over the past 30 years to study the behaviour of the different elements that make up SOFCs.

Gebregergis et al. [43] have realized an efficient lamped-parameter model to allow the real-time simulation and control of a SOFC. They made an equivalent resistor-capacitor (RC) circuit where the capacitance can vary to give the actual dynamic response of the SOFC. Costamagna et al. [47] presented a steady-state two-dimensional model validated with experimental data, which confirms the direct proportionality relationship between the partial pressures of hydrogen and oxygen and the current density. A dynamic three-dimensional model is presented by Ho [48], who analyzed the transient of the temperature, the current density, the activation overpotential and the hydrogen pressure in response to a step input. Bianchi et al. [50] have validated a steady-state two-dimensional model with experimental data. They have based the electrochemical kinetics model on

a semi-empirical relation by fitting experimental results obtained by Electrochemical Impedance Spectroscopy (EIS) analysis and characteristic curves.

These models are solved using commercial CFD simulation or Model-Based Design (MBD) software. An example is the work of Andersson et al. [45], who created a one-dimensional model of a SOFC by integrating the electrolyte model and the fuel flow model with the Modelica programming language. Lakshmi et al. [46] used a phenomenological approach to model a single SOFC with a transfer function that allows the partial pressures of hydrogen, oxygen and water to be calculated.

The models described help study the internal behaviours of SOFCs but can also be used to study the application of SOFC systems, such as power generation in aircraft, with the necessary simplifications to improve computational efficiency.

2.4 Aviation Application of Fuel Cell Models

The application of fuel cells in the aeronautical sector is growing, as explained in the introductory chapter. To study the use of these complex devices, simulation models must be used to analyze fuel cell integration in aeronautical systems, as summarized in Table 2.2. The table shows the type of fuel cell distinguished between PEMFC (P) and SOFC (S), the fuel cell stack size, the source of experimental data used to validate the models, the fuel considered, and the case study.

In the following sections, the aviation application of PEMFC models is reviewed in detail first, followed by the application of SOFC models.

2.5 Aviation Application of PEMFC Models

In aviation, fuel cell simulation models have been used in recent years to study the performance of onboard system architectures powered by hydrogen fuel cell stacks. Inserting a new power source requires a new awareness and knowledge of the behaviour of each part of the new system architecture. Simpler and computationally faster models are often used, such as the zero-dimensional electrochemical model of Vidović et al. [20], that include the behaviour of a compressor and a humidifier to figure out the overall system efficiency. Therefore, studies using PEMFCs as primary or secondary power sources in aircraft of different sizes are shown in this section.

The use of PEMFC in aviation began with replacing individual electrical components, such as the Auxiliary Power Unit (APU) or power generators, due to the reduced power a single stack can provide with current technologies. Pratt et al. [57] studied whether or not the impact of a fuel cell-based electric power system is beneficial to an aircraft: with early 2000s technologies, there was no significant increase in performance, but through reuse of produced water, the benefits could be increased. They also claimed that using the fuel cell at full load for the entire flight duration increased performance. Finally, they studied how the location of the fuel cell, relative to the electrical load, could affect the overall mass of the system. In terms of efficiency, another study conducted by Schröder et al. [61] confirms the possibility of using PEMFC as auxiliary electrical power in commercial aircraft, replacing engine-driven generators and APU. They have developed a one-dimensional low computational cost model for system-level optimization that considers water management effects and is validated with a broad range of operation conditions.

As technologies based on increasingly high-performance PEMFCs develop, configurations for using fuel cells as primary electrical generation for all-electric aircraft have been investigated. Kadyk et al. [58] reiterate the importance of analyzing the system as a whole of all components, considering the presence of hydrogen tanks, in their cost-benefit analysis of a fuel cell system for the primary energy supply of a commercial aircraft. Subsequently, the same authors presented a methodology to guide the design of fuel cell systems by analyzing existing flight data to find a representative average mission profile [67]. Hartmann et al. [15] focused on using PEMFC as a

Ref.	Fuel Cell Type		Power (kW)	Validation with Exp. Data	Fuel		Case study
	P	S			H2	Other	
[55]		X	300	-		Reformed fuel	APU replacement in short-range aircraft
[56]		X	50	-	X		SOFC/Gas turbine system for high altitude aircraft
[25]		X	20	-		Natural gas	SOFC as source of electric and thermal power
[57]	X		12	HyPM 12 PEMFC	X		Impact of fuel cell-based electric power system
[58]	X		27600	[59]	X		Fuel cel as primary energy supply
[60]		X	-	NASA data	X		SOFC/GT/Battery architecture
[61]	X		845	[62]	X		APU replacement
[20]	X		1.2	Nexa 1200	X		BoP modelling
[15]	X		4100	[61, 63]	X		Cryogenic hydrogen feds fuel cell primary power source system in regional aircraft
[64]		X	120	-		Hydrocarbon	SOFC /PEMFC comparison
[65]		X	6	[66]		Ammonia fuel	SOFC/ICE hybrid power systems

Table 2.2: Application of PEMFC and SOFC models to aeronautical case studies, sorted by year of publication.

power source for regional aircraft, taking advantage of hydrogen stored at cryogenic temperature to cool all electrical components and then power the fuel cell stack.

Different approaches can be used to analyze complex electrical power systems in new-generation aircraft. However, PEMFCs present challenges during flight, such as membrane water distribution, as seen in the introductory chapter of the thesis. For this reason, other fuel cell types are also considered.

2.6 Aviation Application of SOFC Models

The complexities of an aircraft electrical system powered by fuel cells differ depending on whether PEMFC or SOFC technology is used, as explained in the introductory Chapter. Many studies have tried to find a solution to this problem by using the SOFC system as a primary or auxiliary source of electric power. In addition, the great flexibility of this type of cell in using fuels other than hydrogen has encouraged its study to improve propulsion efficiency compared to jet engines.

Using current fuels, correctly transformed inside a reformer, can be the first application of SOFC in the aeronautical sector to avoid excessively modifying aircraft configuration due to bulky hydrogen tanks. Gummalla et al. [55] have studied the benefits of using SOFC instead of an APU for future short-range commercial aircraft, recommending a limit for the power-to-weight ratio of

0.07 kW/kg above which there may be a benefit in the use of this technology. Other uses of SOFC as APUs are reviewed by Fernandes et al. [68]. Also, using exhaust gases at high temperatures is fundamental to increase the efficiency of SOFCs, as in the study by Santarelli et al. [25], where different SOFC systems powered by natural gas were studied as a source of electrical and thermal power.

Many configurations and fuels have been studied to use SOFC as a primary energy source in aviation, as reviewed by Li et al. [65] in various hybrid systems with SOFC and Internal Combustion Engine (ICE). Himansu et al. [56] have studied the performances of a SOFC/Gas turbine system, fed with cryogenic hydrogen, that provides primary and secondary electrical power to a high altitude (21 km) aircraft. They found that missions lasting 10 to 20 days are highly favoured for increased efficiency. One of the disadvantages of using this fuel cell-based technology is the low power density that can be achieved due to the heavy BoP. SOFC - Gas turbine - battery hybrid system is studied by Collins et al. [60] for medium and long-range aircraft, fed with liquid hydrogen. The authors suggest this technology could play a role if combined with superconducting motors, reaching a power density of 0.9 kW/kg. Finally, a 120 kW SOFC system for small aircraft is studied by Hawa et al. [64]. This paper compares a SOFC generator fed with low sulphur liquid hydrocarbon to a PEMFC system fueled with hydrogen, and it also identifies some key points for the scalability of this type of system.

The great flexibility in using different fuels makes this type of cell promising for the short and long term, although it maintains various challenges related to the system's weight.

2.7 Summary

An in-depth study of all the elements and possible architectures is necessary to create innovative and complex systems. Many researchers have addressed the study of fuel cell modelling, but to integrate them into the hydrogen aircraft of the future, it is essential to have an overall vision of the system architecture [18], of all the components of the BoP, of the tanks [69], of the control strategy [70] and safety - such as PEMFC fault detection model studied by Najafi et al. [71].

This thesis aims to create a scalable hydrogen fuel cell model that can be inserted into a more extensive aircraft architecture in an MBD simulation environment. This model does not aim to investigate the individual elements or intrinsic phenomena of the cell, which can be studied through more detailed and multidimensional models found in literature, but rather calculates the electrical and thermal power performance provided by the fuel cell and required by the Balance of Plant. For this reason, an equivalent electrical circuit is used to model the behavior of a fuel cell so that it can be connected to a load. Many previously mentioned models extensively use this technique, summarized by Runtz et al. [72]. Each circuit includes a voltage source, defined by the thermodynamics of the cell, resistors, which represent the voltage losses within the cell, and capacitors, which model the dynamic effects during transients. Models using equivalent circuits are easily implemented within software such as Simulink® or Modelica.

Among the various models studied and presented in this chapter, the model of Souleman et al. [42] is chosen as the core of this thesis. This model can represent the behaviour of different types of fuel cells with good approximation using only the data in the manufacturer's datasheets. This choice is dictated by the need to use this model to study the behaviour of fuel cell stacks within aeronautical electrical systems, varying the power. This thesis analyzes the model's details, reviewing its critical issues and adding new mathematical models absent in the original study. Furthermore, an acausal interface is created to connect this model more easily with other components of the Balance of Plant. In fact, among the revised models, no model can be easily shared via OpenSource code, which can interface with other components. The models implemented in Matlab® & Simulink® are closed within that development environment, while the models devel-

oped with Modelica do not have the possibility of interfacing with other components of the BoP. Therefore, this work is focused on creating a model that can be used to study innovative electrical systems.

Chapter 3

Modelling Approach

The mathematical and numerical modelling of fuel cells is essential for studying their behaviour in real applications. This chapter addresses the mathematical models necessary to describe the behaviour of fuel cells as the load required and the fluids supplied vary. Initially, the thermodynamics and the main equations that govern the polarization curve of the fuel cells are studied. Subsequently, the mathematical model chosen for implementation in numerical software and the reasons for this choice are described. Finally, an overview of the implementation of the model with Modelica and some considerations on its validation are presented.

3.1 Fuel Cell Thermodynamics

Fuel cells are devices used to generate electrical energy to feed electrical systems. A fuel cell converts the internal energy (U) of the reactants, such as hydrogen or oxygen, into electrical energy stored in the electrical field generated by electrical charges. To study the thermodynamics of fuel cells the book by O'Hayre et al. [73] is followed.

The first law of thermodynamics describes this conversion and says that energy can never be created or destroyed but can be transformed from one form to another. So, the total energy of the thermodynamic universe can never change, but the energy can be exchanged between the parts of the universe, from a system to its surroundings.

There are two ways to transfer energy between these two components of the thermodynamic universe: heat (Q) or work (W). The variation in the internal energy (dU) has to be the difference between the heat transferred to the system (dQ) and the work done by the system (dW), considered as positive the work done by the system on the surroundings. It can be assumed that only mechanical work is done by a system, i.e., the expansion of a system (dV) against a pressure (p).

$$dU = dQ - dW = dQ - pdV \tag{3.1}$$

The second law of thermodynamics defines entropy the number of possible states of configuring a system. Due to the difficulty of measuring the absolute entropy of systems, the law defines the system's entropy change (dS) related to the reversible transfer of heat (dQ_{rev}) at a constant temperature (T).

$$dS = \frac{dQ_{rev}}{T} \tag{3.2}$$

Four thermodynamic potentials are defined to study energy transfer between systems, detailed in O'Hayre et al. [73] book.

The first one is the internal energy of the system, which can be rewritten as:

$$dU = TdS - pdV \tag{3.3}$$

This equation shows that the internal energy is a function of entropy and volume, but these two parameters are difficult to measure, so other thermodynamic potentials are developed.

The Gibbs free energy (G) is a different description of the thermodynamic system that depends on temperature and pressure.

$$dG = -SdT + Vdp \tag{3.4}$$

In addition, enthalpy (H) is defined as a function of entropy and pressure.

$$dH = TdS + Vdp \tag{3.5}$$

Ultimately, the fourth thermodynamic potential defined as the Helmholtz free energy is not considered in this study.

Thermodynamic potentials and extrinsic quantities, such as entropy, can be written as molar quantities as they depend on the scale of the system. The energy per mole changes (Δ) due to a reaction are:

$$\Delta\hat{g}_{rxn}, \Delta\hat{s}_{rxn}, \Delta\hat{h}_{rxn}$$

Sometimes, these values are followed by a superscript zero, which means the standard-state thermodynamic conditions. Under this set of reference conditions, the values of thermodynamic quantities are given.

$$\Delta\hat{g}^0, \Delta\hat{s}^0, \Delta\hat{h}^0$$

In a fuel cell, the amount of heat energy that can be extracted from a fuel is determined by the fuel's reaction enthalpy, for a constant-pressure process. The heat evolved by a reaction is due to changes in the system's internal energy, i.e. the reconfiguration of chemical bonds and the energy used for work.

$$dH = TdS = dU + dW \tag{3.6}$$

The reaction enthalpy ($\Delta\hat{h}^0_{rxn}$) for a general reaction:

$$aA + bB \rightarrow mM + nN \tag{3.7}$$

Is calculated from the difference between the molar weighted reactant and product formation enthalpies ($\Delta\hat{h}^0_f$)[1]:

$$\Delta\hat{h}^0_{rxn} = \Big[m\Delta\hat{h}^0_f(M) + n\Delta\hat{h}^0_f(N)\Big] - \Big[a\Delta\hat{h}^0_f(A) + b\Delta\hat{h}^0_f(B)\Big] \tag{3.8}$$

An analogous expression can be written to calculate the standard-state entropy of a reaction ($\Delta\hat{s}^0_{rxn}$):

$$\Delta\hat{s}^0_{rxn} = \big[m\hat{s}^0(M) + n\hat{s}^0(N)\big] - \big[a\hat{s}^0(A) + b\hat{s}^0(B)\big] \tag{3.9}$$

Obtaining Gibbs free energy is necessary to calculate the work potential provided by the system. $\Delta\hat{g}_{rxn}$ value is calculated remembering the definition of this potential as a function of $\Delta\hat{h}_{rxn}$ and $\Delta\hat{s}_{rxn}$ values, that are already calculated. The following equations are obtained differentiating the definition of Gibbs free energy, considering an isothermal process, and writing the equation in terms of molar quantities:

$$G = H - TS \tag{3.10}$$

$$dG = dH - TdS - SdT \tag{3.11}$$

$$\Delta\hat{g}_{rxn} = \Delta\hat{h}_{rxn} - T\Delta\hat{s}_{rxn} \tag{3.12}$$

[1] A standard-state formation enthalpy tells how much enthalpy is required to form 1 mol of chemical species i at standard temperature and pressure (STP) from the reference species.

The electrical work is the involved potential in a fuel cell, so the Gibbs free energy can be redefined considering the work term in dU as composed of mechanical and electrical work, in a constant-pressure and constant-temperature process - an assumption valid in fuel cells operating at constant pressure and temperature.

$$\begin{aligned} dG &= dU - TdS - \cancel{SdT} + pdV + \cancel{VdP} \\ &= (TdS - dW) - TdS + pdV \\ &= (TdS - pdV - dW_{elec}) - TdS + pdV \\ &= \cancel{TdS} - \cancel{pdV} - dW_{elec} - \cancel{TdS} + \cancel{pdV} \\ &= -dW_{elec} \end{aligned}$$

Using molar quantities, the equation can be written as:

$$W_{elec} = -\Delta\hat{g}_{rxn} \tag{3.13}$$

In a fuel cell, the value of ΔG has to be less than zero to produce a spontaneous reaction generating electrical work. The electrical work moves a charge Q through an electrical potential difference E.

$$W_{elec} = QE \tag{3.14}$$

The charge is made up of electrons and is measured in coulombs.

$$Q = zF \tag{3.15}$$

where z is the number of moving electron moles, and $F = 96485As/mol$ is Faraday's constant. The Gibbs free energy can be expressed as:

$$\Delta\hat{g}_{rxn} = -zFE \tag{3.16}$$

E is defined as the reversible voltage of a fuel cell, and E^0 is defined as the reversible voltage in the standard state.

$$E^0 = -\frac{\Delta\hat{g}^0_{rxn}}{zF} \tag{3.17}$$

The assumption of standard conditions can limit the use of these equations to a few simple cases. For this reason, a reversible voltage of the fuel cell can be considered in different conditions from the standard conditions. The Gibbs free energy is redefined, considering only the temperature variation and the molar reaction quantities.

$$dG = -SdT + \cancel{Vdp} \tag{3.18}$$

$$\left(\frac{dG}{dT}\right)_p = -S \tag{3.19}$$

$$\left(\frac{\Delta\hat{g}_{rxn}}{dT}\right)_p = -\Delta\hat{s}_{rxn} \tag{3.20}$$

Substituting equation 3.16:

$$\left(\frac{dE}{dT}\right)_p = \frac{\Delta\hat{s}_{rxn}}{zF} \tag{3.21}$$

E_T is defined as the reversible cell voltage at the temperature T and constant pressure.

$$E_T = E^0 + \frac{\Delta\hat{s}_{rxn}}{zF}(T - T_0) \tag{3.22}$$

The influence on the Gibbs free energy of the variation in pressures or concentrations of the reactant and product species of the following chemical reaction, placed on a molar basis for species A:

$$1A + bB \rightarrow mM + nN \tag{3.23}$$

This is shown by the *van't Hoff* isotherm equation:

$$\Delta\hat{g}_{rxn} = \Delta\hat{g}^0_{rxn} + RT \ln \frac{p_M^m p_N^n}{p_A^1 p_B^b} \tag{3.24}$$

Where p_i is the partial pressure of species i, expressed in atm, and $R = 8.3145$ J/(mol K) is the gas constant. As previously shown, the Gibbs free energy is related to the reversible potential of the cell:

$$E = E^0 - \frac{RT}{zF} \ln \frac{p_M^m p_N^n}{p_A^1 p_B^b} \tag{3.25}$$

$$= E^0 + \frac{RT}{zF} \ln \frac{p_A^1 p_B^b}{p_M^m p_N^n} \tag{3.26}$$

This is Nernst's equation, and the equations can be combined to obtain a complete expression of the reversible fuel cell voltage:

$$E = E^0 + \frac{\Delta\hat{s}_{rxn}}{z}(T - T_0) + \frac{RT}{zF} \ln \frac{p_A^1 p_B^b}{p_M^m p_N^n} \tag{3.27}$$

These thermodynamic and electrochemical concepts can be applied to particular types of fuel cells.

3.1.1 Thermodynamic of a PEMFC

As explained in Section 1.3.1, the Proton Exchange Membrane Fuel Cell is a low-temperature fuel cell. The operating temperature is around 100°C, depending on the manufacturers. The boiling temperature of water is a crucial point in defining the parameters that model this fuel cell, because many physics parameters depend on the physical state of the water produced in the reaction:

$$H_2O + \frac{1}{2}O_2 \rightarrow H_2O \tag{3.28}$$

Various parameters are now calculated for gaseous and liquid reaction products, using values from the tables in Appendix B of the book *Fuel cell fundamentals*[73], shown in Table 3.1.

Chemical Species	$\Delta\hat{h}^0_f$ (kJ/mol)	$\hat{s}^0$ [J/(molK)]
$H_{2(g)}$	0	130.68
$O_{2(g)}$	0	205.00
$H_2O_{(g)}$	-241.83	188.84
$H_2O_{(g)}$	-285.83	69.95

Table 3.1: Standard enthalpy of formation and standard entropy of the species involved in the chemical reaction of a PEMFC. Extracted from [73].

Starting from a reaction with water vapour as a product:

$$H_{2(g)} + \frac{1}{2}O_{2(g)} \rightarrow H_2O_{(g)} \tag{3.29}$$

The enthalpy of the reaction, the standard-state entropy of the reaction, the Gibbs free energy, and the reversable voltage are calculated.

$$\begin{aligned}
\Delta\hat{h}^0_{rxn} &= \left[\Delta\hat{h}^0_f(H_2O_{(g)})\right] - \left[\Delta\hat{h}^0_f(H_2) + \frac{1}{2}\Delta\hat{h}^0_f(O_2)\right] \\
&= [(-241.83)] - \left[(0) + \frac{1}{2}\cdot(0)\right] \\
&= -241.83 \text{ kJ/mol} \\
\Delta\hat{s}^0_{rxn} &= \left[\hat{s}^0(H_2O_{(g)})\right] - \left[\hat{s}^0(H_2) + \frac{1}{2}\hat{h}^0(O_2)\right] \\
&= [(188.84)] - \left[(130.68) + \frac{1}{2}\cdot(205.00)\right] \\
&= -44.34 \text{ J/(mol K)} \\
\Delta\hat{g}^0_{rxn}(T = 25°C) &= \Delta\hat{h}^0_{rxn} - T\Delta\hat{s}^0_{rxn} \\
&= -241.83 \text{ kJ/mol} - 298.15\text{K}\cdot(-0.04434 \text{ kJ/(mol K)}) \\
&= -228.61 \text{ kJ/mol} \\
E^0 &= -\frac{\Delta\hat{g}^0_{rxn}}{zF} \\
&= -\frac{-228.61 \text{ kJ/mol}}{2\cdot 96485 \text{ As/mol}} \\
&= 1.184 \text{ V}
\end{aligned}$$

The reversible reaction potential is then obtained by substituting the values obtained into the equation 3.27.

$$E = 1.184 \text{ V} + \frac{-44.34 \text{ J/(mol K)}}{zF}(T - 298.15\text{K}) + \frac{RT}{zF}\ln\left(\frac{p_{H_2}p^{0.5}_{O_2}}{p_{H_2O}}\right) \tag{3.30}$$

This equation considers the reaction product as gaseous so that it can be used for operating temperatures above 100°C.

The following chemical reaction is now considered:

$$H_{2(g)} + \frac{1}{2}O_{2(g)} \rightarrow H_2O_{(liq)} \tag{3.31}$$

The enthalpy of the reaction, the standard-state entropy of the reaction, the Gibbs free energy,

and the reversible voltage are calculated.

$$\begin{aligned}
\Delta\hat{h}^0_{rxn} &= \left[\Delta\hat{h}^0_f(H_2O_{(liq)})\right] - \left[\Delta\hat{h}^0_f(H_2) + \frac{1}{2}\Delta\hat{h}^0_f(O_2)\right] \\
&= [(-285.83)] - \left[(0) + \frac{1}{2}\cdot(0)\right] \\
&= -285.83 \text{ kJ/mol} \\
\Delta\hat{s}^0_{rxn} &= \left[\hat{s}^0(H_2O_{(liq)})\right] - \left[\hat{s}^0(H_2) + \frac{1}{2}\hat{h}^0(O_2)\right] \\
&= [(69.95)] - \left[(130.68) + \frac{1}{2}\cdot(205.00)\right] \\
&= -163.23 \text{ J/(mol K)} \\
\Delta\hat{g}^0_{rxn}(T = 25^{\circ}C) &= \Delta\hat{h}^0_{rxn} - T\Delta\hat{s}^0_{rxn} \\
&= -285.83 \text{ kJ/mol} - 298.15\text{K}\cdot(-0.16323 \text{ kJ/(mol K)}) \\
&= -237.16 \text{ kJ/mol} \\
E^0 &= -\frac{\Delta\hat{g}^0_{rxn}}{zF} \\
&= -\frac{-237.16 \text{ kJ/mol}}{2\cdot 96485 \text{ As/mol}} \\
&= 1.229 \text{ V}
\end{aligned}$$

The reversible reaction potential is then calculated by substituting the values obtained into the equation 3.27.

$$E = 1.229 \text{ V} + \frac{-163.23 \text{ J/(mol K)}}{zF}(T - 298.15\text{K}) + \frac{RT}{zF}\ln\left(p_{H_2}p_{O_2}^{0.5}\right) \tag{3.32}$$

This equation considers the reaction product as gaseous so that it can be used for operating temperatures above 100°C.

A fuel cell's potential depends on the operating conditions of pressure and temperature and the amount of current required by the electrical load connected to it. For this, it is necessary to model the polarization curve (described in section 1.3.3) through current equations with the different voltage drops. In the next section, the mathematical model chosen to describe the behavior of these losses will be presented.

3.2 Matemathical Model

In the early stages of the design process, it is necessary to have a mathematical model with specific characteristics. This thesis's mathematical model is based on the detailed model of Souleman et al. [42] with some integration to increase the number of output results and to improve the capability to be integrated with other models. The chosen mathematical model and the corrections made are described, then the thermal model used is discussed.

3.2.1 Assumptions

Mathematical models are characterized by a certain level of accuracy, defined according to the purpose for which the model is used. The level of accuracy must be chosen according to the phenomena one wants to observe, those one wants to neglect, and the numerical complexity. The

starting model chosen in this work is zero-dimensional because it does not consider spatial dimensions in which fuel cell performance may vary. In addition, the authors of this model made assumptions [42], including:

- The gases are ideal[2][74].
- The fuel cell stack is fed with hydrogen and air.
- The stack has a water management system to maintain the correct humidity level inside the cell at any load.
- The stack has a cooling system which maintains the correct temperature level at the exits of the cathode and anode, equal to the stack temperature.
- Pressure drops across the flow channels, the flow of gases and water through the membrane are negligible.
- Cell voltage drops are due to reaction kinetics and charge transport since most fuel cells do not operate at high currents in the mass transport region. In particular, the concentration voltage drop due to mass transport at high current density is neglected. This is explained in Appendix A.
- The internal resistance of the cells is constant under any operating condition, neglecting the effect of temperature and humidity variations.

To make the model more realistic, in the second part of this chapter, equations modeling heat transfer will be added, which, if properly integrated with the cooling system model, can avoid the constant temperature assumption.

3.2.2 Equivalent Circuit of a Fuel Cell

The model represents a fuel cell stack by an equivalent electrical circuit shown in Figure 3.1. The circuit consists of a controlled voltage source, a resistor, an ideal diode, and a current sensor. The controlled voltage source has within it several contributions, shown in the equation:

$$E = E_{oc} - NA \ln\left(\frac{i_{fc}}{i_0}\right) \cdot \frac{1}{sT_d/3 + 1} \tag{3.33}$$

The first term on the right-hand side represents the reversible reaction potential that the fuel cell can supply, calculated considering the operating temperature and the pressure of the reagents, as shown below. A term is subtracted from this voltage which considers the contribution of the activation losses, modelled by the Tafel equation, and the Double-Layer Charge effect, modelled by a first-order transfer function.

[2]The properties of an ideal gas are:

- Molecules are considered point-like, so their volume is negligible.
- Interactions between the molecules and with the vessel walls occur through perfectly elastic collisions, with no dissipation of kinetic energy.
- There are no remote interaction forces between the gas molecules.
- The gas molecules are identical and indistinguishable from each other.
- The motion of the molecules is random and disordered in all directions but underlying deterministic laws.

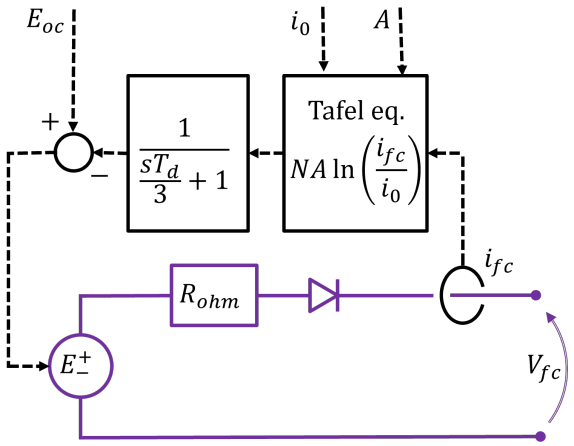

Figure 3.1: Equivalent Circuit of the fuel cell stack. Adapted from [42].

The Tafel equation describes the highly nonlinear behaviour of the polarization curve for low currents.

$$\Delta V_{act} = NA\ln\left(\frac{i_{fc}}{i_0}\right) \tag{3.34}$$

where N is the number of series cells in the stack, A is the Tafel slope (V), i_{fc} is the current provided by the fuel cell stack (A), i_0 is the exchange current (A).

The double-layer charge effect is considered in the voltage source by delaying the Tafel equation with a first-order transfer function, where T_d is the stack settling time, i.e. the time needed for the fuel cell voltage to reach a desired value. The settling time is approximately three times the time constant of the equivalent RC circuit used by Larminie et al.[22] to describe this delay effect.

$$\tau = RC = T_d/3 \tag{3.35}$$

Continuing to examine the components of the equivalent circuit, a resistor that models the losses due to the Ohmic resistance R_{ohm} (Ω) is found. Therefore, the voltage V_{fc} obtained at the ends of the fuel cell equivalent circuit is given by:

$$V_{fc} = E - R_{ohm}i_{fc} \tag{3.36}$$

Finally, an ideal diode is used to avoid negative current flow in the circuit, and a current sensor provides the current value i_{fc} (A) to the Tafel equation.

The model studied in [42] can vary inputs such as stack temperature, gas pressures, composition and flow rates.

$$\{V_{fuel}, V_{air}, P_{fuel}, P_{air}, T, x, y\}$$

These variations influence three parameters of the 3.33, which are calculated with some equations in the mathematical model. The model's authors enclose the calculation of these parameters in 3 blocks of equations, which, for simplicity, they calls Block A, Block B and Block C. The three blocks and related inputs and outputs are shown in Figure 3.2 and described in the next sections. Furthermore, the corrections to the different blocks of the model presented by Souleman et al. [42] model are described. Finally, two further blocks are shown, called Block D and Block Simplified D, which extend the model and calculate the thermal power produced by the fuel cell with two different approaches.

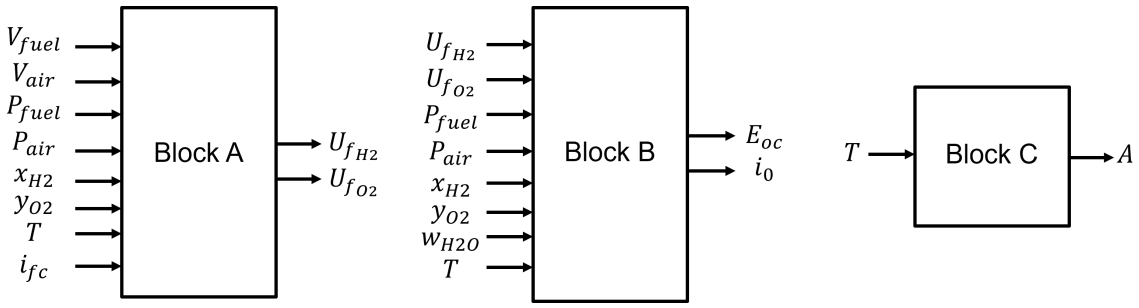

Figure 3.2: Mathematical block for the calculation of E_{oc}, i_0, and A. Adapted from [42]

3.2.3 Block A: Rates of Utilization

Block A has as input all the parameters that can be varied, and the current of the fuel cell $\{V_{fuel}, V_{air}, P_{fuel}, P_{air}, T, x, y, i_{fc}\}$, and it calculates as output the rates of utilization of hydrogen and oxygen $\{U_{f_{H_2}}, U_{f_{O_2}}\}$.

This dimensionless parameter represents the ratio between the number of moles that react in the fuel cell and the total number of moles that enter the gas channel of the anode or cathode. The following expressions are obtained:

$$U_{f_{H_2}} = \frac{n_{H_2}^{react}}{n_{H_2}^{tot}} = \frac{RTNi_{fc}}{zFP_{fuel}V_{fuel}x} \tag{3.37}$$

$$U_{f_{O_2}} = \frac{n_{O_2}^{react}}{n_{O_2}^{tot}} = \frac{RTNi_{fc}}{2zFP_{air}V_{air}y} \tag{3.38}$$

where $R = 8.3145$ J/(mol K) is the gas constant, T is the temperature of operation (K), N is the number of series cells in the stack, i_{fc} is the current provided by the fuel cell stack (A), $z = 2$ is the number of moving electrons, $F = 96485$ As/mol is the Faraday's constant, P_{fuel} is the absolute supply pressure of fuel (Pa), P_{air} is the absolute supply pressure of air (Pa), V_{fuel} is the fuel flow rate (m^3/sec), V_{air} is the airflow rate (m^3/sec), x is the molar fraction of hydrogen in the fuel, y is the molar fraction of oxygen in the air. The utilization rate values are used in [42] to calculate the partial pressures of hydrogen, oxygen and water. As shown in the next paragraph, this formulation was modified because it was deemed incorrect, eliminating Block A from the final mathematical model.

3.2.4 Block B: Open Circuit Voltage and Exchange Current

Block B calculates the open circuit voltage and exchange current. It has as input :

$$\{U_{f_{H_2}}, U_{f_{O_2}}, P_{fuel}, P_{air}, T, x, y, w\}$$

and calculates as output $\{E_{oc}, i_0\}$. To obtain these outputs, the partial pressures of the reactants and the Nernst voltage must be calculated as intermediate steps. The authors obtains the formulation of partial pressures as:

$$P_{H_2} = (1 - U_{f_{H_2}})xP_{fuel} \tag{3.39}$$

$$P_{O_2} = (1 - U_{f_{O_2}})yP_{air} \tag{3.40}$$

$$P_{H_2O} = (w + 2yU_{f_{O_2}})P_{air} \tag{3.41}$$

However, these equations, demonstrated in [75], represent the partial pressures of hydrogen, oxygen and water after the chemical reaction. Partial pressures are used in the Nernst equation, which requires the partial pressures at the fuel cell inlet. For this reason, the original equations were modified as reported in the literature [23] and the partial pressures of hydrogen P_{H_2}, oxygen P_{O_2}, and water vapor P_{H_2O} are expressed in *Pascal* and calculated as follows:

$$P_{H_2} = xP_{fuel} \tag{3.42}$$

$$P_{O_2} = yP_{air} \tag{3.43}$$

$$P_{H_2O} = wP_{air} \tag{3.44}$$

where x is the molar mass of hydrogen in the fuel, y is the molar mass of oxygen in the air, w is the molar mass of water in the oxidant, P_{fuel} is the absolute supply pressure of fuel (Pa), and P_{air} is the absolute supply pressure of air (Pa). The partial pressures are therefore calculated without using the utilization rates obtained in Block A, which will therefore be excluded from the final mathematical model.

The Nernst voltage E_n depends on the operating temperature. If the temperature is below 100 °C, the water generated in the reaction is considered liquid, and equation 3.32 can be used.

$$E_n = 1.229 \text{ V} + (T - 298 \text{ K})\frac{-163.23 \text{ J/mol}}{zF} + \frac{RT}{zF}\ln\left(P_{H_2}P_{O_2}^{0.5}\right) \quad \text{if } T < 373K \tag{3.45}$$

On the other hand, if the operating temperature exceeds 100 °C, the water generated in the chemical reaction is considered vapor, and equation 3.30 can be used.

$$E_n = 1.184 \text{ V} + (T - 298 \text{ K})\frac{-44.34 \text{ J/mol}}{zF} + \frac{RT}{zF}\ln\left(\frac{P_{H_2}P_{O_2}^{0.5}}{P_{H_2O}}\right) \quad \text{if } T \geq 373K \tag{3.46}$$

where $z = 2$ is the number of moving electrons, $F = 96485$ As/mol is the Faraday's constant, T is the operational temperature, and $T_0 = 298$K is the reference temperature to calculate E^0. The remaining parameters of the equations 3.45 and 3.46 are calculated in 3.42, 3.43, and 3.44. The partial pressures are expressed in *bar*.

The parameters obtained can calculate the open circuit voltage and the exchange current.

$$E_{oc} = K_c \cdot E_n \tag{3.47}$$

$$i_0 = \frac{zFk(P_{H_2} + P_{O_2})\Delta v}{Rh}\exp\left(\frac{-\Delta G}{RT}\right) \tag{3.48}$$

where K_c is the voltage constant at the nominal condition of operation, $F = 96485$ As/mol is the Faraday's constant, $k = 1.38 \cdot 10^{-23}$J/K is the Boltzmann's constant, P_{H_2} is the partial pressure of hydrogen (Pa), P_{O_2} is the partial pressure of oxygen (Pa), $\Delta v = 1m^3$ is the activation barrier volume factor, $R = 8.3145$ J/(mol K) is the gas constant, $h = 6.626 \cdot 10^{-34}$Js is the Planck's constant, ΔG is the activation energy barrier (J/mol) calculated in 3.79, and T is the operational temperature (K) of the fuel cell stack. Now only the Tafel Slope remains to be calculated, the value obtained in Block C.

3.2.5 Block C: Tafel Slope

Block C calculates the Tafel slope A (V) with only the operational temperature as input:

$$A = \frac{RT}{z\alpha F} \tag{3.49}$$

where $R = 8.3145$ J/(mol K) is the gas constant, T is the temperature of operation (K), $z = 2$ is the number of moving electrons, $F = 96485$ As/mol is the Faraday's constant, and α is the *charge transfer coefficient* calculated in 3.75, i.e. the percentage of supplied electrical energy devoted to altering the rate of an electrochemical reaction [22].

The Blocks originally defined by Souleman et al. [42] have been exposed and corrected with small changes. The two blocks that make up the thermal model, which are not present in the original model, will be shown.

3.2.6 Blocks D: Thermal Model

The original model considers that there is a sufficient cooling to maintain a constant temperature inside the fuel cell. The cooling systems are part of the BoP and are chosen and sized depending on the fuel cell size. There are different cooling systems as the power of the fuel cell varies, shown in Figure 3.3 and summarized by Zhang et al.[76] and Bargal et al.[77]. Liquid cooling methods are mainly used for fuel cell stacks used in aviation, with high power released.

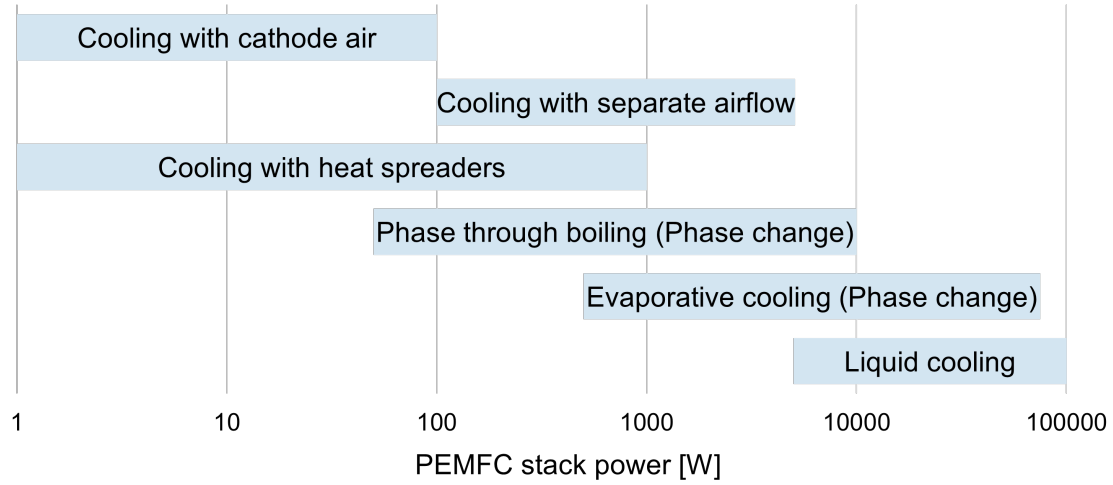

Figure 3.3: Stack cooling methods as power varies. Data from [76, 77]

These cooling systems remove the heat generated by the fuel cell, composed of the sum of various contributions. In the case of PEMFC, the heat is generated by:

- Reversible Heat (Entropic Heat): it is the difference between the total chemical energy of reactants and the maximum useful energy, as expressed by the 2nd law of thermodynamics.
- Irreversible Heat: it originates from irreversible electrochemical reactions within the fuel cell.
- Ohmic Heat: it is caused by the resistance to ion flow and electron flow through electrically conductive FC components.
- Heat from Water Vapor Condensation: it contributes less to the total heat than the other sources.

To model heat generation in a fuel cell, follow the two models presented by Spiegel [28], one simplified and one detailed. The energy balance of a fuel cell stack is defined as:

$$\sum Q_{in} - \sum Q_{out} = W_{el} + Q_{dis} + Q_c \tag{3.50}$$

Where Q_{in} is the enthalpy of the reactants (J/s), Q_{out} is the enthalpy of the products (J/s), W_{el} is the electrical power generated (W), Q_{dis} is the heat dissipated to the environment (W), and Q_c is the heat removed through the cooling system (J/s). Heat can be dissipated via exhaust fluids exiting the gas channels or dispersed into the environment by convection, but most are removed by a cooling system. To estimate the heat generated, a simplified treatment can initially be considered that examines the difference between the energy of the fuel reacting in the fuel cell and the electricity produced.

$$\frac{I_{fc}}{2F}HN = Q_{gen} + I_{fc}V_{cell}N \tag{3.51}$$

Where $F = 96485$ As/mol is the Faraday's constant, H is the energy stored in the fuel (hydrogen) (J/mol), N is the number of cells in series, Q_{gen} is the heat generated (W), and the second factor on the second member represents the electrical power supplied by the fuel cell, obtained by multiplying the voltage of the single cell, the current delivered, and the number of cells in series. This formulation is the basis of the simplified Block D and depends on the temperature of the operation. In the first case, for temperatures below 100°C, the energy of the fuel is considered equal to the high heating value ($HHV_{H_2} = 286$ kJ/mol), i.e. the energy that would be developed from the complete combustion of hydrogen, producing water in liquid form.

$$Q_{gen} = \frac{I_{fc}}{2F}H_{HHV}N - I_{fc}V_{cell}N \tag{3.52}$$

$$= \left(\frac{H_{HHV}}{2F} - V_{cell}\right) I_{fc}N \tag{3.53}$$

$$= (1.482 - V_{cell})I_{fc}N \tag{3.54}$$

In the second case, for temperatures above 100°C, the energy of the fuel is considered equal to the lower heating value ($LHV_{H_2} = 242$ kJ/mol), i.e. the energy that would be developed from the complete combustion of the hydrogen, also considering the energy of vaporization of water.

$$Q_{gen} = (1.254 - V_{cell})I_{fc}N \tag{3.55}$$

The problem of this formulation, which will be used in the final model within the simplified Block D, does not consider the enthalpies of the substances entering and leaving the fuel cell thermodynamic system. For this reason, a more accurate energy balance now needs to be defined.

$$\sum(h_i)_{in} = W_{el} + \sum(h_i)_{out} + Q_{gen} \tag{3.56}$$

The inputs of the thermodynamic system represented by the equation and shown in Figure 3.4 are the enthalpies of the fuel, the oxidant, and the water vapour present at the inlet of the fuel cell. The outputs of this energy balance are the enthalpies of the exhausted fluids, the electrical power and the heat that leaves the fuel cell by convection, radiation or by using the cooling system. The enthalpy of a gas mixture is calculated as:

$$h = \dot{m}c_pT \tag{3.57}$$

where m is the mass flow rate of the gas mixture (kg/s), c_p is the specific heat (J/(kg K)), and T is the flow temperature (°C). In the case of hydrogen, i.e. a combustible gas, the enthalpy is

$$h_{H2} = \dot{m}_{H2}(c_{p,H2}T + h^0_{HHV}) \tag{3.58}$$

where h^0_{HHV} is the higher heating value of the gas at 0°C (J/kg). This value in the case of PEMFC is obtained from the value of HHV in standard conditions of 25°C ($h^{25}_{HHV} = 141.9 \cdot 10^3\ J/(g \cdot K)$)

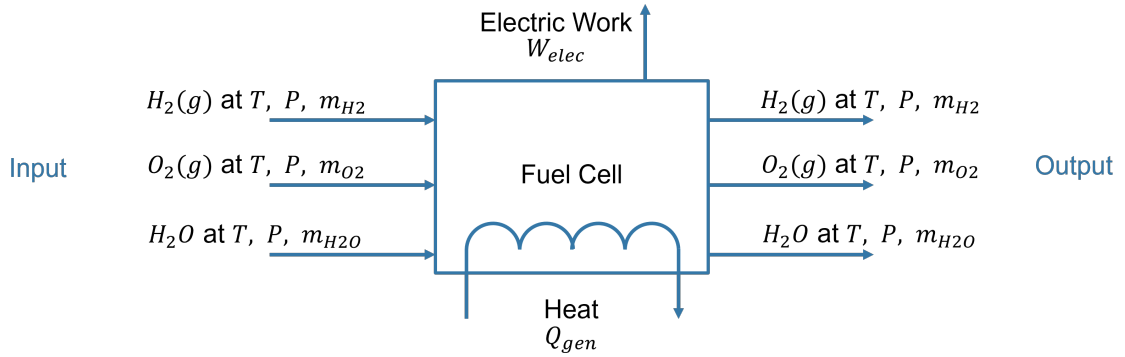

Figure 3.4: Energy balance of the thermodynamic system considered. Adapted from [28].

and converted with the equation:

$$h^0_{HHV} = h^{25}_{HHV} - \left(c_{p,H2} + \frac{1}{2}\frac{M_{O2}}{M_{H2}}c_{p,O2} - \frac{M_{H2O}}{M_{H2}}c_{p,H2O(l)}\right) \cdot 25 \tag{3.59}$$

$$= 141.9 \cdot 10^3 - \left(14.3 + 0.5\frac{31.9988}{2.01568}0.918 - \frac{18.0152}{2.01568}4.1816\right) \cdot 25 \tag{3.60}$$

$$= 142.29\dot{1}0^3 J/(g \cdot K) \tag{3.61}$$

where $c_{p,i}$ is the specific heat (J/(g K)) and M_i is the molar mass (g/mol). The enthalpy of water depends on its physical state, whether in the form of steam:

$$h_{H2O} = \dot{m}_{H2O(g)}c_{p,H2O(g)}T + h^0_{fg} \tag{3.62}$$

where $h^0_{fg} = 2259$ (J/g) is the water heat of vaporization. If in liquid form:

$$h_{H2O} = \dot{m}_{H2O(l)}c_{p,H2O(l)}T \tag{3.63}$$

This mathematical model calculates the heat generated more accurately than the previous one. Its implementation and the necessary data will be discussed in the discussion of the Modelica language code in Section 3.3. In conclusion, figure 3.5 illustrates the four blocks used in the OpenModelica implementation. Furthermore, it is necessary to obtain the parameters to populate the model equations, a process described in the following paragraphs.

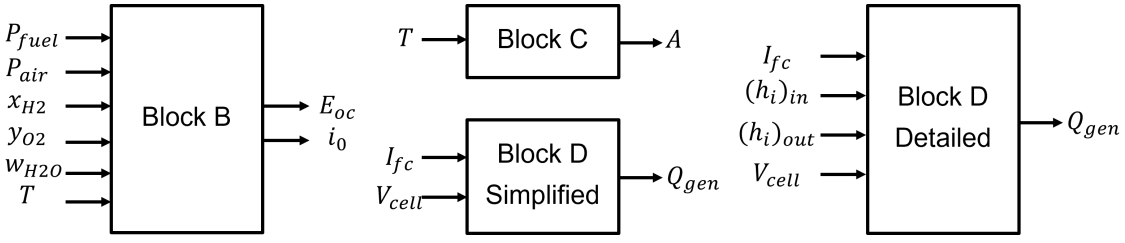

Figure 3.5: Equation blocks after original model corrections.

3.2.7 Model Parameters

The mathematical model calculates the variations to the nominal condition, described through the parameters in the manufacturer's datasheet (see Appendix C). The parameters present in the

mathematical model are:

$$\{E_{oc}, N, T_d, i_0, R_{ohm}, \alpha, \Delta G, K_c\}$$

Some values can be derived directly from the datasheet, and others require intermediate equations. Usually, the fuel cell manufacturing company shows the polarization curve (see Section 1.3.3), from which four valuable points can be extrapolated.

- Voltage at 0 A to determine the Open Circuit Voltage E_{oc}.
- Voltage at 1 A to determine V_1.
- Voltage V_{nom} and current I_{nom} at the nominal operating point.
- Voltage V_{min} and current I_{max} at the maximum operating point.

In addition to the polarization curve, a table in the datasheets provides other important information about the device, from which the following can be obtained:

- the number of cells in series N;
- the nominal LHV stack efficiency η_{nom} expressed as a ratio;
- the nominal operating temperature T_{nom} (K);
- the nominal air flow rate $V_{air(nom)}$ (l/min);
- absolute supply pressures of the fuel $P_{fuel(nom)}$ and of the air $P_{air(nom)}$ (atm);
- nominal compositions of the fuel and the air expressed as a ratio (x_{nom},y_{nom},w_{nom});
- the response time T_d (sec).

Three new parameters can be obtained by solving the equations 3.33 and 3.36 for steady state condition ($s = 0$) and in three different operation conditions: for a current of 1 A, for the nominal operating condition, and for the maximum operating condition.

$$V_1 = [V_{fc}]_{i_{fc}=1A} = E_{oc} + NA\ln(i_0) - R_{ohm} \cdot 1A \tag{3.64}$$

$$V_{nom} = [V_{fc}]_{i_{fc}=I_{nom}} = E_{oc} - NA\ln\left(\frac{I_{nom}}{i_0}\right) - R_{ohm}I_{nom} \tag{3.65}$$

$$V_{min} = [V_{fc}]_{i_{fc}=I_{max}} = E_{oc} - NA\ln\left(\frac{I_{max}}{i_0}\right) - R_{ohm}I_{max} \tag{3.66}$$

Deriving the exchange current i_0 (A) from equation 3.64.

$$i_0 = \exp\left(\frac{V_1 - E_{oc} - R_{ohm}}{NA}\right) \tag{3.67}$$

By substituting 3.67 into 3.65, the internal ohmic resistance R_{ohm} (Ω) is obtained:

$$V_{nom} = \cancel{E_{oc}} - NA\ln(I_{nom}) + V_1 - \cancel{E_{oc}} + R_{ohm} - R_{ohm}I_{nom} \tag{3.68}$$

$$V_{nom} + NA\ln(I_{nom}) - V_1 = R_{ohm}(1 - I_{nom}) \tag{3.69}$$

$$R_{ohm} = \frac{V_{nom} + NA\ln(I_{nom}) - V_1}{1 - I_{nom}} \tag{3.70}$$

By substituting 3.67 and 3.70 into 3.65:

$$V_{min} = \cancel{E_{oc}} - NA\ln(I_{max}) + V_1 - \cancel{E_{oc}} + \frac{V_{nom} + NA\ln(I_{nom}) - V_1}{1 - I_{nom}}(1 - I_{max}) \tag{3.71}$$

Collecting the NA parameter on the left side and multiplying both members by $1 - I_{nom}$:

$$NA\left[\ln(I_{max}) - \frac{1 - I_{max}}{1 - I_{nom}}\ln(I_{nom})\right] = V_1 - V_{min} + \frac{1 - I_{max}}{1 - I_{nom}}(V_{nom} - V_1) \tag{3.72}$$

$$NA\left[\ln(I_{max})(1 - I_{nom}) - (1 - I_{max})\ln(I_{nom})\right] = (V_1 - V_{min})(1 - I_{nom}) + (1 - I_{max})(V_{nom} - V_1) \tag{3.73}$$

The factor NA (V) is obtained:

$$NA = \frac{(V_1 - V_{min})(1 - I_{nom}) + (1 - I_{max})(V_{nom} - V_1)}{\ln(I_{max})(1 - I_{nom}) - (1 - I_{max})\ln(I_{nom})} \tag{3.74}$$

The following equation obtains the dimensionless α parameter, required in 3.49:

$$\alpha = \frac{NRT_{nom}}{zFNA} \tag{3.75}$$

where N is the number of cells in series, $R = 8.3145$ J/(mol K) is the gas constant, T_{nom} is the nominal operating temperature (K), $z = 2$ is the number of moving electrons, $F = 96485$ As/mol is the Faraday's constant, and NA (V) is obtained from 3.74.

The activation energy barrier ΔG (J), required in the equation 3.48, is obtained at the nominal conditions and, as in block B, it is necessary to calculate the partial pressures. In this case, Souleman et al. [42] calculate the nominal partial pressures using nominal utilization rates. As previously explained, the partial pressures of hydrogen $P_{H_2(nom)}$ and oxygen $P_{O_2(nom)}$ at nominal condition (atm) are instead calculated by multiplying the total pressure by the molar fraction of the single component, as follows:

$$P_{H_2(nom)} = x_{nom}P_{fuel(nom)} \tag{3.76}$$

$$P_{O_2(nom)} = y_{nom}P_{air(nom)} \tag{3.77}$$

where x_{nom} is the molar fraction of hydrogen in the fuel at nominal condition, y_{nom} is the molar fraction of oxygen in the air at nominal condition, $P_{fuel(nom)}$ is the absolute supply pressure of fuel at nominal conditions (atm), $P_{air(nom)}$ is the absolute supply pressure of air at nominal conditions (atm).

The parameter K_1 (A) is calculated with the partial pressures of hydrogen $P_{H_2(nom)}$ and oxygen $P_{O_2(nom)}$ at nominal condition (atm) as follows:

$$K_1 = \frac{2Fk(P_{H_2(nom)} + P_{O_2(nom)})P_{std}\Delta v}{Rh} \tag{3.78}$$

where $F = 96485$ As/mol is the Faraday's constant, $k = 1.38 \cdot 10^{-23}$J/K is the Boltzmann's constant, $P_{std} = 101325$ Pa/atm is a unit of measure conversion factor, $\Delta v = 1m^3$ is the activation barrier volume factor, $R = 8.3145$ J/(mol K) is the gas constant, and $h = 6.626 \cdot 10^{-34}$Js is the Planck's constant. Finally, the parameter K_1 is used to calculate the activation energy barrier ΔG (J/mol):

$$\Delta G = -RT_{nom}\ln\left(\frac{i_0}{K_1}\right) \tag{3.79}$$

where $R = 8.3145$ J/(mol K) is the gas constant, T_{nom} is the nominal operating temperature (K), and i_0 is the exchange current (A) calculated in 3.67.

The dimensionless parameter K_c, found in 3.47, is calculated as follows:

$$E_{n(nom)} = 1.229 + (T_{nom} - 298)\frac{-163.23}{zF} + \frac{RT_{nom}}{zF} \ln\left(P_{H_2(nom)} P_{O_2(nom)}^{0.5}\right) \tag{3.80}$$

$$K_c = \frac{E_{oc}}{E_{n(nom)}} \tag{3.81}$$

where $E_{n(nom)}$ is the Nernst voltage at nominal conditions (V), $E^0 = 1.229$V is the standard-state reversible voltage (V), $\Delta\hat{s} = -163.23$ J/(mol K) is the variation in molar entropy due to the reaction, $z = 2$ is the number of moving electrons, $F = 96485$ As/mol is the Faraday's constant, T is the operational temperature in nominal condition, $T_0 = 298$ K is the reference temperature to calculate E^0, and E_{oc} is the Open Circuit Voltage obtained from the datasheet (V). The remaining parameters of the equations 3.80 are calculated in 3.76 and 3.77. The difference between the units *atm* and *bar* is neglected when calculating the Nernst voltage.

The equations that describe the fuel cell are solved using a calculator and coding the model with a programming language. In this thesis, an open-source programming language called Modelica is used.

3.3 Model in OpenModelica

Computer calculators are of utmost importance to speed up the process of calculating equations describing complex systems. This section describes the implementation of the fuel cell stack model with a mathematical modelling and simulation language called Modelica. Modelica is an equation-based, object-oriented language for complex and dynamic applications. For further information about this programming language and the main structures used in this thesis, consult Appendix B.

The mathematical model of the fuel cell is coded in Modelica within the OpenModelica environment. Below, the implementation of the model is shown, including the composition of its different blocks and the process of making the model acausal.

3.3.1 Fuel Cell Core

The fuel cell model described previously is contained in the block `Fuel_Cell_Core`, which is shown in Figure 3.6. This block has several inputs, outputs, parameters, and acausal interfaces, as well as several sub-blocks that constitute it. Every single part is now analyzed, from the interfaces with the outside to the internal structure.

Inputs

The inputs are enclosed in four type `record` elements. These records collect six pieces of information regarding different parts of the cathode and anode circuit of the fuel cell. Subsequently, it will be shown how this data is collected; at the moment, the focus is on the format in which it arrives. Specifically, the `record` is defined as:

```
record SensorFluid
  Real pressure;            // Total pressure (Pa)
  Real mass_flow_rate;      // Mass flow rate (kg/s)
  Real density;             // Density (kg/m3)
  Real temperature;         // Temperature (K)
```

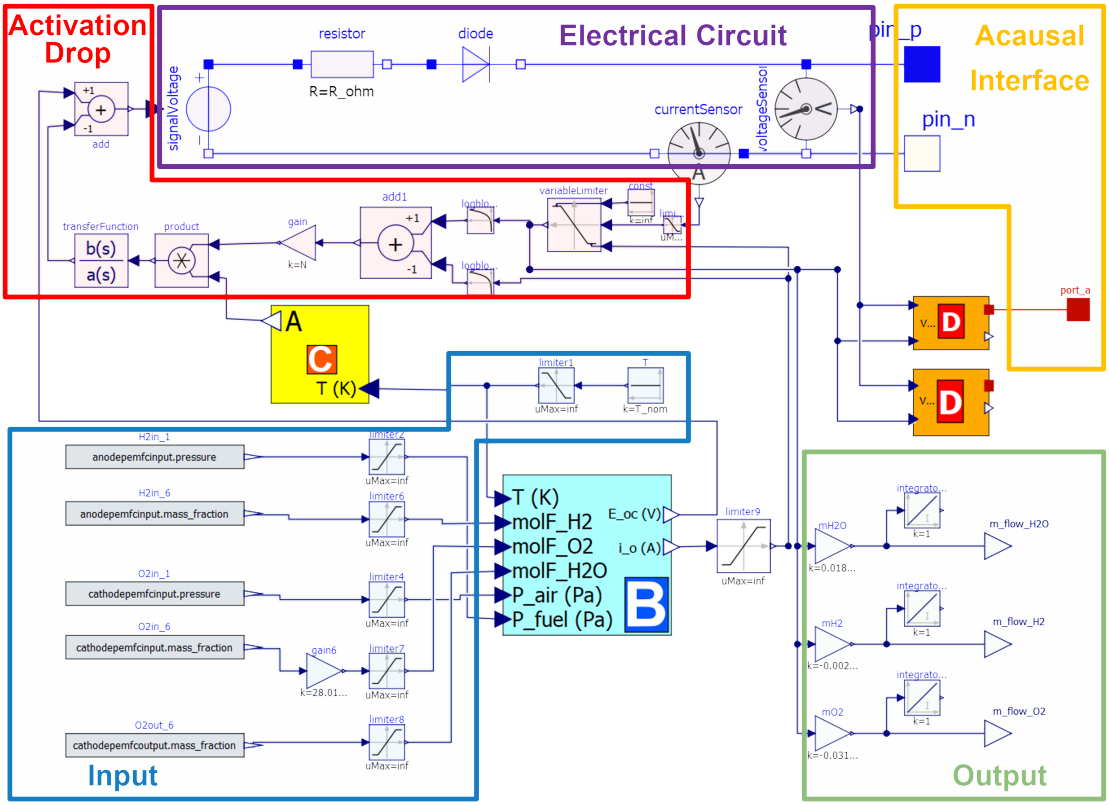

Figure 3.6: `Fuel_Cell_Core` structure and internal configuration.

```
6     Real specific_enthalpy;    // Specific enthalpy (J/kg)
7     Real mass_fraction;        // Mass fraction of a single element
8   end SensorFluid;
```

Listing 3.1: Record structure.

The four records collect data from the input and output of the cathode and anode gas channels to transmit to the block analyzed at each simulation instant. For this, there are real value sources within the block called `Blocks.Sources.RealExpression` from which all the parameters collected from the records are injected into the model.

These four elements are inserted directly into the OpenModelica code and are called:

```
1  input SensorFluid anodepemfcinput;
2  input SensorFluid cathodepemfcinput;
3  input SensorFluid anodepemfcoutput;
4  input SensorFluid cathodepemfcoutput;
```

Listing 3.2: Records input.

Where `sensorfluid` is the name of the previously defined class. Once the signals enter the model, they are subjected to control to avoid, mainly, incurring numerical or mathematical errors due, for example, to negative or null values as arguments of the logarithms. For this reason, limiters are

placed with values shown in Table 3.2 (in other parts of the model, there are limiters which, for simplicity, will be listed in the same table).

Limiter n.	1 (K)	2 (Pa)	3	4 (Pa)	5	6	7 (A)
Max	inf	inf	inf	inf	inf	inf	inf
Min	200	1	1e-4	1	1e-4	1e-4	1e-3

Table 3.2: Maximum and minimum values of the limiters present in the fuel cell core block.

Since the input of block B, which will be discussed later, requires the mole fraction rather than the mass fraction, this value is adjusted by certain blocks according to the relationship (for example, oxygen):

$$x_{O_2} = w_{O_2} \frac{M_{air}}{M_{O_2}} \tag{3.82}$$

where x_{O_2} is the molar fraction, w_{O_2} is the mass fraction, $M_{O_2} = 31.9988$ g/mol is the molar mass of molecular oxygen, and $M_{air} = 28.013$ g/mol is the molar mass of air.

Outputs

The block's outputs are identified in the mass flow rate of hydrogen $\dot{m}_{H_2}$ and oxygen $\dot{m}_{O_2}$ removed from the gas channels and water $\dot{m}_{H_2O}$ produced at the cathode. To calculate these quantities, it is necessary to use some formulas that define the number of moles $\dot{n}_i$ (mol/s) that react as a function of the electric current I_{fc} (A) supplied by the fuel cell. The number of moles per second is multiplied by the molar mass of the substance to obtain the mass flow rate.

$$\dot{m}_{H_2} = -M_{H_2} \cdot \dot{n}_{H_2} = -M_{H_2} N \frac{I_{fc}}{2F} \tag{3.83}$$

$$\dot{m}_{O_2} = -M_{O_2} \cdot \dot{n}_{O_2} = -M_{O_2} N \frac{I_{fc}}{4F} \tag{3.84}$$

$$\dot{m}_{H_2O} = M_{H_2O} \cdot \dot{n}_{H_2O} = M_{H_2O} N \frac{I_{fc}}{2F} \tag{3.85}$$

Where $M_{H_2} = 2.01568$ g/mol is the molar mass of molecular hydrogen, $M_{O_2} = 31.9988$ g/mol is the molar mass of molecular oxygen, $M_{H_2O} = 18.01528$ g/mol is the molar mass of water, N is the number of cells in series, and $F = 96485$ As/mol is the Faraday's constant. Some values are placed negative because mass is removed from the gas channels. In addition, some blocks integrate the above quantities to determine, after a certain time interval, the quantity of oxygen and hydrogen consumed, and the quantity of water produced.

Acausal Interfaces

The last interfaces with the outside are the so-called acausal interfaces, that is, they are neither inputs nor outputs but transmit a series of signals. Three different acausal connectors exist for two physical signals. The first two are the electrical poles of the fuel cell stack, which represent the termination of the equivalent circuit, and the third is related to heat transfer, which is used to study the one-dimensional heat flow between components. The variables of this last connector are the temperature (K) and the heat flow (W), and a heat flow that flows inside a component is considered positive.

Parameters

Equations can only be solved if correctly populated with data from the datasheet. The block being analyzed has a graphical interface that, when used, requires the insertion of certain parameters. Appendix C shows the parameters and the method for obtaining them.

Block B

Block B calculates the fuel cell stack's exchange current and the open circuit voltage. The inputs of Block B are the stack temperature, the pressure and mole fraction of hydrogen, the pressure of air, the mole fraction of oxygen in the air, and the mole fraction of water in the cathode at the exit of the fuel cell. From the graphic interface, it is possible to insert the K_c parameter and the activation energy barrier as block parameters.

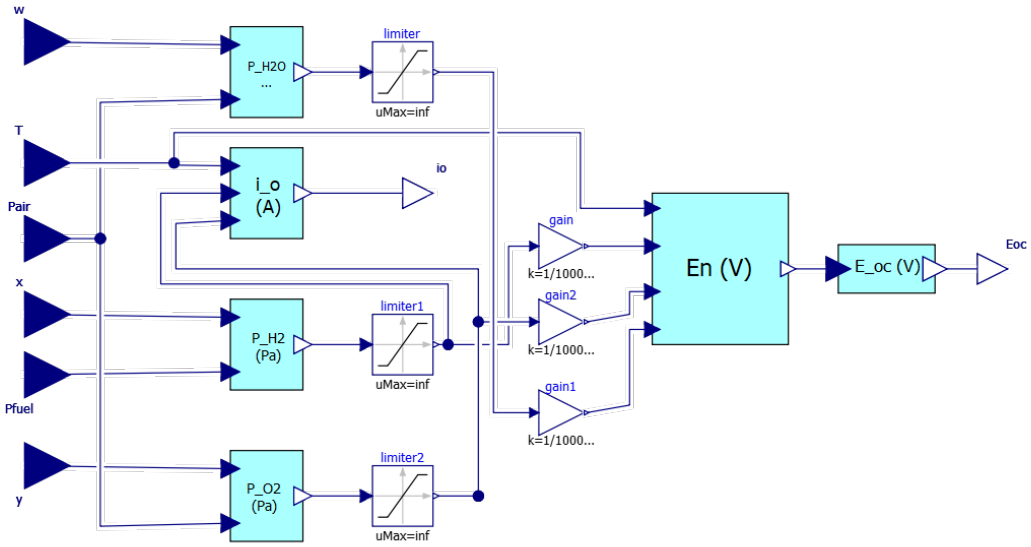

Figure 3.7: Block B

Block B contains other code blocks with some model equations, expressed in the previous section and shown in Figure 3.7. The partial pressures of hydrogen, oxygen, and water are calculated in `BlockB3`, `BlockB2`, and `BlockB1`, respectively. The partial pressures are limited at the bottom by limiters, which must be greater than zero, and are used to calculate the exchange current in `BlockB4`. To calculate the Nernst voltage in `BlockB5`, partial pressures are converted to *bar*, and a different equation is used depending on the temperature. In particular, the three contributions of equation 3.27 are defined among the variables. Subsequently, these are calculated according to the temperature and added together to obtain the final potential. The three contributions are calculated separately to observe the different influences on the final voltage subsequently. The code is shown below.

```
block BlockB5
    Real En1;
    Real En2;
    Real En3;
    ...
```

```
equation
    if T >= 373 then
        En1 = 1.184;
        En2 = (T - 298)*(-44.34)/(z*F);
        En3 = (R*T*Modelica.Math.log(PH2*(PO2^(0.5))/PH2O))/(z*F);
        En = En1 + En2 + En3;
    else
        En1 = 1.229;
        En2 = (T - 298)*(-163.23)/(z*F);
        En3 = (R*T*Modelica.Math.log(PH2*(PO2^(0.5))))/(z*F);
        En = En1 + En2 + En3;
    end if;
end BlockB5;
```

Listing 3.3: Block B5

Finally, the Nernst voltage of a single cell is converted into the open circuit voltage of the fuel cell, i.e. the voltage when no electrical load is connected, in `BlockB6`, multiplying it by K_c.

Block C

Block C calculates the Tafel slope. The real input of Block C is the temperature of the stack. Inserting the parameter α as a block parameter is possible from the graphical interface. The core of the block is expressed through the equation 3.49.

Activation Drop

To calculate the losses due to the activation energy the equation 3.33 is implemented. The fuel cell stack current is measured via a current sensor and is limited to be greater than the exchange current value via a variable limiter. This assumption derives from the study of the implementation of this model in the Simulink® Fuel Cell Stack block, which is discussed in Chapter 2. Therefore, this part of the circuit receives as input the current circulating in the fuel cell via a current sensor applied in series to the equivalent circuit, the exchange current calculated in Block B, and the Tafel slope calculated in Block C. This equation returns the voltage drop due to the activation energy damped by the first-order transfer function representing the dynamic effects of the fuel cell. This loss is subtracted from the open circuit voltage calculated in block B, and the result is inputted to the equivalent circuit voltage source.

Electrical Circuit

Modelling fuel cell stack voltage behaviour through an electrical circuit is a common analogy in this field, as summarized in the work of Runtz et al. [72]. The equivalent circuit of the fuel cell stack is depicted with different electrical elements. The first is the voltage source `signalVoltage`, which is controlled by the algebraic sum between the open circuit voltage and the activation losses. Ohmic losses are represented by a resistor with a R_{ohm} value, not temperature-dependent. The presence of the diode forces the current flow in only one direction, avoiding a negative current. Finally, two sensors measure the voltage at the ends of the fuel cell stack equivalent circuit and the current generated.

Block D Simplified

Simplified block D contains the simplified heat production modelling previously exposed, shown in Figure 3.8. This block receives the voltage and current of the fuel cell as input, obtained through

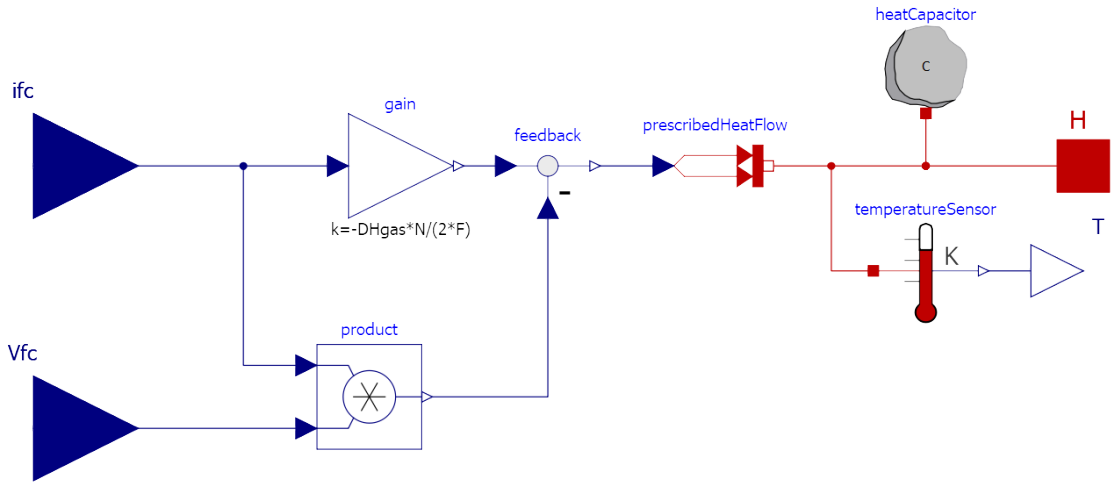

Figure 3.8: Block D simplified implemented in OpenModelica

the sensors applied on the equivalent circuit. The block outputs the temperature of the fuel cell, which can be connected to other elements of the fuel cell core only when a cooling system is present. Otherwise, it grows without limits, distorting the modelling. A thermal connector can be connected to a cooling system to keep the temperature constant. The block parameters, set out in detail and obtained in Appendix C, refer to the fuel cell stack: the specific heat capacity, the mass, the initial temperature, and the number of cells in series. Inside the block, the generated heat is calculated with equation 3.51 and is fed with a `PrescribedHeatFlow` block into a thermal circuit modelled using OpenModelica thermal libraries. Inside this circuit there is also a lumped thermal element that stores heat, which describes, employing the heat capacity, the thermal mass of the fuel cell stack. Finally, there is a thermal mass temperature sensor.

Block D Detailed

Detailed block D contains the detailed heat production modelling previously exposed, shown in Figure 3.9. This block receives the voltage and current of the fuel cell as input, obtained through the sensors applied on the equivalent circuit, and the two gas channels' input and output enthalpy values. The block provides the temperature of the fuel cell, which can be connected to other elements of the fuel cell core only when a cooling system is present. Otherwise, it grows without limits, turning modelling upside down. A thermal connector can be connected to a cooling system to maintain a constant temperature. The block parameters, detailed and obtained in Appendix C, refer to the fuel cell stack: the specific heat capacity, mass, initial temperature and the number of cells in series. Inside the block, the generated heat is calculated with the equation 3.56 and is provided with a `PrescriptionHeatFlow` block in a thermal circuit modelled using OpenModelica thermal libraries. Within this circuit there is also a concentrated thermal element that stores heat, which describes, using thermal capacity, the thermal mass of the fuel cell stack. Finally, there is a thermal mass temperature sensor.

3.3.2 PEMFC Stack Model in OpenModelica

It is necessary to create acausal interfaces for the mathematical model discussed to interface the fuel cell stack model with other elements of the Balance of Plant within the OpenModelica development environment. The fuel cell core provides the acausal interfaces for the electrical and thermal

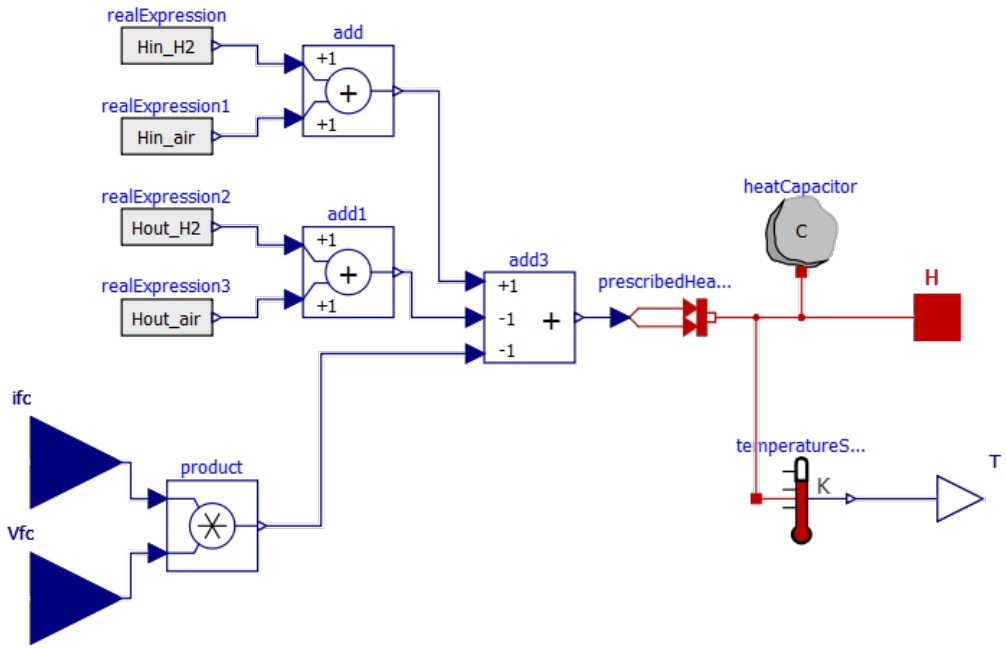

Figure 3.9: Block D detailed implemented in OpenModelica

circuits but still has causal input and output elements that must be converted. For this reason, the PEMFC Stack block is created, which contains three main elements: the anode, the cathode and the previously modelled membrane.

The interfaces of this block, as shown in Figure 3.10, are all of the acausal type. In addition to the fuel cell core, the four input and output ports of the two gas channels are created with the fluid ports of the standard OpenModelica library. The parameters of this block are exposed in the appendix C. The contents of the anode and cathode blocks are now shown.

Anode

The two electrodes are modelled similarly through a simplified approach. The anode is made with the OpenModelica fluid library, where the gas channels' inlet and outlet are made utilizing a fluid connector. A fundamental component uses a flow source that represents hydrogen consumption, controlled via an input signal directly from the fuel cell core, representing the amount of mass that reacts and passes inside the fuel membrane cell. To force the flow to move from the gas channel inlet to the outlet, non-return valves are inserted, using a linear valve (provided in the OpenModelica library) completely open but with the setting to avoid flow reversal. Two valves are positioned across the controlled negative hydrogen source, which simulates the consumption of hydrogen in reactions. These valves also separate the conditions at the inlet and outlet of the gas channels to be measured more precisely using six specific sensor models. The six sensors measure total pressure, mass flow, density, temperature, specific enthalpy, and hydrogen mass fraction. The values measured by the sensors are stored and provided to the fuel cell core model employing two `record` classes.

In Modelica, when using circuits with fluids, it is important to define the fluid that flows

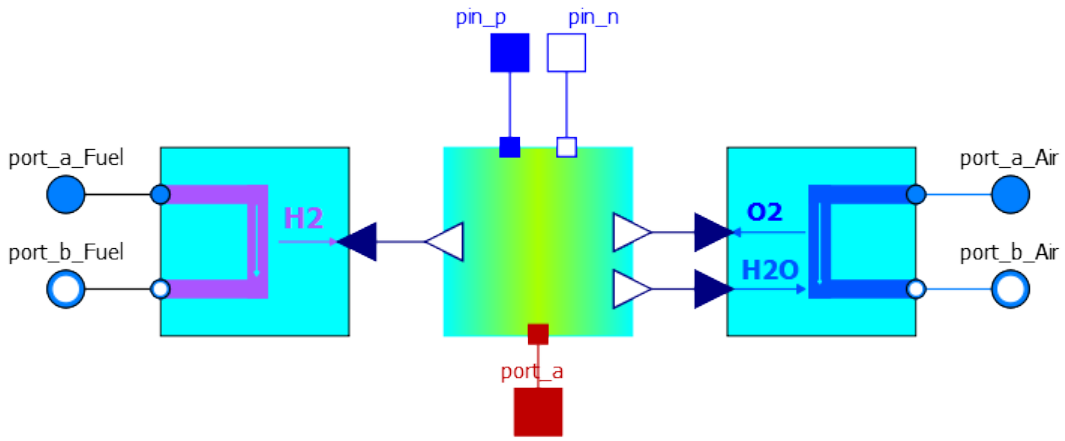

Figure 3.10: Block PEMFC stack implemented in OpenModelica.

through them. In this case, a mixture of hydrogen at high percentages and an inert gas such as nitrogen in low concentrations is considered, to simulate the presence of foreign fluids. The combustible fluid is described by defining a new package called `FuelMixture` in Modelica. This package extends existing Modelica packages to model the gases mentioned above using NASA data. The code shown presents the definition of the customized fluid with the different percentages of hydrogen and nitrogen.

```
package FuelMixture "Mixture of H2 and N2 for anode channel"
extends Modelica.Media.IdealGases.Common.MixtureGasNasa(
        mediumName = "Fuel",
        data = {Modelica.Media.IdealGases.Common.SingleGasesData.H2,
                Modelica.Media.IdealGases.Common.SingleGasesData.N2},
        fluidConstants = {Modelica.Media.IdealGases.Common.FluidData.H2,
                          Modelica.Media.IdealGases.Common.FluidData.N2},
        substanceNames = {"Hydrogen","Nitrogen"},
        reference_X = {1,0}); // default values set on pure hydrogen
            mixture
end FuelMixture;
```

Listing 3.4: Fuel mixture definition's script.

This fluid is then inserted into each component of the anode circuit described above so that the behaviour of the fuel can be represented.

Cathode

The cathode is modelled similarly to the anode through a simplified approach. The cathode is made with the OpenModelica fluid library, where the gas channels' input and output are made using fluid connectors. A fundamental component is the flow source representing the hydrogen consumption, which is controlled via an input signal directly from the fuel cell core. In addition, compared to the anode, there is a second flow source which introduces the water produced by the reactions that occur at the cathode into the circuit. To force the flow to move from the gas channel inlet to the outlet, non-return valves are inserted using a linear valve provided in the OpenModelica library that is completely open but with the setting to avoid flow reversal. Two valves are positioned across the oxygen and water sources. These valves also serve to clearly separate the conditions

at the inlet and outlet of the gas channels so that they can be measured more precisely using six different sensors. The six sensors measure the total pressure, mass flow, density, temperature, specific enthalpy, and hydrogen mass fraction. The values measured by the sensors are stored and provided to the fuel cell core through two `record` classes.

In the case of the cathode, the fluid considered in the circuit is a mixture of nitrogen and oxygen, representing dry air, and water. To describe the combustible fluid, a new package called `AirMixture` is defined in Modelica in which packages already present in Modelica are extended which model the gases mentioned above thanks to NASA data. The code shown presents the definition of the custom fluid with the different percentages of nitrogen, oxygen and water.

```
package AirMixture "Mixture of air (nitrogen and oxygen) and water vapor"
extends Modelica.Media.IdealGases.Common.MixtureGasNasa(
        mediumName = "Air",
        data = {Modelica.Media.IdealGases.Common.SingleGasesData.N2,
                Modelica.Media.IdealGases.Common.SingleGasesData.O2,
                Modelica.Media.IdealGases.Common.SingleGasesData.H2O},
        fluidConstants = {Modelica.Media.IdealGases.Common.FluidData.N2,
                          Modelica.Media.IdealGases.Common.FluidData.O2,
                          Modelica.Media.IdealGases.Common.FluidData.H2O},
        substanceNames = {"Nitrogen","Oxygen","Water"},
        reference_X = {0.78,0.22,0.0});
end AirMixture;
```

Listing 3.5: Air mixture definition's script.

This fluid is then inserted into each component of the cathode circuit described above so that the behaviour of the air can be represented.

Overall PEMFC Stack Block

In conclusion, a block with an acausal interface has been created which can be connected to other elements of the BoP through acausal interfaces. Figure 3.11 shows the icon of the block that can be used in OpenModelica, where there are the seven acausal connectors that represent the input and output of the anodic and cathodic gas channel, the electrical poles of the fuel cell, and the interface for the heat transfer.

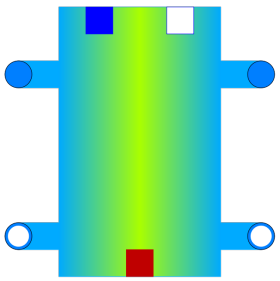

Figure 3.11: PEMFC stack block in OpenModelica.

Once the model has been created, it is necessary to compare the predictions with experimental data to define its level of accuracy. This process is called validation and will be carried out by recreating the polarization curves of some fuel cells on the market.

3.4 Validation

Validation of the model implemented in OpenModelica is necessary to understand the accuracy and limitations of the model itself. To carry out this step in creating the model, the peculiarity of this model can be exploited by populating it with data from the fuel cell datasheet. In the international market, many PEMFC manufacturers publish their catalogues with more or less information regarding the characteristics of their products and the polarization curve. A fuel cell database was therefore created with two main purposes:

- obtain information about the polarization curve and use it in the created model;
- observe the trend of energy density as power increases, for future studies on integrating these devices within system architectures.

The database and these considerations are reported and commented in Appendix C. In this section, the setup created with OpenModelica to validate the model will be presented, followed by the results for three different fuel cell stacks.

3.4.1 Balance of Plant for Validation

Comparing the polarization curve on the datasheet with the polarization curve obtained with the simulation is a method to validate the model. To carry out the simulation, creating a BoP around the fuel cell block is necessary to allow this study. For this reason, a simplified and conceptual BoP was created composed of a few elements, as shown in Figure 3.12. In this configuration, it is observed that the oxygen and hydrogen circuits, as well as the current circuit, are connected, while the thermal circuit is not connected, as the operating temperature is considered constant.

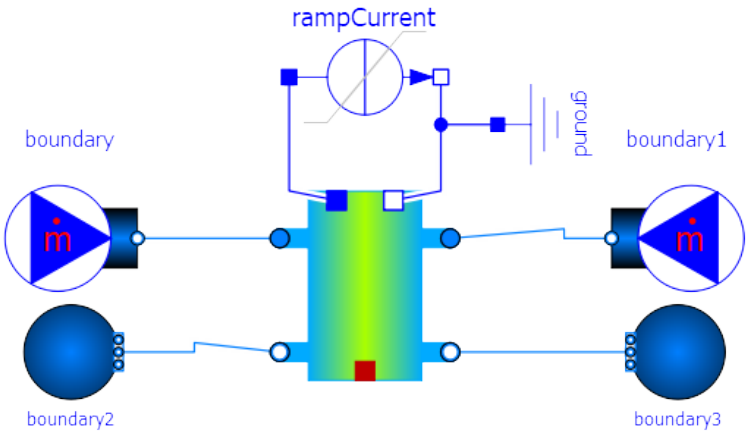

Figure 3.12: Balance of Plant for validation testing.

A constant flow of hydrogen arrives at the anode produced by a `MassFlowSource_T` block, which is set to have a mass flow equal to:

$$\dot{m}_{fuel,max} = \frac{\lambda_{H2} V_{min} I_{max}}{\eta_{nom} \Delta h_{HHV}} \tag{3.86}$$

Where $\lambda_{H2} = 1.1$ is the chosen stoichiometric ratio of the hydrogen considering the recirculation of the unconsumed hydrogen, V_{min} is the minimum voltage of the fuel cell at maximum current

I_{max}, η_{nom} is the nominal efficiency of the fuel cell, and $\Delta h_{HHV} = 141.8$ MJ/kg is the enthalpy of hydrogen formation. The exhaust hydrogen gases end up in a boundary with constant ambient temperature and pressure.

The cathode circuit has the same configuration, with the air source generating a mass flow equal to:

$$\dot{m}_{air,max} = \frac{N I_{max} \lambda_{O2} M_{air}}{4 F y_{O2}} \tag{3.87}$$

Where N is the number of cells in series, $\lambda_{O2} = 1.8$ is the stoichiometric ratio of the oxygen in the air, I_{max} is maximum current, M_{air} is the molar mass of the air, and y_{O2} is the molar fraction of oxygen in the airflow. The connected electrical circuit has a structure composed of two elements. The first is a current source that follows a unit slope ramp, which reaches a maximum current defined by the maximum value present in the datasheet in a time corresponding to the same current value but expressed in seconds. This measure allows the polarization curve to be obtained in a simple and immediate way. The second component of the circuit is the circuit ground, which is necessary to establish a zero reference for the fuel cell stack potential.

This BoP can be populated with data from the fuel cell datasheet, which is obtained as explained in Appendix C. Now, three different examples of model validation will be shown.

NedStack P8 PS6

The first validation example is taken directly from the validation used by the model authors in their article [42]. The *NedStack P8 PS6* Fuel Cell has a nominal power of 5 kW, and once the parameters have been entered into the model, the results are shown in Figure 3.13.

In Figure 3.13a, the polarization curve can be observed on the datasheet, represented by extrapolated points, along with the electrical power curve compared to the current. The simulation is expressed in solid lines. Figure 3.13b analyzes the relative error between the simulated polarization curve and the one obtained by interpolating the curve data on the datasheet. In this case, the error is greater for high currents, with a maximum relative error of 3.2%.

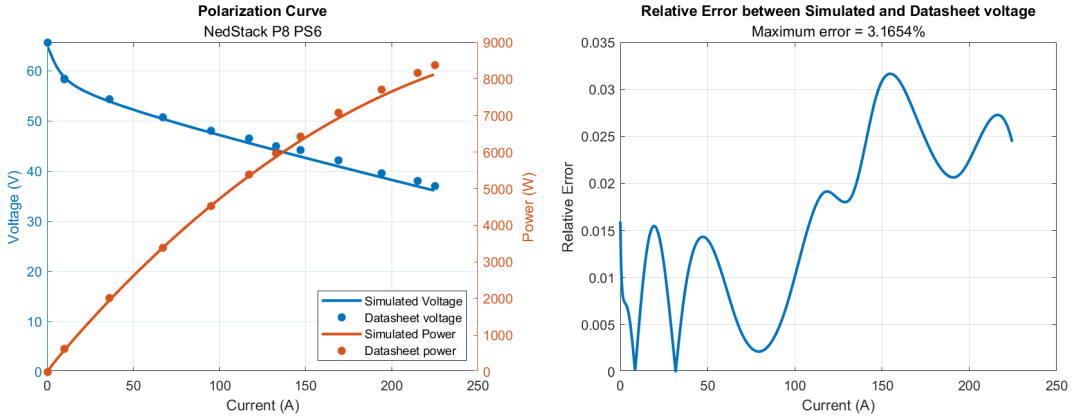

(a) Polarization curve.

(b) Relative error.

Figure 3.13: Validation results for the NedStack P8 PS6 fuel cell

Horizon H5000

The second validation example is taken from the Horizon Fuel Cell Technology catalogue. The *Horizon H5000* fuel cell has a nominal power of 4 kW, and once the parameters have been entered

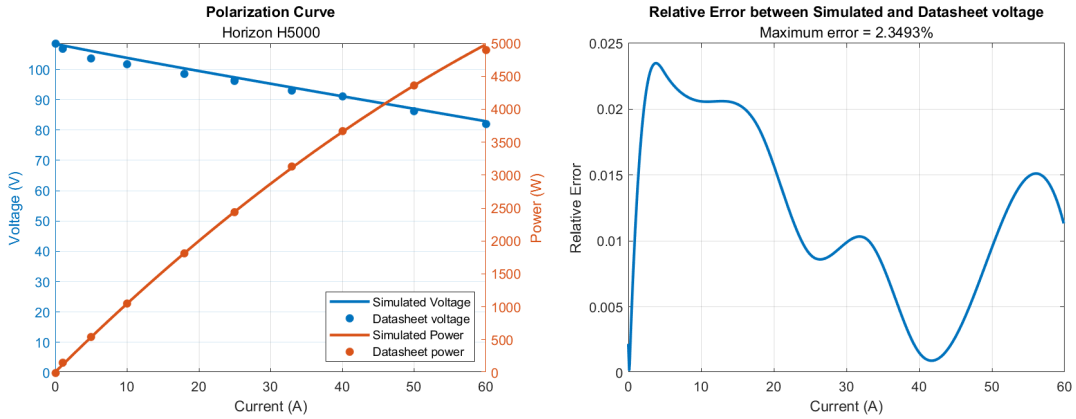

(a) Polarization curve.

(b) Relative error.

Figure 3.14: Validation results for the Horizon H5000 fuel cell

into the model, the results are shown in Figure 3.14.

In Figure 3.14a, the polarization curve on the datasheet is represented by extrapolated points, and the electrical power curve is compared to the current. The simulation is expressed in solid lines. Figure 3.14b analyzes the relative error between the simulated polarization curve and the one obtained by interpolating the curve data on the datasheet. In this case, the error is greater for low currents, with a maximum relative error of 2.4%.

Horizon H1000XP

The third validation example is taken from the Horizon Fuel Cell Technology catalogue. The *Horizon H1000XP* fuel cell has a nominal power of 1 kW, and once the parameters have been entered into the model, the results are shown in Figure 3.15.

In Figure 3.15a, the polarization curve on the datasheet is represented by extrapolated points, and the electrical power curve is compared to the current. The simulation results are shown in solid lines. Figure 3.15b analyzes the relative error between the simulated polarization curve and the one obtained by interpolating the curve data on the datasheet. The error is greater for low currents, with a maximum relative error of 3.8%.

3.4.2 Final Considerations on Validation

The mathematical model can approximate the fuel cells' polarization curve with a low error. Comparing the examples, it is observed in Figure 3.13a that the activation losses are initially modeled with a curve, which then transitions into a line in the Ohmic losses region. In the other examples, the polarization curve is modelled mainly by a straight line, which, however, closely approximates the data provided by the datasheet. This difference is due to the choice of parameters to be inserted within the fuel cell stack block. As explained in Appendix C, selecting points on the original polarization curve is crucial to obtaining a good result from the simulation. The model is validated with good results and can be used to study the integration of PEMFC within system architectures.

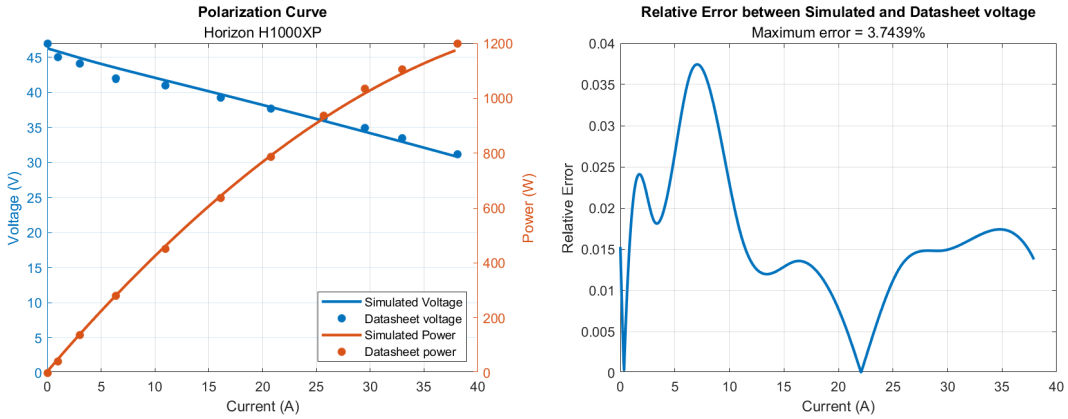

(a) Polarization curve.

(b) Relative error.

Figure 3.15: Validation results for the Horizon H1000XP fuel cell

Chapter 4

Case Study

The model built in OpenModelica can be used to study system architectures. As seen in Chapter 2, fuel cells are analyzed to provide secondary electrical power or generate the power needed to move the electric motors used in propulsion. This chapter describes the Balance of Plant implemented in OpenModelica to perform realistic case studies and analyzes a case study simulation.

4.1 Model of the Balance of Plant

A fuel cell stack can only operate thanks to a series of systems that support its operation. For this reason it is important to simulate the behavior of these devices that make up the Balance of Plant. The BoP built around the fuel cell is shown in Figure 4.1 and consists of several electrical, fluid or signal nature elements. The fuel cell stack is sized according to the application and the required power. Hydrogen source and exhaust gas conditions are present on the anode side. A circuit on the cathode side maintains the correct pressure and mass flow in the fuel cell. The mission profile controls the power demand and defines the atmospheric conditions. In this configuration, used to analyze the case studies, the cooling system is absent and no devices are connected to the thermal port of the block, thus considering the fuel cell to work at a constant operating temperature.

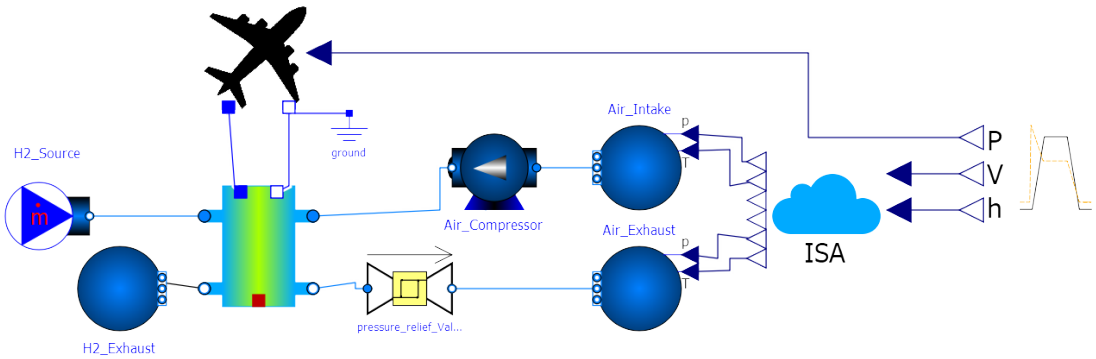

Figure 4.1: Balance of Plant to perform the case study.

4.1.1 Fuel Cells Scaling for Aircraft Applications

The focus of the BoP is always the fuel cell stack, represented by the block described in Chapter 3. To decide which fuel cell stack parameters to include, it is necessary to know the application's power requirements. A database, shown in Appendix C, has been built with many devices for low and medium-power applications. However, if a higher power is required, defining a fictitious fuel cell by scaling actual fuel cells is necessary. The power of the fuel cell stack is defined as:

$$P_{stack} = V_{cell} \cdot N \cdot i \cdot A_{cell} \tag{4.1}$$

where V_{cell} is the voltage of a single cell, N is the number of cells in series, i is the current density, and A_{cell} is the area of the cell. There are two ways to increase the total power of a given stack with nominal conditions V_{cell} and i [58]:

- By increasing the number of cells in series N, the total stack voltage is increased. This technique maintains the cell area and the design of the gas transport channels unchanged. It is equivalent to connecting multiple fuel cell stacks in series.
- By increasing the cell area A_{cell}, thus favouring semi-reactions and increasing the total current supplied by the fuel cell stack. This method requires extensive studies of the bipolar plate, as by increasing the surface area, the gas distribution must be redesigned to be optimal. In addition, increasing the area increases the size of the bipolar plates and seals, which are the heaviest components of the stack.

Both methods have their advantages and disadvantages, but they can be combined and used in a balanced way by increasing both voltage and current. Each manufacturer scales its fuel cells using a proprietary methodology, which will be described in the case study.

4.1.2 Anode Side

The circuit that supplies hydrogen to a fuel cell is complex and has many elements that research is studying to increase the overall performance. These elements include hydrogen tanks, non-return valves, and pumps for recirculation of unconsumed hydrogen. Many of these elements are not considered in the BoP of this thesis, where hydrogen is supplied to the fuel cell using a `MassFlowSource_T` source of constant mass flow rate equal to:

$$\dot{m}_{fuel,max} = \frac{\lambda_{H2} V_{min} I_{max}}{\eta_{nom} \Delta h^0_{HHV}} \tag{4.2}$$

where $\lambda_{H2} = 1.1$ is the hydrogen stoichiometric ratio considering hydrogen recirculation, V_{min} and I_{max} are the voltage and current at maximum power, η_{nom} is the nominal efficiency, and $\Delta h^0_{HHV} = 141.8$ MJ/kg is the higher heating value of hydrogen. Mass flow rate relative to maximum power is used because active control over mass flow for each phase of flight has not yet been implemented. The flow temperature is assumed to be equal to 273 K, and the mass composition is 100% hydrogen. This source is directly connected to the hydrogen channel input of the fuel cell. The exhaust gases, conversely, are determined by the boundary conditions defined by a `Boundary_pT` block, where an outlet pressure equal to 0.8 times the ambient pressure and a temperature equal to the fuel cell use temperature is assumed.

4.1.3 Cathode Side

This model has more accurately implemented the circuit that brings the gas to the cathode. The air inlet conditions are defined by a `Boundary_pT` block that sets the air temperature and pressure.

In this case, the two values are commanded employing a block that calculates, depending on the altitude and speed of flight, the total pressure and temperature conditions following the ISA (International Standard Atmosphere) atmosphere model. The air is subsequently compressed by a pump that maintains a constant flow rate throughout use. The flow rate is equal to:

$$\dot{m}_{air,max} = \frac{NI_{max}\lambda_{O2}M_{air}}{4Fy_{nom}} \tag{4.3}$$

where N is the number of cells in series, I_{max} is current at maximum power, $\lambda_{O2} = 1.8$ is the oxygen stoichiometric ratio, M_{air} is the molar mass of air, and y_{nom} is the nominal molar fraction of oxygen in the air. Mass flow rate relative to maximum power is used because active control over mass flow for each phase of flight has not yet been implemented. Next, the air enters the fuel cell where oxygen reacts with H^+ ions to produce water, and the spent gases are first maintained at a certain operating pressure by a pressure relief valve and finally discharged at the outlet conditions defined by a `Boundary_pT` block controlled with static pressure and temperature at the flight altitude.

ISA Atmosphere Block

According to the ICAO unified ISA atmosphere model, the block that describes the behaviour of atmospheric conditions has the altitude h (m) and flight speed V (m/s) as input. These two pieces of information are fundamental to defining some variables that describe the atmospheric conditions in the troposphere and stratosphere. The tropopause separates these two different regions of the atmosphere at an altitude of $h_{trop} = 11.000$ m. The block, based on [78], allows to calculate the static pressure P_{air} at a specific altitude:

$$\begin{cases} P_{air} = p_0 & \text{for } h \leq 0 \\ P_{air}(h) = p_0 \left(1 - 0.0065\frac{h}{T_0}\right)^{5.2561} & \text{for } 0 < h \leq h_{trop} \\ P_{air}(h) = p_{11} \cdot \exp\left(-\frac{g_0(h-h_{trop})}{RT_{11}}\right) & \text{for } h > h_{trop} \end{cases}$$

where $p_0 = 101.325$ Pa and $T_0 = 288.15$ K are the pressure and the temperature at sea level condition, $g_0 = 9.80665$ m/(s^2) is the gravity acceleration at sea level condition, $p_{11} = 22632$ Pa and $T_{11} = 216.65$ K are the pressure and the temperature at the tropopause, and $R = 287.04$ J/(kg K) is the air gas constant.
The static air temperature at a given altitude is:

$$\begin{cases} T_{air} = T_0 & \text{for } h \leq 0 \\ T_{air}(h) = T_0 - 0.0065 \cdot h & \text{for } 0 < h \leq h_{trop} \\ T_{air} = T_{11} & \text{for } h > h_{trop} \end{cases}$$

The Mach number Ma corresponding to the speed of the aircraft at a certain altitude is:

$$Ma = \frac{V}{\sqrt{\gamma RT_{air}}}$$

where $\gamma = 1.4$ is the air heat capacity ratio. The density ρ of the air is:

$$\rho = \frac{P_{air}}{RT_{air}}$$

And finally, the total pressure P_{air}^{tot} and temperature T_{air}^{tot} are:

$$P_{air}^{tot} = P_{air}(1 + \frac{\gamma - 1}{2}Ma^2)^{\frac{\gamma}{\gamma-1}}$$
$$T_{air}^{tot} = T_{air}(1 + \frac{\gamma - 1}{2}Ma^2)$$

Pressure Relief Valve

The pressure relief valve maintains a certain fluid pressure. In particular, the pressure must be constant inside the cathode gas channel to promote correct fuel cell performance. For this reason, as shown in Figure 4.2, a valve model present in the basic OpenModelica library was used to model the behaviour of this component, which is controlled to open linearly. For a unit signal, the valve is completely open; for a zero signal, it is completely closed. A pressure sensor measures the pressure at the valve inlet and supplies this value to a block that models the hysteresis. Hysteresis was chosen so that the valve can not open and close instantly. This block has the boolean behaviour described in Figure 4.3. The output defines the opening or closing value of the valve. If the valve

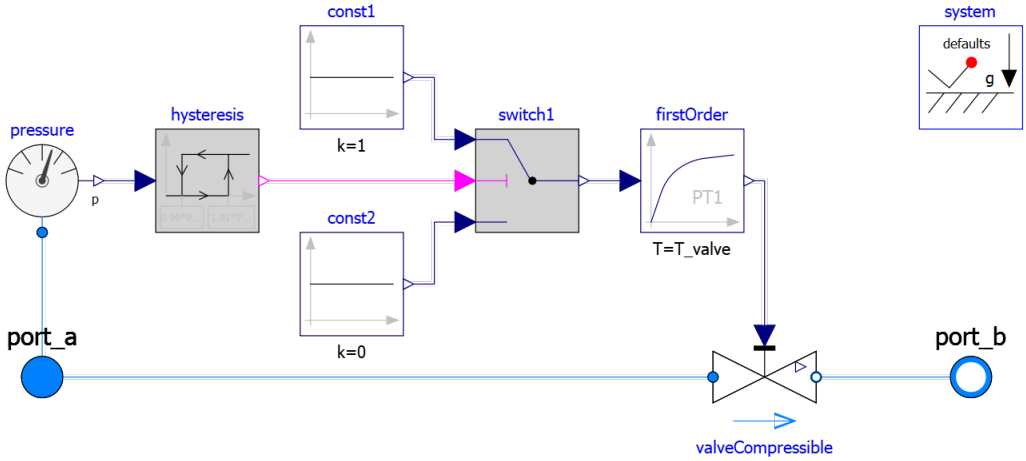

Figure 4.2: Pressure relief valve block.

must open, a switch selects the unitary signal, while if it must close, it selects the null signal. A first-order transfer function is inserted to avoid jerky opening and ensure realism, which delays the signal variation. The parameters to be inserted in this block include the control pressure P_{set}, which is the pressure to be maintained upstream of the valve, the characteristic opening time of the valve T_d, the nominal pressure drop, the nominal airflow rate, and the nominal pressure at the valve inlet.

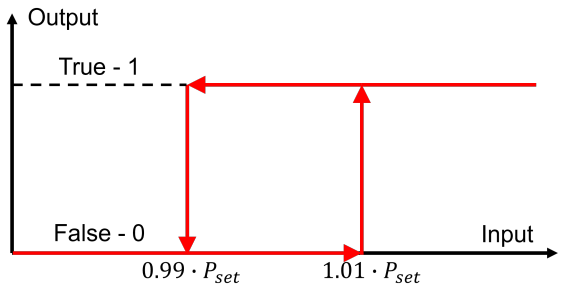

Figure 4.3: Description of the hysteresis present in the pressure relief valve.

4.1.4 Mission Profile

To simulate a real case study, it is necessary to be able to inject conditions into the simulation at different stages of flight. The block that performs this function is called `Mission_Profile` and receives an array of four columns and fifteen rows (editable) as input. The fundamental points of the mission profile are entered into this table, and linear interpolations between successive points will be made to define the flight conditions at each time instant. The first column contains the times for the instants of flight considered. The other columns contain the required power (W), altitude (m), and velocity (m/s) at each instant considered. Figure 4.4 and Figure 4.5 show an example of how the table is composed. This block outputs three signals corresponding to power, velocity, and altitude at each mission instant. As seen earlier, the velocity and altitude are the inputs to the block that calculates the atmospheric conditions.

Time (s)	**Power (W)**	**Altitude (m)**	**Speed (m/s)**
0	200000	0	0
600	200000	0	0
610	4100000	0	0
⋮	⋮	⋮	⋮

Figure 4.4: Mission profile input table

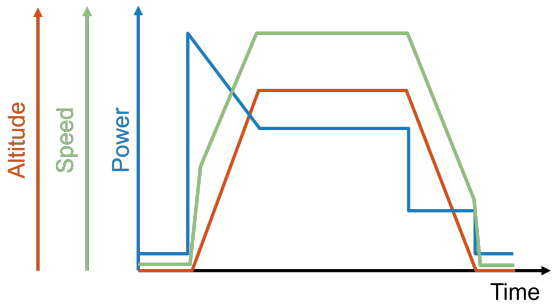

Figure 4.5: Mission profile example

On the other hand, power is needed by the `Electrical_Input` block that defines the current required to the fuel cell stack at each instant. This block generates the required current to the fuel cell through a current source controlled by the equation

$$i_{fc} = \frac{P}{V_{fc}} \tag{4.4}$$

where P is the power at each instant of time, and V_{fc} is the voltage at the ends of the fuel cell. This block is then directly connected to the fuel cell and grounded.

4.2 Case Study

The case study analyzed is inspired by the work of Hartmann et al. [15], who considers an ATR 72-based aircraft with cryogenic propulsion. This example has been slightly modified in this thesis without considering superconductive propulsion. A 70-passenger twin-engine aircraft with a maximum takeoff weight of 23 tons is assumed. The propulsion system is a single fuel cell stack capable of powering two electric motors that replace conventional turboprops in this aircraft type (Figure 4.6). There are no considerations of integrating this system into the aircraft in this case study, but it shows a possible application of the fuel cell model for realistic case simulation.

A flight that can cover the Milan-Barcelona route (725 km) is taken, with the mission profile shown in Figure 4.7 and the data shown in Appendix D. Compared to the original [15], it has been extended by adding taxi phases and defining a specific duration for the cruise phase. The first phase is the taxiing, where the power is low. At takeoff, the engines are pushed up to 4.1 MW for a short interval. After that, the throttle is decreased progressively during the two climb phases, the first up to 4.5 km and the second up to the cruising altitude of 6 km. During the cruise, the

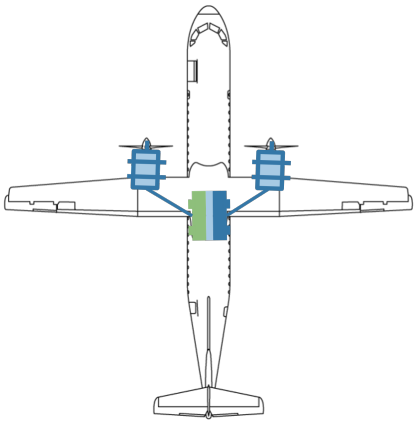

Figure 4.6: ATR 72-based aircraft configuration. Adapted from ATR website.

fuel cell stack power requirement is fixed at 2.5 MW, and the aircraft flies at 520 km/h. After about an hour of cruise, the aircraft prepares for descent by progressively decreasing power until the holding phase, where it is maintained at an altitude of 1 km. After completing the holding circuit, the descent is concluded by landing and taxiing to the airport. From this mission profile, the maximum and nominal powers required of the fuel cell stack at different phases of flight are evident, so it is necessary to size a fuel cell stack to meet these requirements properly.

A PEMFC with those characteristics is not currently on the manufacturers' market, so it is necessary to scale up an existing fuel cell to the desired power ratings. In this example, the voltage of a basic fuel cell is scaled until the desired power is reached. As seen above, this is equivalent to putting many fuel cells in series.
In this case study, two different fuel cell stacks are scaled differently. The first is an old-generation fuel cell, the complete datasheet of which is present and has already been used to validate the model in the previous Chapter. The second fuel cell is a newly developed stack. Both fuel cell stacks do not reach the maximum power required, so they must be scaled up. The first fuel cell stack is the NedStack P8 PS6, which has a very low specific power of approximately 75 W/kg. This fuel cell has a maximum power of 8325 W; therefore, to deliver the power required by the mission profile, the voltage is multiplied by a factor ϕ_1, which is equal to:

$$\phi_1 = \frac{4.1MW}{8325W} = 492.5 \tag{4.5}$$

The second PEMFC stack developed by ZeroAvia has a specific power equal to 2100 W/kg [79], and a maximum power output of 400kW. It can be seen that this device has a very high power density when compared with others in the database. In the information on the ZeroAvia datasheet, however, there is no full polarization curve, which is necessary to input the data into the mathematical model used in this thesis. For this reason, a realistic and optimistic polarization curve was constructed using the process shown in Appendix C. To obtain the desired power from the mission profile, the fuel cell polarization curve is scaled by increasing the voltage by a factor ϕ_2 equal to:

$$\phi_2 = \frac{4.1MW}{400kW} = 10.25 \tag{4.6}$$

A specific fuel cell is created in this case study while putting ten or eleven ZeroAvia stacks in a series, which represents a more realistic solution.

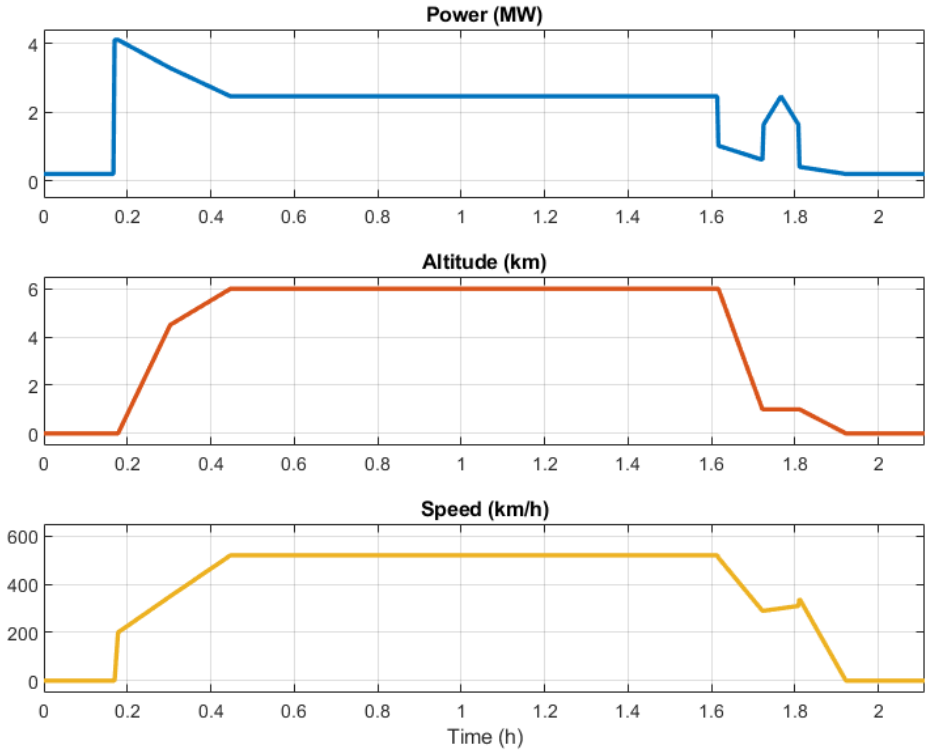

Figure 4.7: Mission profile of the case study. Adapted from [15].

The resulting two fuel cell stacks then have the polarization curves shown in Figure 4.8, and the data and parameters of the original and scaled fuel cell stacks are presented in Appendix D and used within the model in OpenModelica. The comparison shows how it is possible to achieve the same power with different fuel cells, where the first uses a higher voltage, i.e. more cells in series with a smaller area, and the second has a greater surface area of the individual cells, used in fewer numbers. These new fictitious fuel cell stacks and their data are inserted within the model in OpenModelica, and the simulation is started. The equations are solved using the solver implemented in OpenModelica called DASSL, an extension of Newton's method using derivative approximation formulas of orders greater than one [80].

4.2.1 Results

Interesting results can be observed from the simulation of this case study using two different PEMFC stacks. Figure 4.9 shows the voltage and current variations within the fuel cells. This behaviour is typical of fuel cells in that the polarization curve has a negative slope, so as the required current increases, the voltage decreases due to ohmic losses. In the case of the NedStack-based FC, a much higher voltage can be observed.

Despite the losses, increasing the current also increases the total power generated by the fuel cell, as shown in Figure 4.10, where the power follows the energy profile of the mission for both stacks. As can be seen in the graph describing the efficiency, if the efficiency is less than 50 percent, more heat is produced than electricity. This is because, as shown in Appendix A, efficiency decreases for

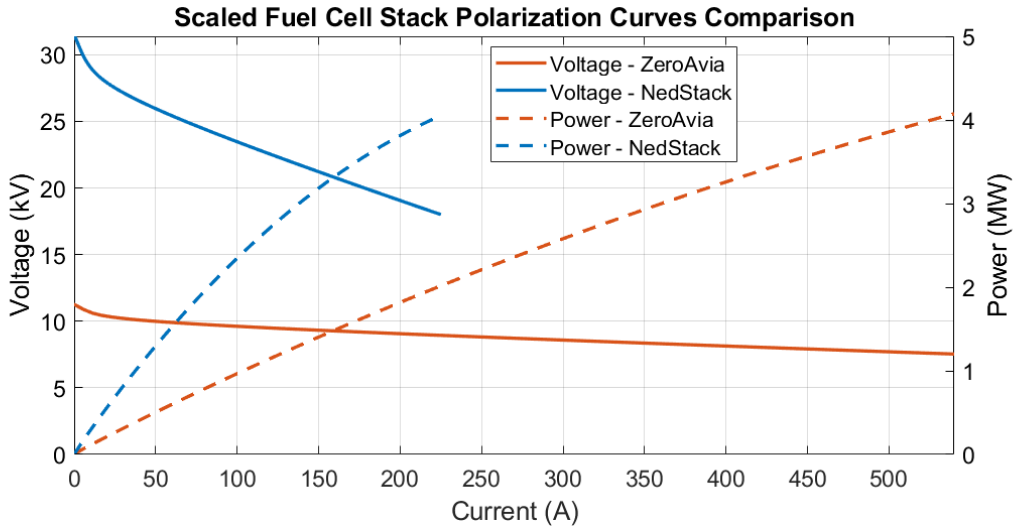

Figure 4.8: Polarization curves of the scaled fuel cell stacks used

high currents, so it is preferable to oversize the fuel cell to improve efficiency. Nevertheless, it is observed that the efficiency decreases only in the initial phase of the mission when maximum power is required from the fuel cell. To avoid this, different architectures can be considered, with the batteries supporting the power demand in the early stages of flight and the fuel cell operating only at nominal conditions equal to cruise conditions. Analyzing the specific cases, it can be seen that in Figure 4.10, the efficiency is consistently below 50 percent, bringing high heat production and again suggesting the oversizing of this device. This behaviour can also be seen by comparing the difference between heat and electrical power dissipation in the take-off phase, which is very high in the case of the NedStack-based FC. To calculate the efficiency, there are several formulas in the literature, but the calculation proposed by Hartmann et al. [15] was used for this representation:

$$\eta = \frac{2FV_{fc}}{N\Delta h_{HHV}} \tag{4.7}$$

where the fuel cell voltage V_{fc} was normalized for the number of cells N and related to the higher heating value of hydrogen Δh_{HHV}.

A comparison of the results of the two different models for heat calculation is shown in Figure 4.11. The results show relative errors of less than 2%, so they can be considered accurate in both FC stack configurations.

Figure 4.12 shows the amount of hydrogen and oxygen consumed in the total mission and the total water produced for both FC stack configurations. This data is important for defining the size of the hydrogen tanks and considering possible water use. It is observed how the study and research on fuel cells can increase their performance by reducing losses and consequently needing less oxygen and hydrogen for the same mission.

This mission of about 800 km requires 200 kg of hydrogen, considering the ZeroAvia-based FC stack. This amount can be scaled approximately to the maximum mission that an ATR 72 can operate, equal to 1350 km fully loaded [81], resulting in about 330 kg of hydrogen required. Compared to 5000 kg of conventional fuel [81], this is, therefore, a significant saving, to which, however, must be added the weight of all the Balance of Plant components, which will not be explored in detail in this thesis. The water produced by the fuel cell stack during the reference mission is about 1800 kg, which can be used in a small part for the internal utilities of the aircraft

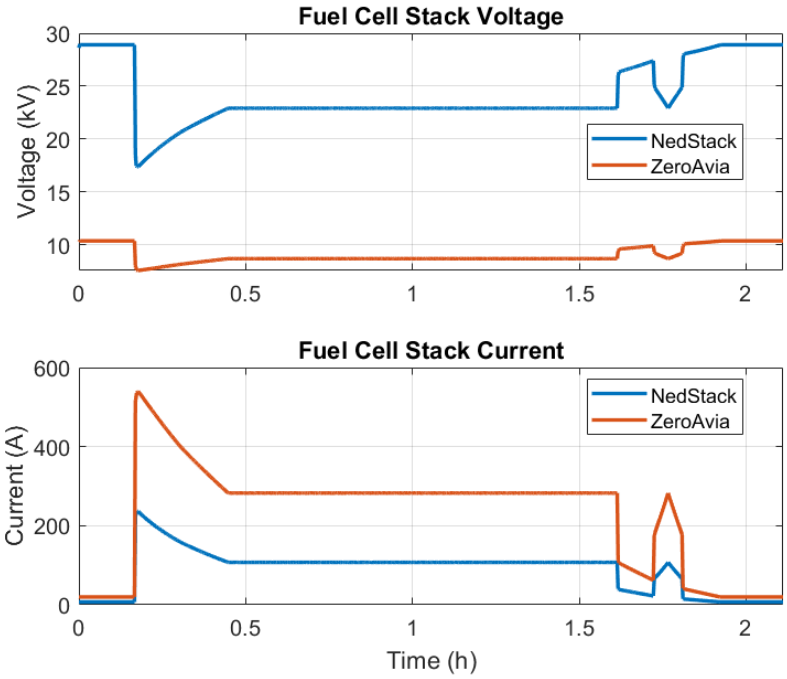

Figure 4.9: Voltage and current generated by the fuel cell stack during the mission.

by filling, in the initial phases of flight, the 15L tank generally present on this type of aircraft. This strategy can avoid dispersing water at low altitudes near the departure airport, considering this architecture produces about 2.3 litres of water per kilometre. The oxygen consumed in this mission is about 1600 kg.

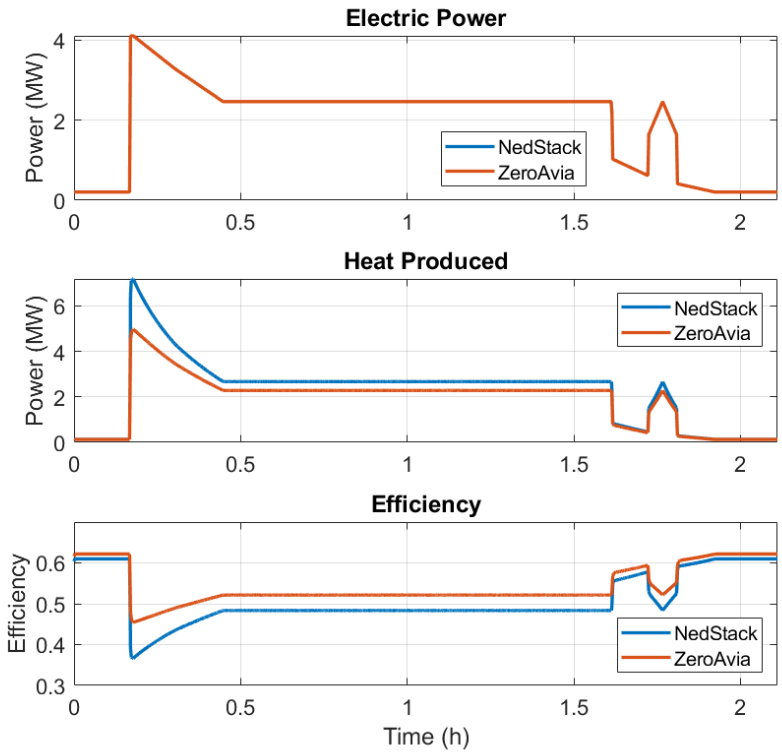

Figure 4.10: Comparison of electrical power and heat generated during the mission by the fuel cell in relation to the efficiency of the reaction process.

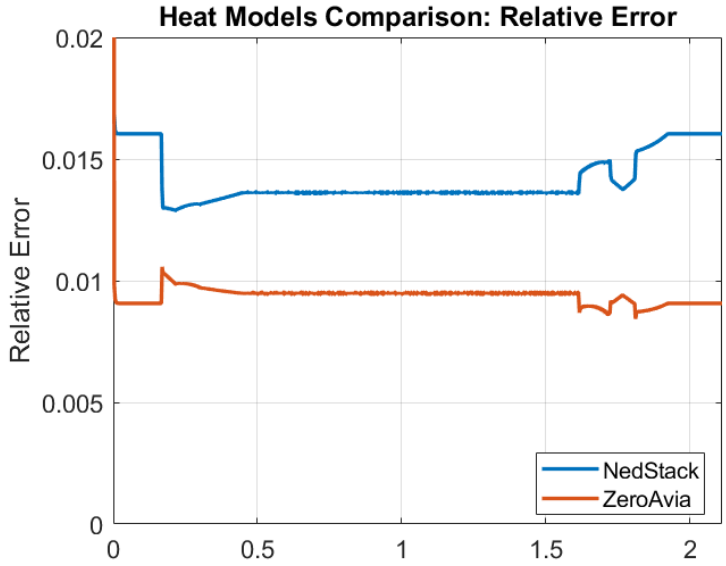

Figure 4.11: Comparison of simplified and detailed models of heat production.

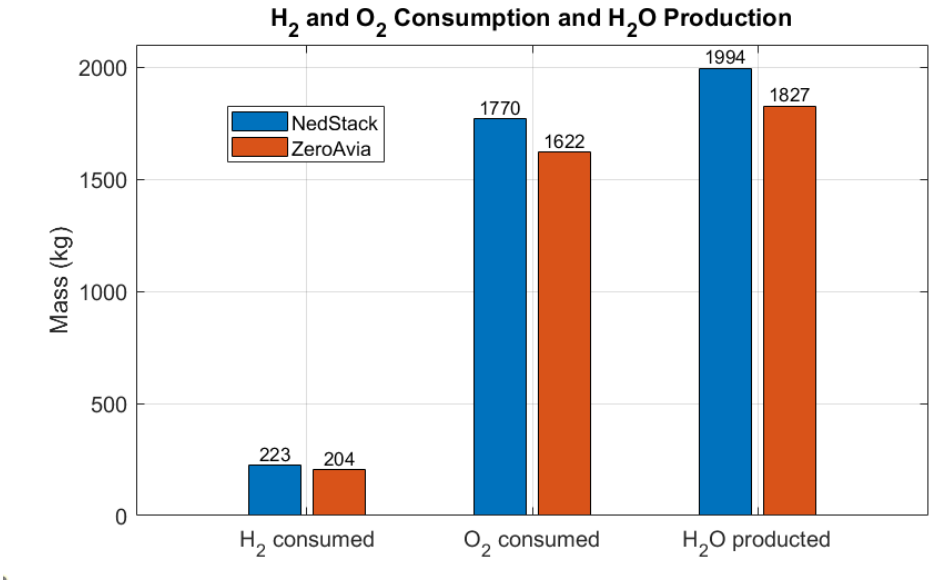

Figure 4.12: Hydrogen and oxygen consumption, water production.

Chapter 5

Conclusion

In this thesis, a mathematical model was developed in the OpenModelica environment to simulate fuel cell system architectures. The final chapter discusses the achievement of the goals set in Chapter 1, the limitations of the mathematical model, and future steps following this research.

5.1 Assessment of Objectives

Intermediate goals were set to realize a mathematical fuel cell model that is scalable and flexible for simulating aircraft electrical system architectures. Of these goals, most have been achieved:

1. An in-depth literature review was conducted for the two fuel cell models, PEMFC and SOFC. Multidimensional and simpler models using the equivalent circuit fuel cell representation were analyzed. Several examples of fuel cell application studies in the aeronautical field have been reviewed.

2. Once a reference model has been chosen, with characteristics such as easy scalability, ability to adapt to different configurations, and good computational speed, the model with Modelica is coded, making it acausal. The chosen model was corrected and revised, implementing the PEMFC simulation. The core of this model can be used for SOFC modelling, which, however, has not yet been done.

3. The mathematical model was validated with data from the polarization curves of some fuel cells on the market after creating a valuable database for collecting the performance of fuel cells applicable to mobility.

4. Different configurations of the Balance of Plant and the models of its devices were studied. A rudimentary Balance of Plant model was created in OpenModelica around the fuel cell stack model to make the simulation more realistic. The air circuit side was more developed. The cooling circuit was not modelled. This model receives data from the mission profile of an aircraft as input.

5. Finally, a case study of an aircraft with fuel cell propulsion architecture was defined and simulated. The mission profile was extended from work in the literature, and the results were discussed.

The objectives were generally followed and achieved, except for realizing the SOFC model. In addition, the rudimentary BoP model is insufficient to properly simulate this system's behaviours, primarily because of the absence of a cooling system.

5.2 Limitations of the Model

The model meets the accuracy requirements for use in the preliminary stages of aircraft design. The mathematical model was developed based on the work of Souleman et al. [42]. This work was modified to allow for an acausal configuration to connect the model with other parts of the BoP. Hydrogen circuits, from tanks, and air, from an air intake, can be connected to this block, which is made with Modelica. In addition, the fuel cell stack can be connected to an electrical load that can model all the devices that help stabilize the voltage for devices requiring electricity. Finally, a cooling circuit can be connected to this block as the fuel cell stack's heat production and thermal mass behaviour are modelled.

The model has some limitations. First of all, the block can simulate the behaviour of PEMFCs only, and the success of the simulation depends on the accuracy with which the parameters are chosen from the FC datasheet, especially those coming from the polarization curve provided by the fuel cell stack manufacturer. In addition, this model does not provide information on the hydration of the polymer membrane since the presence of a humidifier is considered to maintain the optimum humidity under all conditions. Finally, the BoP model has room for improvement, mainly regarding the thermodynamic conditions of exhaust gases. It must be remembered, however, that this model is necessary in the preliminary stages of an aeronautical project, where many physical characteristics of the devices are not necessary. Despite these limitations, the model can approximate polarization curves with an error of less than 5% and has room for improvement.

5.3 Future Steps

The PEMFC model has been implemented, but it is necessary to go deeper to improve it and make it more robust to different configurations. Future work includes model development for SOFC, improvement of PEMFC modelling, and testing with other case studies.

This model can be converted for SOFC simulation, as this device can substantially impact aviation due to its previously described strengths. The core of the model is developed to describe the behaviour of different types of fuel cells, requiring a modification only to the acausal interface and to the fluid models present in the anode and cathode due to the different compositions in using SOFC. Although the model includes fuel cells operating at temperatures above 100°C, more study of the phenomena affecting fluids at high temperatures is needed.

To conclude, further refine and improve the BoP component models and explore advanced configurations for high-temperature fuel cells. Implementing refined control strategies for hydrogen and air flows within the simulations will enable a more detailed study of the parameters and dynamics. This includes accurately defining their properties and simulating phase changes where possible. In addition, with an improved ability to model fuel cells operating at elevated temperatures, investigations can focus on exploiting generated heat or hot exhaust gases to further optimize efficiency.

Appendix A

Consideration on Concentration Voltage Drop

The polarization curve shows the trend of the fuel cell voltage V_{cell} as the current density i_{cell} varies. Figure A.1a shows the polarization curve superimposed with the power density delivered at each current density $P_{cell} = V_{cell} \cdot i_{cell}$. The polarization curve can be converted into the efficiency v curve, obtaining the trend illustrated in Figure A.1b.

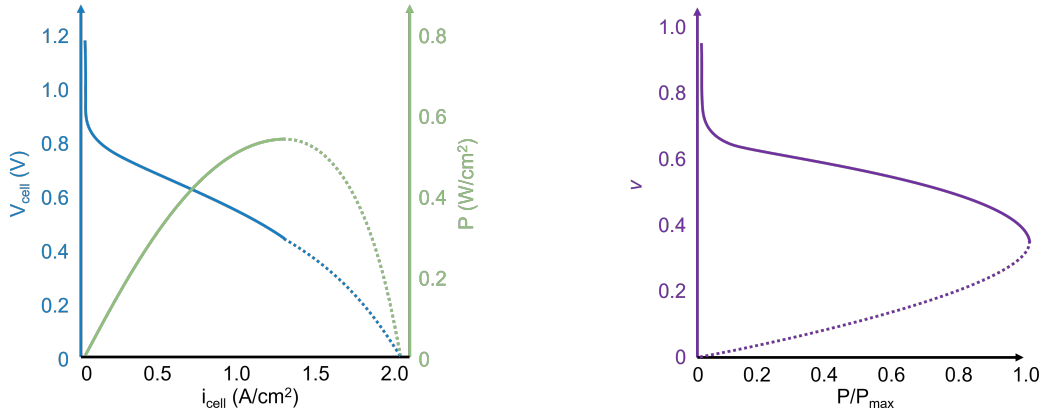

(a) Polarization curve (blue). Power curve (green).

(b) Cell efficiency versus normalized cell power.

Figure A.1: Efficiency considerations of a PEMFC. The dotted line marks the neglected part of the mathematical model. Adapted from [58]

This last curve shows two stability points (bistable curve) for the same power delivered, corresponding to different efficiencies. The points with the highest efficiency are then chosen, i.e. the branch of the polarization curve before reaching the maximum power. In the part considered (solid line), the losses are due to the activation energy and the ohmic resistance. Concentration and mass transport losses come into play in the excluded part (dotted line). In modeling the fuel cell for real applications, high efficiency is maintained by neglecting current densities higher than those related to maximum power. Furthermore, an attempt is made to oversize the fuel cell to use it in greater efficiency conditions. For further information, see the work of Kadyk et al. [58].

Appendix B

Introduction to Modelica

Modelica is an equation-based, object-oriented language for complex and dynamic applications. Modelica is structured to implement acausal models, that is, modelling with no direct correlation or path between input and output variables. However, causality is specified only when the system equations are solved. This allows for better reuse of system components. For example, Figure B.1 compares an acausal model of an RLC electrical circuit (on the left) and its causal representation employing equations and block diagram (on the right). In the first case, there is an overall view of the components of the system, with each piece of information visible, whereas in the second case, the scheme is difficult to understand, and the inputs and outputs are well defined.

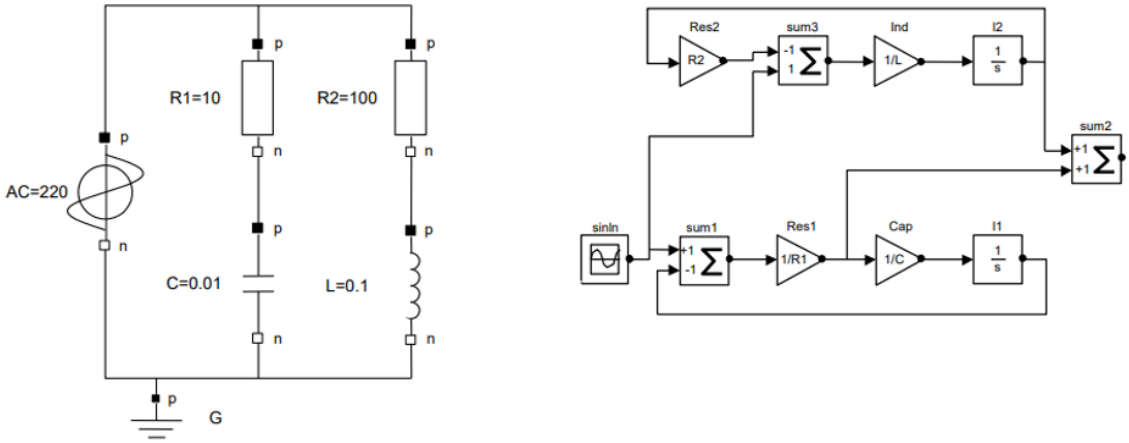

Figure B.1: Comparison between an acausal model (on the left) and a causal model (on the right). Source [27].

The development environment identified is OpenModelica, a free and open-source software developed by the Open Source Modelica Consortium. Modelica is a complex programming language with many facets to optimize its use. In this section, only the essential elements to understand the fuel cell stack and Balance of the plant models will be addressed; for a better and more in-depth explanation, refer to [27].

A Modelica program is built from classes or models containing the declaration of variables and the equations of the system. Below is an example code depicting a mass-spring-damper system showing some major components of a Modelica model.

```
model System_mck
  Real x(start=0);                // mass displacement
  Real vx(start=0);               // mass speed
  Real F;                         // applied force
  parameter Real m=1, c=1, k=1; // system parameter
  parameter Real F0=1;            // maximum force
equation
  der(x)=vx;
  F=F0*sin(time);                 // force definition
  m*der(vx)+c*vx+k*x=F;           // force balance equation
end System_mck;
```

Listing B.1: Example's script of Modelica model.

In this example of Modelica code, the two distinct parts are as follows: the first part declares the system variables, and the second part states the equations. The mathematical model must have the same number of variables and equations to be determined. In this case, there are three real-type variables, representing body displacement, body velocity and applied force, and three equations.

The first two dynamic variables (or state variables) are initialized on a value with the command `start=0`. Variables can be of different types, such as `Boolean`, `Integer`, `Real`, or `String`. Conversely, constants can be created with the prefixes `constant` or `parameter`. The difference between the two types is that parameters can be modified through the graphical user interface tool of OpenModelica.

The three equations are written in the `equation` part of the script. In this part, the variable's order or position in the equation is not essential.

Each element of Modelica is defined within a class. There are different types of classes, depending on the specific use to be made of them. The `model` class used in the example is the most generic and general. A `block` class can also be found that maintains causality, as each connector must specify whether it is input or output. The same `connector` is a class that defines the interface between different components. Finally, another class used within the fuel cell stack model is the `record` class, which is used to declare a data structure.

In Modelica, a block representation of the system to be modeled is enabled, utilizing components that contain Modelica classes and can be connected through connectors, typically referred to as ports. Components are essential to the reusability of the model in different configurations. Connections correspond to real physical connections, such as fluid pipes, electrical cables or rotating shafts, or can be signals between blocks requiring some causality.

Acausal modelling is powerful because individual blocks can be reused in different contexts by changing the system architecture. A package called `Modelica`, or more commonly *Modelica Standard Library*, provides numerous models, functions and blocks for building models of complex and multi-physical systems. Four libraries are mainly used within the fuel cell stack model: `Modelica.Electrical`, `Modelica.Fluid`, `Modelica.Thermal`, and `Modelica.Blocks`.

Appendix C

Model Parameter and Fuel Cell Database

The fuel cell stack model exhibited in this thesis needs some parameters to be simulated. This appendix will define what parameters need to be entered within the block in OpenModelica, how to obtain these parameters through equations or by looking at the datasheet, a database created to collect and study the parameters of different types of PEMFCs, and finally, show the parameters used for the three model validations.

C.1 Parameter of the Model

The parameters within the model are distinguished between electrical parameters, which represent the polarization curve; fluid parameters, which show the nominal characteristics of the reactants; and thermal parameters, which are useful for the thermal model. Among the electrical parameters are:

- The number of cells N in series within the stack. This parameter is generally written in the datasheet, but if not, it can be calculated as an approximation through the equation:

$$N = \frac{2FV_{nom}}{\Delta h^0_{H2O(g)}\eta_{nom}} \tag{C.1}$$

  Where the different factors are explained below.

- The response time T_d is the time required to reach 95% of the desired value during a transient due to step input. If not present, it can be considered between 10 and 30 seconds for PEMFCs.

- The open-circuit voltage E_{oc} is often found in the datasheet but can be derived by observing the polarization curve for zero current.

- The voltage at unity current V_1 is obtained by analyzing the polarization curve found on the datasheet.

- The nominal voltage V_{nom} is often present throughout the datasheets; otherwise, it must be obtained from the polarization curve.

- The minimum voltage V_{min} corresponds to the maximum power output; it is important to remember that this model neglects the effects due to high currents beyond the maximum

power point. Therefore, if the polarization curve is more extensive, it is necessary to truncate it. It is also preferred that this point is still in the linear part of the ohmic losses.

- The maximum current I_{max} is derived with the same considerations as the minimum voltage.
- The rated current I_{nom} corresponds to the rated power point on the datasheet.

Among the fluid parameters are:

- The rated temperature T_{nom} expressed in *Kelvin*, obtained from the datasheet. This will be considered the temperature for exhaust gases.
- The nominal fuel cell efficiency η_{nom} for the LHV. A value between 0.45 and 0.55 can be considered if not present.
- The enthalpy of formation of water under standard conditions $\Delta h^0_{H2O(g)} = 241830$ J/mol.
- The nominal air pressure $P_{air,nom}$ at the fuel cell inlet expressed in *atm*. This value can be found in the datasheet; otherwise, atmospheric pressure is considered.
- The volumetric air flow rate $V_{air,nom}$ at rated conditions found on the datasheet and converted to litres per minute. If this value is absent, it can be derived from the mass flow velocity, considering a stoichiometric ratio of about $\lambda_{O2} = 1.8$.

$$\dot{m}_{air,nom} = \frac{NI_{nom}\lambda_{O2}M_{air}}{4Fy_{nom}} \tag{C.2}$$

$$\dot{V}_{air,nom} = \frac{60000 \text{ dm}^3 \text{ s}/(\text{m}^3 \text{ min}) \cdot 287.05 \text{ J}/(\text{kg K}) \, \dot{m}_{air,nom}T_{nom}}{P_{air,nom} \cdot 101325 \text{ Pa/atm}} \tag{C.3}$$

- The nominal fuel pressure $P_{fuel,nom}$ is a value on the datasheet, usually in a certain range, expressed in *atm*.
- The nominal concentration of hydrogen x_{nom} in the fuel corresponds to the molar fraction; if not present, it can be considered unitary.
- The nominal oxygen concentration in air y_{nom} is the molar fraction equal to about 0.21.

Thermal parameters include:

- The specific heat capacity of the fuel cell stack c_p, which can be calculated by knowing the thickness t_i, the surface area A_i, and the density ρ_i of the individual layers of the fuel cell and their specific heat capacity $c_{p,i}$:

$$c_p = \frac{\sum_i c_{p,i} \cdot t_i \cdot A_i \cdot \rho_i}{\sum_i t_i \cdot A_i \cdot \rho_i} \tag{C.4}$$

  An example is shown in Table C.1. Or by considering a value between 1000 and 1300 J/(kg K) [82, 83].
- The total mass M of the fuel cell stack on the datasheet.
- The initial ambient temperature T_{start}.

	Anode Side					Cathode Side				
	BPP	**GC**	**GDL**	**CL**	**MEM**	**CL**	**GDL**	**GC**	**BPP**	**Unit**
Density	1850	0.084	440	3212	1771	3212	440	0.084	1850	kg/m^3
Specific Heat Capacity	1200	14290	840	1528	4189	1528	840	14290	1200	$\frac{J}{kg\ K}$
Thickness	2	2	0.3	0.03	0.1	0.03	0.3	2	2	μm

Table C.1: Parameters for calculating the specific heat capacity of a PEMFC. Adapted from [82]

C.2 PEMFC Dataset

The data needed for the PEMFC model are obtained from the datasheet from the fuel cell stack. Therefore, fuel cell datasheets were collected to study their performance at different sizes. Tables C.2, C.3, C.4, and C.5 show the database obtained through the study of fuel cell datasheets for mobility applications from the following companies: H3 Dynamics, Plug Power, Intelligent Energy, Ballard, Horizon Fuel Cell Technologies, Cummins inc., and Nuvera.
This collection of data, in addition to helping to select parameters for simulation, is interesting in understanding the performance of these devices' characteristics as power changes. Indeed, it is important to know their size and weight to study the integration of fuel cell stacks inside aircraft.

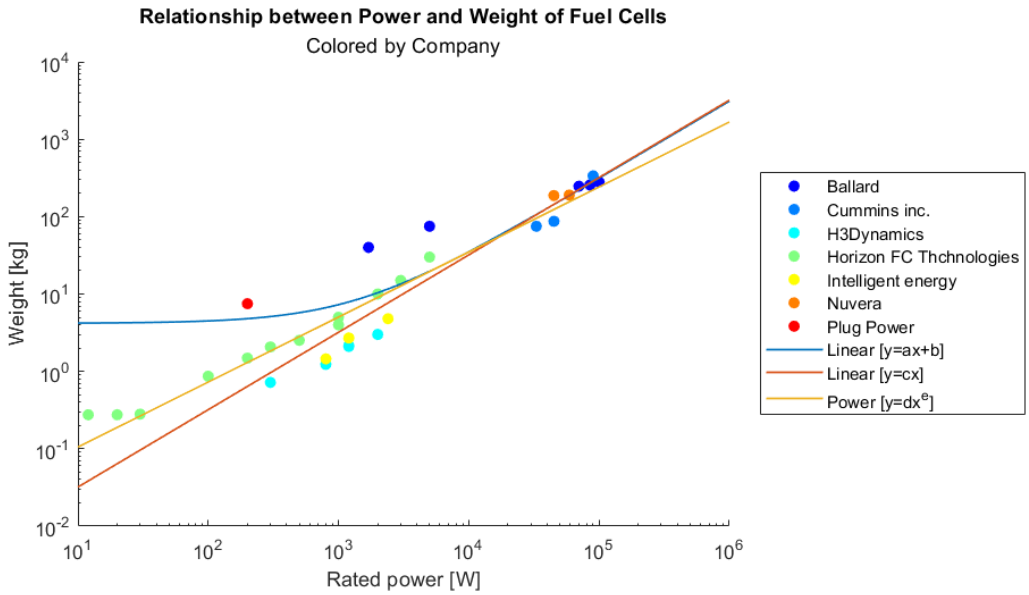

Figure C.1: Analysis of the relationship between weight and nominal power for different types of fuel cells.

First, the weight trend as the fuel cell power rating changes was studied. Figure C.1 shows the collected fuel cells coloured according to the manufacturer. It can be seen that there are trends according to different companies, as they may use criteria to scale the fuel cells. Three trend lines obtained by averaging the least squares method are shown in this data. The functions describing these lines can assist in determining the weight of a fictitious fuel cell being analyzed. However, it must be remembered that this trend is in the range of a maximum of 100kW. The three lines

represent three different functions describing the trend: two linear and one exponential. The functions are expressed as (followed by the coefficient of determination R^2):

$$y_1 = 0.0031x + 4.18 \quad (R^2 = 0.95) \tag{C.5}$$

$$y_2 = 0.0032x \quad (R^2 = 0.96) \tag{C.6}$$

$$y_3 = 0.0152x^{0.84} \quad (R^2 = 0.95) \tag{C.7}$$

The curves all have a high coefficient of determination. Nonetheless, it is possible that a single curve may not correctly represent the weight trend as a function of power for each power.

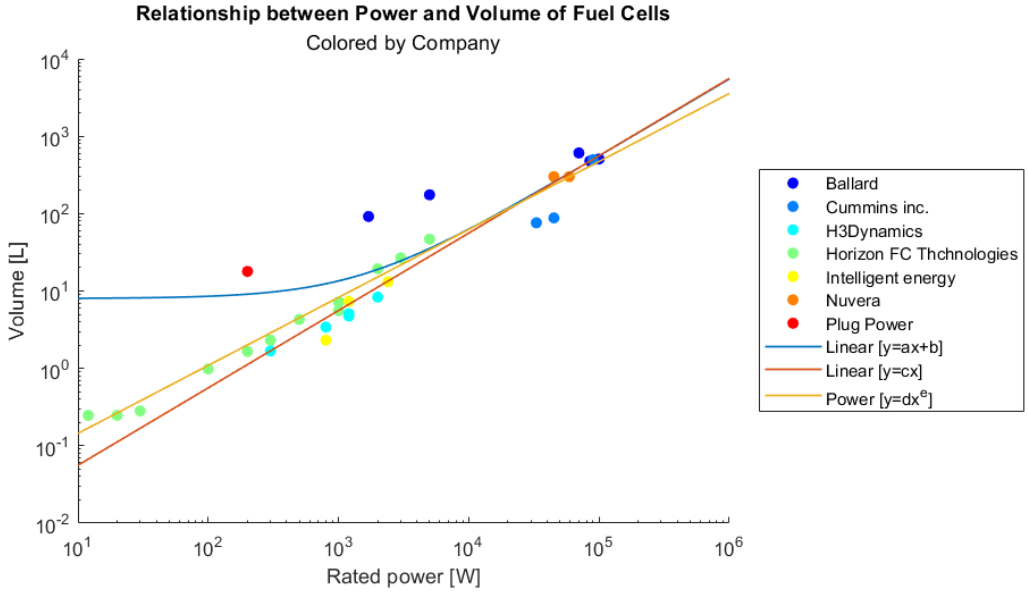

Figure C.2: Analysis of the relationship between volume and nominal power for different types of fuel cells.

Next, the volume trend as the fuel cell power rating changes was similarly studied. Figure C.2 shows the collected fuel cells coloured according to the manufacturer company. It can be seen that, again, trends are depending on the different companies. The three trend lines are expressed as (followed by the coefficient of determination R2):

$$y_1 = 0.0055x + 8 \quad (R^2 = 0.88) \tag{C.8}$$

$$y_2 = 0.0056x \quad (R^2 = 0.91) \tag{C.9}$$

$$y_3 = 0.0191x^{0.88} \quad (R^2 = 0.88) \tag{C.10}$$

The curves all have a high coefficient of determination, but the one that best represents the total trend is the linear one that intercepts the origin. Nonetheless, it is possible that a single curve may not correctly represent the weight trend as a function of power for each power.
This data collection may, therefore, be necessary for studying the application of fuel cells in aviation. However, it still needs to be updated to consider PEMFCs with higher power or other types of fuel cells, such as SOFCs. Some fuel cells in this database were used to validate the mathematical model described in this thesis.

Name	**Company**	**Number of cells**	**Rated power [W]**	**Max power [W]**	**Voltage [V]**	**Current [A]**
A-2000	H3Dynamics	55	2000	2200	33-53	0-60
A-1200 HV	H3Dynamics	65	1200	1400	39-61.8	0-32
A-1200 LV	H3Dynamics	50	1200	1400	32-47.5	0-47
A-800	H3Dynamics	45	800	1000	27-42.8	0-30
A-300	H3Dynamics	37	300	350	22.2-35.2	0-13
IE-SOAR 2.4kW	Intelligent energy		2400			
IE-SOAR 1.2kW	Intelligent energy		1200			
IE-SOAR 800 W	Intelligent energy		800		24-48	
FCmove-HD	Ballard		70000		250-500	20-240
FCveloCity-HD85	Ballard		85000		260-419	10-284
FCveloCity-HD100	Ballard		100000		357-577	10-257
FCgen-H2PM	Ballard		1700		47-57	
FCgen-H2PM	Ballard		5000		48-55	
Gensure E-200	Plug Power		200			
H-12	Horizon FC Technologies	13	12		7.0-12.0	0-2
H-20	Horizon FC Technologies	13	20		7.0-12	0-3.4
H-30	Horizon FC Technologies	14	30		8.0-14	0-4.2
H-100	Horizon FC Technologies	16	100		8.0-15	0-12.0
H-200	Horizon FC Technologies	32	200		16-30	0-12
H-300	Horizon FC Technologies	48	300		24-46	0-12
H-500	Horizon FC Technologies	24	500		12.0-23	0-42
H-1000	Horizon FC Technologies	48	1000		24-46	0-42
H-1000XP	Horizon FC Technologies	50	1000		29-45	0-40
H-2000	Horizon FC Technologies	48	2000		24-45	0-80
H-3000	Horizon FC Technologies	72	3000		36-65	0-80
H-5000	Horizon FC Technologies	120	5000		60-110	0-80
HD 30	Cummins inc.		33000		60-120	0-500
HD 45	Cummins inc.		45000		88-180	0-450
HD 90	Cummins inc.		90000		176-360	0-450
E-45-HD	Nuvera		45000		170-290	0-312.5
E-60-HD	Nuvera		59000		175-290	0-375

Table C.2: Dataset of Proton Exchange Membrane Fuel Cell (Part 1)

Name	**Weight [kg]**	**Specific power [W/kg]**	**Power density [W/L]**	**Volume [L]**	**Cooling**	**Air input temperature [°C]**
A-2000	3	667	240	8.338	Air	0-40
A-1200 HV	2.1	570	252	4.755	Air	0-40
A-1200 LV	2.15	560	236	5.067	Air	0-40
A-800	1.23	645	235	3.422	Air	0-40
A-300	0.72	486	208	1.681	Air	0-40
IE-SOAR 2.4kW	4.8	500	182	13.18		
IE-SOAR 1.2kW	2.7	444	163	7.34		
IE-SOAR 800 W	1.45	552	346	2.315		
FCmove-HD	247	283	115	608.2	Ethylene glycol	
FCveloCity-HD85	256	332	178	478.2		
FCveloCity-HD100	280	357	197	507.8		
FCgen-H2PM	40	43	19	91.8		
FCgen-H2PM	75	67	29	174.9		
Gensure E-200	7.5	27	11	17.9		
H-12	0.275	44	49	0.2468	Air	5.0-30
H-20	0.275	73	81	0.2468	Air	5.0-30
H-30	0.28	107	106	0.282	Air	5.0-30
H-100	0.865	116	102	0.9814	Air	5.0-30
H-200	1.485	135	121	1.657	Air	5.0-30
H-300	2.07	145	129	2.323	Air	5.0-30
H-500	2.52	198	117	4.285	Air	5.0-30
H-1000	4	250	139	7.219	Air	5.0-30
H-1000XP	5	200	179	5.574	Air	5.0-35
H-2000	10	200	103	19.41	Air	5.0-30
H-3000	15	200	112	26.77	Air	5.0-30
H-5000	30	167	107	46.75	Air	5.0-30
HD 30	75	440	434	76	De-ionized water or glycol mix	
HD 45	87	517	511	88		
HD 90	336	268	181	498		
E-45-HD	187	241	150	300	De-ionized water or glycol mix	
E-60-HD	190	311	197	300	De-ionized water or glycol mix	

Table C.3: Dataset of Proton Exchange Membrane Fuel Cell (Part 2)

Name	**H2 input presssure [bar]**	**H2 purity required [%]**	**Fuel max consump. [L/min]**	**Start-up time [s]**	**Voltage at 0A [V]**
A-2000	0.6-0.8	99.998	21	20	51
A-1200 HV	0.6-0.8	99.998	12.5	20	61
A-1200 LV	0.6-0.8	99.998	12.5	20	47
A-800	0.6-0.9	99.998	8.3	20	42
A-300	0.6-0.9	99.998	3.1	20	35
IE-SOAR 2.4kW					
IE-SOAR 1.2kW					
IE-SOAR 800 W					
FCmove-HD					500
FCveloCity-HD85					419
FCveloCity-HD100					577
FCgen-H2PM		99.95			57
FCgen-H2PM					55
Gensure E-200					
H-12	0.45-0.55	99.995	0.18	30	12
H-20	0.45-0.55	99.995	0.28	30	12
H-30	0.45-0.55	99.995	0.42	30	14
H-100	0.45-0.55	99.995	1.3	30	15
H-200	0.45-0.55	99.995	2.6	30	30
H-300	0.45-0.55	99.995	3.9	30	46
H-500	0.45-0.55	99.995	6.5	30	23
H-1000	0.45-0.55	99.995	13	30	46
H-1000XP	0.45-0.55	99.995	12.5	30	45
H-2000	0.45-0.55	99.995	26	30	45
H-3000	0.45-0.55	99.995	39	30	65
H-5000	0.45-0.55	99.995	65	30	110
HD 30		99.98			
HD 45					
HD 90					
E-45-HD	12.5-15				
E-60-HD	12.5-15				

Table C.4: Dataset of Proton Exchange Membrane Fuel Cell (Part 3)

Name	**Voltage at 1A [V]**	**Operat. current [A]**	**Operat. Voltage [V]**	**Max. current [A]**	**Min. voltage [V]**
A-2000	50	53	37	72	35
A-1200 HV	60	26	48	32	46
A-1200 LV	45	35	35	46	33
A-800	41	24	33	29	31
A-300	35	10	30	11	29
IE-SOAR 2.4kW					
IE-SOAR 1.2kW					
IE-SOAR 800 W					
FCmove-HD	500			40	250
FCveloCity-HD85	418			284	260
FCveloCity-HD100	576			257	357
FCgen-H2PM	56	35	48	38	47
FCgen-H2PM	54	104	48	105	48
Gensure E-200					
H-12	9	1.5	7	2	7
H-20	10	2.6	7.8	3.4	7
H-30	12	3.6	8.4	4.2	8
H-100	14	10.4	9.6	12	8
H-200	28	10.4	19.2	12	16
H-300	40	10.4	28.8	12	24
H-500	22	35	14.4	42	12
H-1000	44	35	28.8	42	24
H-1000XP	44	33.5	30	50	25
H-2000	44	70	28.8	80	24
H-3000	64	70	43.2	80	36
H-5000	105	70	72	80	60
HD 30					
HD 45					
HD 90					
E-45-HD					
E-60-HD					

Table C.5: Dataset of Proton Exchange Membrane Fuel Cell (Part 4)

C.3 Parameter for Validation

To validate the mathematical model, as described in Section 3.4, three different fuel cells are used. Table C.6 gives the parameters for performing these validations. Article [42] provides more information on extrapolating these values from datasheets.

	NedStack P8 PS6	Horizon H5000	Horizon H1000XP	*Unit*
N	65	120	50	
T_d	10	20	30	s
E_{oc}	65	110	46	V
V_1	63	108	44	V
V_{nom}	45	95	35	V
V_{min}	37	83	31	V
I_{max}	225	60	38	A
I_{nom}	133.3	33	30	A
T_{nom}	338	333	338	K
η_{nom}	0.55	0.4	0.45	
$P_{air,nom}$	1	1	1	atm
$V_{air,nom}$	320	144	55.4	l/min
$P_{fuel,nom}$	1.5	0.65	0.55	atm
x_{nom}	1	1	1	
y_{nom}	0.21	0.21	0.21	
c_p	1300	1300	1300	$J/(kg\ K)$
M	80	30	30	kg
T_{start}	300	300	300	K
$\dot{m}_{flow,air}$	9.41	4.63	1.22	g/s
$\dot{m}_{flow,fuel}$	0.117	0.0966	0.0203	g/s

Table C.6: Data used for model validation with different fuel cells.

Appendix D

Data for the Case Study

This appendix provides the main data for running the case study simulation. The data used to create the mission profile, the parameters of the two fuel cells compared, and the methodology used to obtain these parameters in the absence of the polarization curve are shown.

D.1 Mission Profile

Table D.1 shows the parameters of the mission profile considered in the Milan-Barcelona route (Figure D.1). This table represents, for some key moments of time, the power required from the propulsion system, the flight altitude, the speed and the distance travelled up to that moment.

Time (s)	**Power (W)**	**Altitude (m)**	**Speed (m/s)**	**Range (m)**
0	205000	0	0	0
600	205000	0	0	0
610	4100000	0	0	0
640	4100000	0	55.556	833.333
1090	3280000	4500	97.222	35208.333
1610	2460000	6000	144.444	98041.667
5810	2460000	6000	144.444	704708.333
5820	1025000	6000	141.667	706138.889
6200	615000	1000	80.556	748361.111
6210	1640000	1000	80.5556	749166.667
6360	2460000	1000	83.333	761458.333
6510	1640000	1000	86.111	774166.667
6520	410000	1000	94.444	775069.445
6920	205000	0	0	793958.334
7600	205000	0	0	793958.334

Table D.1: Case study mission profile data. Adapted from: [15]

D.2 First Fuel Cell Stack Data

The case study compares the results of two fictitious fuel cells obtained by scaling two real fuel cells with different performances. The first is an older, low-performance fuel cell. The second is a modern fuel cell stack developed for aeronautical applications.

Figure D.1: Flight route Milan-Barcelona of the case study.

The first fuel cell stack was obtained by scaling the one used in the validation phase, called NedStack P8 PS6. The latter is a very old device that is far from the current state of the art, as it has a low power density. The maximum power of this device is:

$$P_{max} = 225A \cdot 37V = 8325W \tag{D.1}$$

Therefore, to reach the maximum power required by the mission profile (4.1 MW), it is necessary to scale the fuel cell by a factor:

$$\phi = \frac{4.1MW}{8325W} = 492.5 \tag{D.2}$$

The results are shown in Table D.2 and used in the simulation.

D.3 Second Fuel Cell Stack Data

The second fuel cell stack is ZeroAvia's product called Superstack [79]. This FC has advanced performance for its product class. For this low-temperature PEMFC, the datasheet only has some necessary values, and the complete polarization curve is absent. However, knowing the complete polarization curve is essential before inserting the data into the model. Therefore, a strategy was implemented to draw the polarization curve starting from the data provided and from the experience of reading the polarization curves on the market. In particular, in the datasheet, only the two extreme points of the polarization curve and the maximum power delivered are present. Starting from this data, a polarization curve that is as realistic as possible is sought.

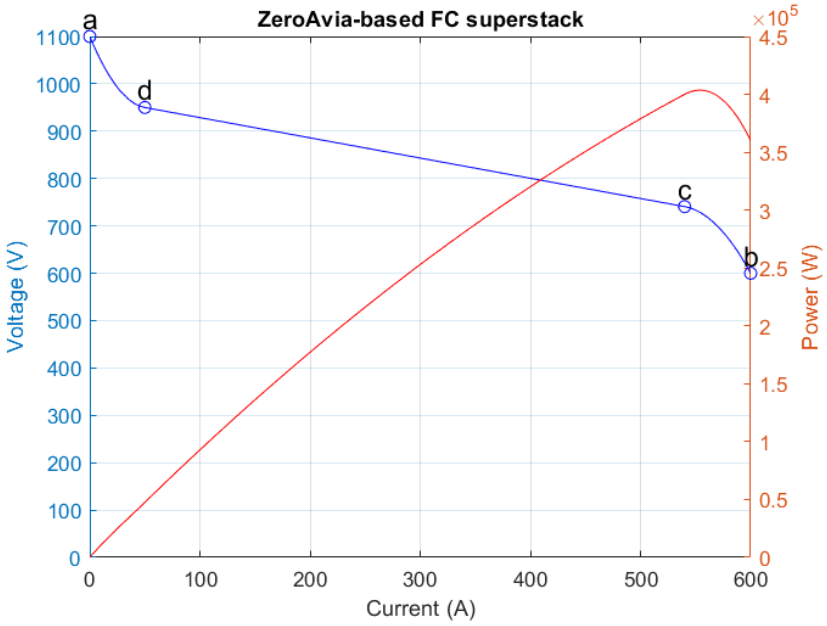

Figure D.2: Reference for finding the ZeroAvia polarization curve.

To obtain this curve, referring to Figure D.2, start by positioning the two endpoints in a Cartesian graph, corresponding to a) zero current and maximum voltage (1100 Volts) and b) maximum current (600 Amperes) and minimum voltage (600 Volts). The maximum power delivered is equal to 400 kW, which is higher than the power delivered at the end point b), which is equal to

$$P_{I_{max}} = I_{max} \cdot V_{min} = 360kW \tag{D.3}$$

By observing the power-current curve shown in figure A.1a, and assuming that the maximum power is reached in the range shown in the datasheet (0-600 Amperes), it can be deduced that the maximum power point c) is before point b), which is in the curve portion with a negative slope of the power, corresponding to the losses due to mass transport. To correctly identify point c), it is necessary to find all the points that satisfy the condition

$$I_c \cdot V_c = 400kW \tag{D.4}$$

$$V_c = \frac{400kW}{I_c} \tag{D.5}$$

and on this branch of hyperbola, it will be possible to choose the optimal point.

The polarization curve is hypothesized as a function defined in segments, which, for simplicity, are a parabolic segment between point a) and point d) defined subsequently, a linear segment between point d) and c), and finally, a parabolic segment between point c) and b). To define the three functions, start with the linear section, choosing point d) in a manner consistent with other polarization curves on the market (remember that it is an approximate curve), which also provides an estimate of the slope of this curve, around $-0.4 : -0.5$.

After defining this curve, the coefficients representing the two parabola branches are determined by satisfying the passage conditions for the endpoints and tangency with the linear curve. At the end of this procedure, a very rudimentary polarization curve is obtained, which makes it possible to vary the position of point c) along the hyperbola branch to satisfy the maximum power condition.

To remove this last degree of freedom, the power curve is represented as a current function, and an attempt is made to obtain a curve by varying point c), such that the maximum power is around 400kW and not too sharp around this point. For example, the power increases beyond the maximum value for low current values, while the curve tends to behave sharply for high values. The current value of point c) is then chosen, and the polarization curve based on the ZeroAvia Superstack data can be used within the model, dutifully scaled. The data obtained and those scaled by a factor $\phi = 10.25$ (used in the simulation) are shown in Table D.2. The process was carried out using the following MATLAB script.

```
%ZEROAVIA polarization curve
close all
clear
clc

% Definition of the main points
X3=540; % Variable abscissa of the maximum power point
P1 = [0,1100]; % Endpoint a)
P2 = [50,950]; % Point defined by analogy with other polarization curves.
     Also called d)
P3 = [X3,400000/X3]; % Maximum power point, variable with X3. Also called
     c)
P4 = [600,600]; % Endpoint b)

% Vectors for graphic representation of the three parts of the curve
x1=P1(1):P2(1);
x2=P2(1):P3(1);
x3=P3(1):P4(1);

% Linear curve definition between points d) and c)
lin = @(x) (x-P2(1))*(P3(2)-P2(2))/(P3(1)-P2(1))+P2(2); % Definition of
    the equation of a straight line passing through two points.
y2 = lin(x2);
a=(P3(2)-P2(2))/(P3(1)-P2(1)); % Slope of the straight line

% Definition of the functions of the two parabolas that satisfy the
    requirements.
parab = @(coeff,x) coeff(1)*x.^2 + coeff(2)*x + coeff(3); % Parabola
    function
A = @(x1,x2,x3d) [x1^2 x1 1;x2^2 x2 1;2*x3d 1 0];
b = @(y1,y2,y3d) [y1;y2;y3d];
c1 = A(P1(1),P2(1),P2(1))\b(P1(2),P2(2),a); % Calculation of parabola
    coefficients between a) and d)
c2 = A(P3(1),P4(1),P3(1))\b(P3(2),P4(2),a); % Calculation of parabola
    coefficients between c) and b)
y1 = parab(c1,x1);
y3 = parab(c2,x3);

% Representation of the polarization curve
yyaxis left;
plot(x2,y2,'-b')
hold on
plot(x1,y1,'-b')
plot(x3,y3,'-b')
grid on
```

```
xlabel('Current (A)');
ylabel('Voltage (V)');
ylim([0,1100])

% Representation of the power curve
yyaxis right;
Pow1 =x1.*y1;
Pow2 =x2.*y2;
Pow3 =x3.*y3;
plot(x1,Pow1,'-r',x2,Pow2,'-r',x3,Pow3,'-r')
ylabel('Power (W)');
title("ZeroAvia-based FC superstack")
```

Listing D.1: Code to obtain the polarization curve of the ZeroAvia Superstack

Table D.2: FC stack parameters for the case study

	NedStack P8 PS6	NedStack P8 PS6 Scaled Up	ZeroAvia Superstack	ZeroAvia Superstack Scaled Up	*Unit*
N	65	32010	1100	11275	
T_d	10	10	20	20	s
E_{oc}	65	32010	1100	11275	V
V_1	63	31030	1094	11213.5	V
V_{nom}	45	22160	848	8692	V
V_{min}	37	18220	740	7585	V
I_{max}	225	225	540	540	A
I_{nom}	133.3	133.3	287	287	A
T_{nom}	338	338	360	360	K
η_{nom}	0.55	0.55	0.55	0.55	
$P_{air,nom}$	1	1	1	1	atm
$V_{air,nom}$	320	157600	8285	84919	l/min
$P_{fuel,nom}$	1.5	1.5	1	1	atm
x_{nom}	1	1	1	1	
y_{nom}	0.21	0.21	0.21	0.21	
c_p	1300	1300	1300	1300	$J/(kg\ K)$
M	80	39400	190	1950	kg
T_{start}	300	300	300	300	K
$\dot{m}_{flow,air}$	0.00941	4.634	0.381	3.91	kg/s
$\dot{m}_{flow,fuel}$	0.000117	0.0576	0.00563	0.0577	kg/s

Bibliography

[1] *Aviation Benefits Report 2019*. 2019. URL: https://www.icao.int/sustainability/Documents/AVIATION-BENEFITS-2019-web.pdf (visited on 04/10/2024).

[2] Mission Possible Partnership. *Making Net-Zero Aviation possible*. 2022. URL: https://missionpossiblepartnership.org/wp-content/uploads/2023/01/Making-Net-Zero-Aviation-possible.pdf (visited on 04/10/2024).

[3] IATA. *Executive Summary - Net Zero Roadmaps*. 2022. URL: https://www.iata.org/contentassets/8d19e716636a47c184e7221c77563c93/executive-summary---net-zero-roadmaps.pdf (visited on 04/10/2024).

[4] IATA. *Aircraft Technology Net Zero Roadmab*. 2023. URL: https://www.iata.org/contentassets/8d19e716636a47c184e7221c77563c93/aircraft-technology-net-zero-roadmap.pdf (visited on 04/10/2024).

[5] European Aviation Safety Agency. and European Environment Agency. *European aviation environmental report 2019.* LU: Publications Office, 2019. URL: https://data.europa.eu/doi/10.2822/309946 (visited on 05/07/2024).

[6] European Aviation Safety Agency. and European Environment Agency. *European aviation environmental report 2022*. LU: Publications Office, 2022. URL: https://www.easa.europa.eu/eco/sites/default/files/2023-02/230217_EASA%20EAER%202022.pdf (visited on 05/07/2024).

[7] Benjamin J. Brelje and Joaquim R. R. A. Martins. "Electric, hybrid, and turboelectric fixed-wing aircraft: A review of concepts, models, and design approaches". In: *Progress in Aerospace Sciences* 104 (Jan. 1, 2019), pp. 1–19. ISSN: 0376-0421. DOI: 10.1016/j.paerosci.2018.06.004. URL: https://www.sciencedirect.com/science/article/pii/S0376042118300356 (visited on 04/11/2024).

[8] Ibrahim Dincer. "Green methods for hydrogen production". In: *International Journal of Hydrogen Energy*. 10th International Conference on Clean Energy 2010 37.2 (Jan. 1, 2012), pp. 1954–1971. ISSN: 0360-3199. DOI: 10.1016/j.ijhydene.2011.03.173. URL: https://www.sciencedirect.com/science/article/pii/S0360319911019823 (visited on 04/11/2024).

[9] Eytan Adler and Joaquim Martins. *Hydrogen-Powered Aircraft: Fundamental Concepts, Key Technologies, and Environmental Impacts*. July 1, 2023.

[10] Talal Yusaf et al. "Sustainable hydrogen energy in aviation – A narrative review". In: *International Journal of Hydrogen Energy* 52 (Jan. 2, 2024), pp. 1026–1045. ISSN: 0360-3199. DOI: 10.1016/j.ijhydene.2023.02.086. URL: https://www.sciencedirect.com/science/article/pii/S0360319923009187 (visited on 04/23/2024).

[11] Adam Reiman. "AMC's Hydrogen Future: Sustainable Air Mobility". PhD thesis. June 1, 2009. 116 pp.

[12] Kate Barabanova. *ZeroAvia and PowerCell sign deal for serial delivery of LTPEM hydrogen fuel cell stacks*. ZeroAvia. Oct. 5, 2022. URL: https://zeroavia.com/powercell-mou/ (visited on 01/06/2024).

[13] Kate Barabanova. *ZeroAvia Successfully Completes Initial Dornier 228 Flight Test Campaign*. ZeroAvia. July 19, 2023. URL: https://zeroavia.com/complete-flight-test/ (visited on 01/06/2024).

[14] Hanneke Weitering and 2023 March 3. *Universal Hydrogen Flies Hydrogen-Powered Dash 8*. FutureFlight. URL: https://www.futureflight.aero/news-article/2023-03-02/universal-hydrogen-flies-hydrogen-powered-dash-8 (visited on 01/06/2024).

[15] Christian Hartmann et al. "Dual Use of Liquid Hydrogen in a Next-Generation PEMFC-Powered Regional Aircraft With Superconducting Propulsion". In: *IEEE Transactions on Transportation Electrification* 8.4 (Dec. 2022). Conference Name: IEEE Transactions on Transportation Electrification, pp. 4760–4778. ISSN: 2332-7782. DOI: 10.1109/TTE.2022.3170827. URL: https://ieeexplore.ieee.org/document/9765468 (visited on 12/15/2023).

[16] G. Daniel Brewer. *Hydrogen aircraft technology*. Boca Raton: CRC Press, 1991. 430 pp. ISBN: 978-0-8493-5838-8.

[17] Rolls Royce. *Leading the transition to net zero carbon*. 2021. URL: https://www.rolls-royce.com/~/media/Files/R/Rolls-Royce/documents/others/rr-net-zero-full-report.pdf (visited on 05/30/2024).

[18] Marty Bradley. "Identification and Descriptions of Fuel Cell Architectures for Aircraft Applications". In: *2022 IEEE Transportation Electrification Conference & Expo (ITEC)*. 2022 IEEE/AIAA Transportation Electrification Conference and Electric Aircraft Technologies Symposium (ITEC+EATS). Anaheim, CA, USA: IEEE, June 15, 2022, pp. 1047–1050. ISBN: 978-1-66540-560-7. DOI: 10.1109/ITEC53557.2022.9814063. URL: https://ieeexplore.ieee.org/document/9814063/ (visited on 11/08/2023).

[19] *Fuel cell handbook*. Seventh edition. OCLC: 957455519. Morgantown, WV: U.S. Department of Energy, Office of Fossil Energy, National Energy Technology Laboratory, 2016. ISBN: 978-1-365-10113-7.

[20] Tino Vidović et al. "Proton-Exchange Membrane Fuel Cell Balance of Plant and Performance Simulation for Vehicle Applications". In: *Energies* 15.21 (Oct. 31, 2022), p. 8110. ISSN: 1996-1073. DOI: 10.3390/en15218110. URL: https://www.mdpi.com/1996-1073/15/21/8110 (visited on 11/22/2023).

[21] Jay T. Pukrushpan, Anna G. Stefanopoulou, and Huei Peng. *Control of fuel cell power systems: principles, modeling, analysis, and feedback design*. Advances in industrial control. London ; New York: Springer, 2004. 161 pp. ISBN: 978-1-85233-816-9.

[22] James Larminie and Andrew Dicks. *Fuel cell systems explained*. 2nd ed. New York: Wiley, 2003. ISBN: 978-0-470-84857-9.

[23] Mohammad Hashem Nehrir and Caisheng Wang. *Modeling and control of fuel cells: distributed generation applications*. IEEE Press series on power engineering. Hoboken, N.J: Wiley, 2009. 296 pp. ISBN: 978-0-470-23328-3.

[24] Tatiana Santos Andrade and Torbjörn Thiringer. "Low platinum fuel cell as enabler for the hydrogen fuel cell vehicle". In: *Journal of Power Sources* 598 (Apr. 2024), p. 234140. ISSN: 0378-7753. DOI: 10.1016/j.jpowsour.2024.234140. URL: https://www.sciencedirect.com/science/article/pii/S0378775324000910 (visited on 07/15/2024).

[25] M. Santarelli, M. Cabrera, and M. Calì. "Analysis of Solid Oxide Fuel Cell Systems for More-Electric Aircraft". In: *Journal of Aircraft* 46.1 (Jan. 2009), pp. 269–283. ISSN: 0021-8669, 1533-3868. DOI: 10.2514/1.38408. URL: https://arc.aiaa.org/doi/10.2514/1.38408 (visited on 11/08/2023).

[26] Catarina Mendonça, António Ferreira, and Diogo M. F. Santos. "Towards the Commercialization of Solid Oxide Fuel Cells: Recent Advances in Materials and Integration Strategies". In: *Fuels* 2.4 (Oct. 9, 2021), pp. 393–419. ISSN: 2673-3994. DOI: 10.3390/fuels2040023. URL: https://www.mdpi.com/2673-3994/2/4/23 (visited on 11/10/2023).

[27] Peter Fritzson. *Principles of Object-Oriented Modeling and Simulation with Modelica 3.3: A Cyber-Physical Approach — IEEE eBooks — IEEE Xplore*. 2015. URL: https://ieeexplore-ieee-org.lib-ezproxy.concordia.ca/book/7022515 (visited on 12/19/2023).

[28] Colleen Spiegel. *PEM fuel cell modeling and simulation using Matlab*. OCLC: 1033832673. Amsterdam: Academic Press/Elsevier, 2011. ISBN: 978-0-08-055901-8.

[29] Ilenia Rossetti. "Modelling of Fuel Cells and Related Energy Conversion Systems". In: *ChemEngineering* 6.3 (June 2022). Number: 3 Publisher: Multidisciplinary Digital Publishing Institute, p. 32. ISSN: 2305-7084. DOI: 10.3390/chemengineering6030032. URL: https://www.mdpi.com/2305-7084/6/3/32 (visited on 11/22/2023).

[30] E. A. Ticianelli et al. "Methods to Advance Technology of Proton Exchange Membrane Fuel Cells". In: *Journal of The Electrochemical Society* 135.9 (Sept. 1, 1988). Publisher: IOP Publishing, p. 2209. ISSN: 1945-7111. DOI: 10.1149/1.2096240. URL: https://iopscience.iop.org/article/10.1149/1.2096240/meta (visited on 05/14/2024).

[31] Dawn M. Bernardi. "Water-Balance Calculations for Solid-Polymer-Electrolyte Fuel Cells". In: *Journal of The Electrochemical Society* 137.11 (Nov. 1, 1990), pp. 3344–3350. ISSN: 0013-4651, 1945-7111. DOI: 10.1149/1.2086220. URL: https://iopscience.iop.org/article/10.1149/1.2086220 (visited on 01/03/2024).

[32] Dawn M. Bernardi and Mark W. Verbrugge. "Mathematical model of a gas diffusion electrode bonded to a polymer electrolyte". In: *AIChE Journal* 37.8 (1991), pp. 1151–1163. ISSN: 1547-5905. DOI: 10.1002/aic.690370805. URL: https://onlinelibrary.wiley.com/doi/abs/10.1002/aic.690370805 (visited on 01/04/2024).

[33] T. E. Springer, T. A. Zawodzinski, and S. Gottesfeld. "Polymer Electrolyte Fuel Cell Model". In: *Journal of The Electrochemical Society* 138.8 (Aug. 1, 1991), pp. 2334–2342. ISSN: 0013-4651, 1945-7111. DOI: 10.1149/1.2085971. URL: https://iopscience.iop.org/article/10.1149/1.2085971 (visited on 12/11/2023).

[34] Dawn M. Bernardi and Mark W. Verbrugge. "A Mathematical Model of the Solid-Polymer-Electrolyte Fuel Cell". In: *Journal of The Electrochemical Society* 139.9 (Sept. 1, 1992). Publisher: IOP Publishing, p. 2477. ISSN: 1945-7111. DOI: 10.1149/1.2221251. URL: https://iopscience.iop.org/article/10.1149/1.2221251/meta (visited on 01/04/2024).

[35] Hubertus P. L. H. van Bussel, Frans G. H. Koene, and Ronald K. A. M. Mallant. "Dynamic model of solid polymer fuel cell water management". In: *Journal of Power Sources* 71.1 (Mar. 15, 1998), pp. 218–222. ISSN: 0378-7753. DOI: 10.1016/S0378-7753(97)02744-4. URL: https://www.sciencedirect.com/science/article/pii/S0378775397027444 (visited on 12/29/2023).

[36] S. Dutta, S. Shimpalee, and J.W. Van Zee. "Three-dimensional numerical simulation of straight channel PEM fuel cells". In: *Journal of Applied Electrochemistry* 30.2 (Feb. 1, 2000), pp. 135–146. ISSN: 1572-8838. DOI: 10.1023/A:1003964201327. URL: https://doi.org/10.1023/A:1003964201327 (visited on 12/29/2023).

[37] Jung Seok Yi and Trung Van Nguyen. "Multicomponent Transport in Porous Electrodes of Proton Exchange Membrane Fuel Cells Using the Interdigitated Gas Distributors". In: *Journal of The Electrochemical Society* 146.1 (Jan. 1, 1999). Publisher: IOP Publishing, p. 38. ISSN: 1945-7111. DOI: 10.1149/1.1391561. URL: https://iopscience.iop.org/article/10.1149/1.1391561/meta (visited on 05/14/2024).

[38] Thomas F. Fuller and John Newman. "Water and Thermal Management in Solid-Polymer-Electrolyte Fuel Cells". In: *Journal of The Electrochemical Society* 140.5 (May 1, 1993), pp. 1218–1225. ISSN: 0013-4651, 1945-7111. DOI: 10.1149/1.2220960. URL: https://iopscience.iop.org/article/10.1149/1.2220960 (visited on 05/14/2024).

[39] Andrew Rowe and Xianguo Li. "Mathematical modeling of proton exchange membrane fuel cells". In: *Journal of Power Sources* 102.1 (Dec. 1, 2001), pp. 82–96. ISSN: 0378-7753. DOI: 10.1016/S0378-7753(01)00798-4. URL: https://www.sciencedirect.com/science/article/pii/S0378775301007984 (visited on 01/04/2024).

[40] T. Berning, D. M. Lu, and N. Djilali. "Three-dimensional computational analysis of transport phenomena in a PEM fuel cell". In: *Journal of Power Sources*. Proceedings of the Seventh Grove Fuel Cell Symposium 106.1 (Apr. 1, 2002), pp. 284–294. ISSN: 0378-7753. DOI: 10.1016/S0378-7753(01)01057-6. URL: https://www.sciencedirect.com/science/article/pii/S0378775301010576 (visited on 01/05/2024).

[41] K.K.T. Thanapalan et al. "MODELLING OF A PEM FUEL CELL SYSTEM". In: *IFAC Proceedings Volumes* 41.2 (2008), pp. 4636–4641. ISSN: 14746670. DOI: 10.3182/20080706-5-KR-1001.00780. (Visited on 11/10/2023).

[42] Njoya M. Souleman, Olivier Tremblay, and Louis-A. Dessaint. "A generic fuel cell model for the simulation of fuel cell vehicles". In: *2009 IEEE Vehicle Power and Propulsion Conference*. 2009 IEEE Vehicle Power and Propulsion Conference. ISSN: 1938-8756. Sept. 2009, pp. 1722–1729. DOI: 10.1109/VPPC.2009.5289692. URL: https://ieeexplore.ieee.org/document/5289692 (visited on 11/21/2023).

[43] Abraham Gebregergis et al. "Solid Oxide Fuel Cell Modeling". In: *IEEE Transactions on Industrial Electronics* 56.1 (Jan. 2009). Conference Name: IEEE Transactions on Industrial Electronics, pp. 139–148. ISSN: 1557-9948. DOI: 10.1109/TIE.2008.2009516. URL: https://ieeexplore.ieee.org/document/4682693 (visited on 11/30/2023).

[44] Miguel Angel Rubio Gonzalez, Alfonso Urquia, and S. Dormido. "Dynamic modelling of PEM fuel cells using the FuelCellLib Modelica library". In: *Mathematical and Computer Modelling of Dynamical Systems* 16 (June 1, 2010), pp. 165–194. DOI: 10.1080/13873954.2010.506758.

[45] Daniel Andersson et al. "Dynamic modeling of a solid oxide fuel cell system in Modelica". In: (2011).

[46] T V V S Lakshmi, P Geethanjali, and Prasad S Krishna. "Mathematical modelling of solid oxide fuel cell using Matlab/Simulink". In: *2013 Annual International Conference on Emerging Research Areas and 2013 International Conference on Microelectronics, Communications and Renewable Energy*. 2013 Annual International Conference on Emerging Research Areas and 2013 International Conference on Microelectronics, Communications and Renewable Energy. June 2013, pp. 1–5. DOI: 10.1109/AICERA-ICMiCR.2013.6576016. URL: https://ieeexplore.ieee.org/abstract/document/6576016 (visited on 11/30/2023).

[47] Paola Costamagna et al. "Integrated Planar Solid Oxide Fuel Cell: Steady-State Model of a Bundle and Validation through Single Tube Experimental Data". In: *Energies* 8.11 (Nov. 2015). Number: 11 Publisher: Multidisciplinary Digital Publishing Institute, pp. 13231–13254. ISSN: 1996-1073. DOI: 10.3390/en81112364. URL: https://www.mdpi.com/1996-1073/8/11/12364 (visited on 01/08/2024).

[48] Thinh X. Ho. "Dynamic characteristics of a solid oxide fuel cell with direct internal reforming of methane". In: *Energy Conversion and Management* 113 (Apr. 1, 2016), pp. 44–51. ISSN: 0196-8904. DOI: 10.1016/j.enconman.2016.01.049. URL: https://www.sciencedirect.com/science/article/pii/S0196890416000662 (visited on 01/08/2024).

[49] Andraz Kravos et al. "Thermodynamically consistent reduced dimensionality electrochemical model for proton exchange membrane fuel cell performance modelling and control". In: *Journal of Power Sources* 454 (Apr. 1, 2020), p. 227930. ISSN: 0378-7753. DOI: 10.1016/j.jpowsour.2020.227930. URL: https://www.sciencedirect.com/science/article/pii/S0378775320302330 (visited on 11/22/2023).

[50] Fiammetta Rita Bianchi et al. "Solid Oxide Fuel Cell Performance Analysis through Local Modelling". In: *Catalysts* 10.5 (May 2020). Number: 5 Publisher: Multidisciplinary Digital Publishing Institute, p. 519. ISSN: 2073-4344. DOI: 10.3390/catal10050519. URL: https://www.mdpi.com/2073-4344/10/5/519 (visited on 01/08/2024).

[51] Sandip Dutta, Sirivatch Shimpalee, and J.W. Van Zee. "Numerical prediction of mass-exchange between cathode and anode channels in a PEM fuel cell". In: *International Journal of Heat and Mass Transfer* 44.11 (June 2001), pp. 2029–2042. ISSN: 00179310. DOI: 10.1016/S0017-9310(00)00257-X. URL: https://linkinghub.elsevier.com/retrieve/pii/S001793100000257X (visited on 12/14/2023).

[52] Sreekissoon Sumeshan, Dreepaul Raj Kumar, and Busawon Krishna. "Simulink Model of Proton Exchange Membrane Fuel Cell". In: *2022 7th International Conference on Environment Friendly Energies and Applications (EFEA)*. 2022 7th International Conference on Environment Friendly Energies and Applications (EFEA). Bagatelle Moka MU, Mauritius: IEEE, Dec. 14, 2022, pp. 1–4. ISBN: 9798350333213. DOI: 10.1109/EFEA56675.2022.10063799. URL: https://ieeexplore.ieee.org/document/10063799/ (visited on 11/16/2023).

[53] "Designing Fuel Cell Systems Using System-Level Design". In: (2022). URL: https://www.mathworks.com/campaigns/offers/fuel-cell-systems-for-electrical-mobility.html.

[54] Steven B. Beale et al. "Continuum scale modelling and complementary experimentation of solid oxide cells". In: *Progress in Energy and Combustion Science* 85 (July 1, 2021), p. 100902. ISSN: 0360-1285. DOI: 10.1016/j.pecs.2020.100902. URL: https://www.sciencedirect.com/science/article/pii/S036012852030112X (visited on 01/08/2024).

[55] Mallika Gummalla et al. "Fuel Cell Airframe Integration Study for Short-Range Aircraft". In: 1 (2006).

[56] Ananda Himansu et al. "Hybrid Solid Oxide Fuel Cell/Gas Turbine System for High Altitude Long Endurance Aerospace Missions". In: Jan. 1, 2006. DOI: 10.1115/FUELCELL2006-97095.

[57] Joseph W. Pratt et al. "Proton exchange membrane fuel cells for electrical power generation on-board commercial airplanes". In: *Applied Energy*. Sustainable Development of Energy, Water and Environment Systems 101 (Jan. 1, 2013), pp. 776–796. ISSN: 0306-2619. DOI: 10.1016/j.apenergy.2012.08.003. URL: https://www.sciencedirect.com/science/article/pii/S0306261912005727 (visited on 11/08/2023).

[58] Thomas Kadyk et al. "Analysis and Design of Fuel Cell Systems for Aviation". In: *Energies* 11.2 (Feb. 2018). Number: 2 Publisher: Multidisciplinary Digital Publishing Institute, p. 375. ISSN: 1996-1073. DOI: 10.3390/en11020375. URL: https://www.mdpi.com/1996-1073/11/2/375 (visited on 01/05/2024).

[59] A. A. Kulikovsky. "A Physically–Based Analytical Polarization Curve of a PEM Fuel Cell". In: *Journal of The Electrochemical Society* 161.3 (Dec. 28, 2013). Publisher: IOP Publishing, F263. ISSN: 1945-7111. DOI: 10.1149/2.028403jes. URL: https://iopscience.iop.org/article/10.1149/2.028403jes/meta (visited on 05/14/2024).

[60] Jeffrey M. Collins and Dustin McLarty. "All-electric commercial aviation with solid oxide fuel cell-gas turbine-battery hybrids". In: *Applied Energy* 265 (May 1, 2020), p. 114787. ISSN: 0306-2619. DOI: 10.1016/j.apenergy.2020.114787. URL: https://www.sciencedirect.com/science/article/pii/S0306261920302993 (visited on 01/06/2024).

[61] M. Schröder et al. "Optimal operating conditions of PEM fuel cells in commercial aircraft". In: *International Journal of Hydrogen Energy* 46.66 (Sept. 24, 2021), pp. 33218–33240. ISSN: 0360-3199. DOI: 10.1016/j.ijhydene.2021.07.099. URL: https://www.sciencedirect.com/science/article/pii/S0360319921027634 (visited on 12/28/2023).

[62] F. Becker, F. Pillath, and J. Kallo. "Cathode Exhaust Gas Recirculation for Polymer Electrolyte Fuel Cell Stack". In: *Fuel Cells* 18.5 (2018), pp. 568–575. ISSN: 1615-6854. DOI: 10.1002/fuce.201700219. URL: https://onlinelibrary.wiley.com/doi/abs/10.1002/fuce.201700219 (visited on 05/14/2024).

[63] Kui Jiao et al. "Designing the next generation of proton-exchange membrane fuel cells". In: *Nature* 595 (July 15, 2021), pp. 361–369. DOI: 10.1038/s41586-021-03482-7.

[64] Hani A.E. Hawa, Subir Roychoudhury, and Christian Junaedi. "Hybridized, High Pressure, Liquid Fueled Solid Oxide Fuel Cell (SOFC) for Aircraft Primary Power". In: *2022 IEEE Transportation Electrification Conference & Expo (ITEC)*. 2022 IEEE/AIAA Transportation Electrification Conference and Electric Aircraft Technologies Symposium (ITEC+EATS). Anaheim, CA, USA: IEEE, June 15, 2022, pp. 1051–1056. ISBN: 978-1-66540-560-7. DOI: 10.1109/ITEC53557.2022.9813817. URL: https://ieeexplore.ieee.org/document/9813817/ (visited on 12/04/2023).

[65] Chengjie Li et al. "Comparative study on the performance of the application of clean alternative fuels in SOFC/ICE hybrid power systems on electric aircraft". In: *Frontiers in Energy Research* 11 (2023). ISSN: 2296-598X. URL: https://www.frontiersin.org/articles/10.3389/fenrg.2023.1146587 (visited on 12/04/2023).

[66] Feng Zhao and Anil V. Virkar. "Dependence of polarization in anode-supported solid oxide fuel cells on various cell parameters". In: *Journal of Power Sources* 141.1 (Feb. 16, 2005), pp. 79–95. ISSN: 0378-7753. DOI: 10.1016/j.jpowsour.2004.08.057. URL: https://www.sciencedirect.com/science/article/pii/S0378775304009528 (visited on 05/14/2024).

[67] Thomas Kadyk et al. "Design of Fuel Cell Systems for Aviation: Representative Mission Profiles and Sensitivity Analyses". In: *Frontiers in Energy Research* 7 (2019). ISSN: 2296-598X. URL: https://www.frontiersin.org/articles/10.3389/fenrg.2019.00035 (visited on 12/12/2023).

[68] M.D. Fernandes et al. "SOFC-APU systems for aircraft: A review". In: *International Journal of Hydrogen Energy* 43.33 (Aug. 2018), pp. 16311–16333. ISSN: 03603199. DOI: 10.1016/j.ijhydene.2018.07.004. URL: https://linkinghub.elsevier.com/retrieve/pii/S0360319918320986 (visited on 12/04/2023).

[69] Maria Massaro et al. "Potential and technical challenges of on-board hydrogen storage technologies coupled with fuel cell systems for aircraft electrification". In: *Journal of Power Sources* 555 (Jan. 1, 2023), p. 232397. DOI: 10.1016/j.jpowsour.2022.232397.

[70] Tri Cuong Do et al. "Energy Management Strategy of a PEM Fuel Cell Excavator with a Supercapacitor/Battery Hybrid Power Source". In: *Energies* 12 (Nov. 15, 2019), p. 4362. DOI: 10.3390/en12224362.

[71] Masoud Najafi et al. "Modeling and simulation of a reformate supplied PEM fuel cell stack, application to fault detection". In: (Jan. 1, 2007).

[72] K.J. Runtz and M.D. Lyster. "Fuel cell equivalent circuit models for passive mode testing and dynamic mode design". In: *Canadian Conference on Electrical and Computer Engineering, 2005.* (2005). Conference Name: Canadian Conference on Electrical and Computer Engineering, 2005. ISBN: 9780780388857 Place: Saskatoon, SK, Canada Publisher: IEEE, pp. 794–797. DOI: 10.1109/CCECE.2005.1557048. URL: http://ieeexplore.ieee.org/document/1557048/ (visited on 04/05/2024).

[73] Ryan P. O'Hayre et al. *Fuel cell fundamentals*. Third edition. 1 online resource vols. Hoboken, New Jersey: John Wiley & Sons Inc., 2016. ISBN: 978-1-5231-1024-7. URL: http://public.eblib.com/choice/publicfullrecord.aspx?p=4505263 (visited on 01/31/2024).

[74] Yunus A. Çengel. *Thermodynamics*. In collab. with Internet Archive. McGraw-Hill, 2001. 970 pp. ISBN: 978-0-07-238332-4. (Visited on 04/10/2024).

[75] Souleman NJOYA MOTAPON. "A GENERIC FUEL CELL MODEL AND EXPERIMENTAL VALIDATION". PhD thesis. Montreal: ECOLE DE TECHNOLOGIE SUPERIEURE, 2008. URL: https://espace.etsmtl.ca/id/eprint/620/1/NJOYA_MOTAPON_Souleman.pdf (visited on 04/24/2024).

[76] Guangsheng Zhang and Satish G. Kandlikar. "A critical review of cooling techniques in proton exchange membrane fuel cell stacks". In: *International Journal of Hydrogen Energy* 37.3 (Feb. 2012), pp. 2412–2429. ISSN: 03603199. DOI: 10.1016/j.ijhydene.2011.11.010. URL: https://linkinghub.elsevier.com/retrieve/pii/S0360319911024980 (visited on 12/05/2023).

[77] Mohamed H.S. Bargal et al. "Liquid cooling techniques in proton exchange membrane fuel cell stacks: A detailed survey". In: *Alexandria Engineering Journal* 59.2 (Apr. 2020), pp. 635–655. ISSN: 11100168. DOI: 10.1016/j.aej.2020.02.005. URL: https://linkinghub.elsevier.com/retrieve/pii/S1110016820300600 (visited on 12/05/2023).

[78] Mustafa Cavcar. "The International Standard Atmosphere (ISA)". In: ().

[79] ZEROAVIA. *SuperStack Datasheet*. URL: https://zeroavia.com/wp-content/uploads/2024/05/SuperStack-Datasheet-6-digital.pdf (visited on 06/04/2024).

[80] L. R. Petzold. *Description of DASSL: a differential/algebraic system solver*. SAND-82-8637; CONF-820810-21. Sandia National Labs., Livermore, CA (USA), Sept. 1, 1982. URL: https://www.osti.gov/biblio/5882821 (visited on 06/06/2024).

[81] ATR Aricraft. *ATR 72-600 Flyer*. URL: https://www.atr-aircraft.com/wp-content/uploads/2022/06/ATR_Fiche72-600-3.pdf (visited on 06/07/2024).

[82] Emil Skoglund. "A NUMERICAL MODEL OF HEAT- AND MASS TRANSFER IN POLYMER ELECTROLYTE FUEL CELLS". In: (2021).

[83] Eric Mueller and Anna Stefanopoulou. "Analysis, Modeling, and Validation for the Thermal Dynamics of a Polymer Electrolyte Membrane Fuel Cell System". In: *Journal of Fuel Cell Science and Technology - J FUEL CELL SCI TECHNOL* 3 (May 1, 2006). DOI: 10.1115/1.2173663.